Kinetic Studies on the University of London Nuclear Reactor

A Thesis submitted for the award of the Degree of Doctor of Philosophy in the Faculty of Engineering, University of London.

By

Alan Jebb, B.Sc.(Hons.), D.I.C.

Nuclear Power Section
Mechanical Engineering Department
Imperial College of Science and Technology
London S.W.7.

November 1973.

CONTENTS

ABSTRACT

In many reactor dynamic studies use is made of the reactor transfer function for zero power and full operational power. The latter in fact consisting of the zero power transfer function modified to take account of power dependent reactivity feedbacks due to temperature, density and pressure changes. For many studies, particularly control studies, the point reactor kinetic equations are sufficient. However, the increased size of power reactors and the pressure of spatial effects has lead to the non-separable space-time kinetic transfer functions.

Finally the growth of noise analysis with respect to reactor behaviour has led to many theoretical and experimental studies.

This thesis covers an investigation into the determination of the zero power transfer function of the University of London Reactor (U.L.R.) CONSORT and its spatial dependency, if any, utilising a specially designed reactivity oscillator and the use of noise measurements as an alternative method of zero power transfer function derivation.

The results provide a zero power transfer function that fits closely to theoretical predictions. Certain basic nuclear parameters such as prompt neutron lifetime were obtained and agreed reasonably well with design values. No spatial dependency was obtained for the oscillator/detector configurations used in the experiments.

The noise measurements provided an adequate check for the zero power transfer function in the upper frequency range. Again no spatial dependency was observed.

Spatial dependency may exist but it would require the detector to be much nearer to the oscillator, than was possible with the present core configuration. The practical benefits to be gained from such an investigation on the CONSORT reactor would, of course, require careful study before implementation.

During the course of the experimentation use was made of existing alternative standard measurement equipment to facilitate the production of a student experiment.

ACKNOWLEDGEMENTS

I would like to thank my supervisor, Professor P.J. Grant for his guidance, encouragement and assistance during the experimental work and the invaluable discussions during the writing period of the thesis.

My thanks are due to the staff of the U.L.R. Reactor Centre, particularly Mr. M. Kerridge, Mr. E.A. Caesar and Mr. T. Jones, for their help during the design and experimental phase of the work.

I must extend my gratitude to Dr. C.B. Besant for his selfless support during the final stages of the thesis.

May I finally thank Mrs. J. Campion for her patience during her typing of this thesis.

NOMENCLATURE

α	Sub-critical Rossi-Alpha.
$\overline{\gamma\beta}(\beta)^*$	Effective delayed neutron fraction.
n	Neutron density.
C_i	Precursor density.
t	Time.
ρ	Reactivity.
β	Delayed neutron fraction.
ℓ	Neutron generation time.
λ	Decay constant for precursor density.
S	Effective source strength.
$\overline{\gamma}$	Average effectiveness (in producing fission) of delayed neutrons compared with prompt neutrons.
K	Effective reproduction factor.
$H(p)$	System transfer function.
W	Angular frequency.
$I(p)$	La place impulse response.
$G(p)$	Zero power transfer function.
ϕ_r	Neutron flux at radius r.
B	Material buckling.
ϕ_n, ϕ_r	Neutron and gamma flux respectively.
S_n, S	Neutron and gamma sensitivity of neutron detectors, respectively.
ν	Mean number of neutrons produced per fission event.
Cd	Cadmium.
$\not\beta$	Dollars unit of reactivity.

db	Decibels.
α_{DC}	Delayed critical Rossi-Alpha.
PDF	Probability density function.
ACF	Auto-correlation function.
CCF	Cross-correlation function.
APSD	Auto power spectral density function.
CPSD	Cross power spectral density function.
F	Fourier transform.
τ	Time lag in correlation functions.
R_{xx}, R_{xy}	Auto and cross-correlation functions respectively.
G(f)	Greens function.
M	Migration length.
G	Amplitude or gain in decibels.
D	Diffusion coefficient.
$\frac{1}{K}$	Penetration depth (neutrons).
V	Neutron velocity.
$\Sigma_{\bar{a}}$	Macroscopic absorption cross-section.

CHAPTER 1

1.1. General Introduction

Most dynamic characteristics of nuclear reactors cannot be evaluated by static techniques, kinetic characteristics are best measured by kinetic experiments. These experiments provide precise values of dynamic parameters such as neutron lifetime, α, reactor period, they also provide many of the static parameters determined by exponential column experiments for example.

Kinetic techniques for the determination of reactivity have been developed and used over the years placing an increased emphasis upon the accuracy of fundamental kinetic data and the interpretation of kinetic experiments.

Common to static and kinetic measurements are the perturbations caused by the presence of higher flux modes. In static measurements use is made of spatial separation between detector and source to avoid higher mode perturbations whilst dynamic measurements use separation in time (e.g. one can allow higher modes to die away before taking measurements).

Experimental difficulties arise in static experiments when spatial flux sampling is involved. Flux time decay curves can be observed externally by a single detector. Spatial modal effects sensitive to detector location are difficult to interpret. In a dynamic experiment the presence or absence of higher modes is more easily established.

The three most important parameters of reactor kinetics are reactivity, prompt neutron lifetime and the effective delayed neutron fraction $\bar{\beta}$. Dynamic techniques available for their evaluation are:

1. Asymptotic period measurements.

2. Reactivity perturbations i.e. rod drop and oscillators.

3. Source perturbation i.e. source jerk, Rossi-Alpha pulsed neutron.

4. Controlled step and impulse reactivity responses.

5. Statistical correlation methods i.e. noise analysis.

1.2. Reactor Transfer Function

A very important aspect of reactor dynamics and safety is the stability of the reactor under power oscillations caused either spontaneously or due to some malfunction of the reactor system.

The response of a reactor when subjected to small periodic disturbances of reactivity or neutron sources is described by the Reactor Transfer Function. This Function is the complex function of frequency relating the power oscillation to the reactivity oscillation.

In control system synthesis and analysis use is often made of Transfer Functions and a Reactor Transfer Function is necessarily of great value[1, 2].

1.2(1). Zero Power Reactor Transfer Function

The geometry and spectrum of a given reactor are explicitly involved in the detailed analysis of the kinetic behaviour of the reactor.

In a space independent one group approximation the fundamental spatial and spectral mode of neutron flux distribution is assumed constant. The kinetic response is then governed by

the prompt neutron lifetime and the delayed neutron behaviour.

Space independent kinetic equations are valid for many studies, notably those undertaken in the design of reactor control systems. Several groups of delayed neutron precursors can more easily be incorporated into a transfer function than can be spatial effects. In many reactor control system studies a two group approximation has proved to be very suitable, e.g. a control system design study carried on the Prototype Fast Reactor by the author[3] involves the use of a two group delayed neutron approximation.

The basic transfer function for any reactor is that known as the Zero-Power Transfer Function. This is derived either analytically or experimentally for a given reactor at zero power nominally at which condition no power-feedback effects are present.

1.2(2). Power Reactor Transfer Function

Reactor transfer functions are necessary so that a designer can study kinetic effects when the reactor is operating at different steady power levels. For these operations it is more normal to use a zero-power transfer function modified by the appropriate power reactivity feedback effects. These may differ in magnitude and type for different power levels dependent upon the reactor type.

In a non-critical operation such as start-up and shut-down it can be important to know how the transfer function differs from its usual equilibrium value, this leads to a non-equilibrium or 'instantaneous' type reactor transfer function. The importance of this has been shown by Singer[4].

1.2(3). Space Dependent Reactor Transfer Function

As stated before the transfer function equations most commonly used for reactors are derived from the time dependent kinetic or diffusion equations after the spatial dependency has been removed by assuming that the flux shape stays in its fundamental mode, the reactor often being treated as a 'black box' or a 'lumped parameter' model[5, 6]. This type of transfer function predicts reactor behaviour very well (Harrer et al[7]) especially for low frequencies where the neutron flux appears to respond simultaneously throughout the entire reactor and for critical systems where the bandwidth is narrow and the higher frequencies are heavily attenuated.

A reactor however is not a lumped parameter system, the distances between input and output devices as well as their relative locations in the system can have a large effect upon the measured attenuation and phase shift of a disturbance as it propagates through a system. For example in the case of a large thermal power reactor the slow withdrawal of a poison rod could produce continuous changes in flux shape as well as an overall increase in flux level. This change in flux shape would affect the three aforementioned, most important kinetic parameters reactivity, prompt neutron lifetime and delayed neutron fraction. These effects, if significant, would have to be considered in a kinetic study, i.e. space and time dependency. Other such examples are coupled systems, mixed fuel and isotope systems and fast breeder reactors.

1.3. The Present Work

The main objectives of the present study were to determine the zero-power transfer function of the University of London Research Reactor and to investigate its spatial dependency, if any, using a sinusoidal oscillator and detector system in one series of experiments and a one/two detector noise measuring system for a second series of experiments. Reversibility of the reactor transfer function was to be investigated during the first series of experiments.

The study consisted of four main tasks:

(1) The design, construction, test and calibration of an accurate sinusoidal oscillator with its associated speed control and measurement system. This section involved the computer prediction of reactivity levels using the CRAM[8] program and basic experimental reactivity tests on the reactor.

(2) A series of experiments with the oscillator and detector in various geometric positions in and outside the actual reactor core, tests being repeated with the positions of the oscillator and detector reversed.

(3) Using the same detector measurement system as (2) to carry out one and two detector noise experiments.

(4) The evaluation and analysis of the results using computer techniques and the correlation between the two series of experiments.

CHAPTER 2

2.1. Zero Power Reactor Transfer Functions

2.1(1) Point Reactor Equations (Space Independent)

The well established point reactor equations are as follows:

$$\frac{dn}{dt} = \frac{\rho - \beta}{\ell} n + \Sigma_i \lambda_i C_i + S \qquad \ldots.2.1$$

$$\frac{dC_i}{dt} = \frac{\beta_i}{\ell} n - \lambda_i C_i \qquad \ldots.2.2$$

Where

n = neutron density (or power, etc.)

C_i = precursor density, same units as n

t = time

ρ = reactivity $\frac{k-1}{k}$, the fractional change in neutron reproduction factor

β = delayed neutron fraction ($\Sigma_i \beta_i$)

ℓ = neutron generation time

λ_i = decay constant for precursor decay

S = effective source strength (same units as $\frac{dn}{dt}$)

The summation in equation 2.1 is from i = 1 to m where m is the number of delayed neutron group.

Since the equations are for a spatial independent model n can be regarded as an integral or volume averaged property that is proportional to the instantaneous neutron density at some point in the reactor, thus the terms power and neutron density can be interchanged (care must be taken since this viewpoint could be misleading). Neutron energy effects which can be very complicated

are excluded from these equations, i.e. if the neutron density is regarded as that for a thermal reactor terms in the equation can be multiplied by correction factors to allow for leakage and absorption above thermal energies. These factors can be calculated using Fermi age theory, two-energy group theory etc.[9, 10, 11]. Different correction factors are needed for prompt, delayed and extraneous source neutrons since they are produced at different energy levels.

Delayed neutrons are born at lower energies than prompt neutrons and on the average suffer less epithermal leakage and capture. This fact is allowed for by using effective delayed neutron fractions $\gamma_i\beta_i$ and $\bar{\gamma}\beta$ where $\bar{\gamma}$ could be as large as 1.3 for a small water moderated thermal reactor[12, 13].

A further refinement would be to allow for the fact that each delayed neutron emitter has a different neutron emission spectrum, thus requiring a different correction factor for each β_i, in the point model β is interpreted as the effective fraction, the ratios β_i/β being assumed fixed for a given fuel.

A shift in the reactor spectrum during a transient would affect the spectrum weighted average parameters. This spectral shift is one component in a complex interrelationship between reactor parameters such as density and temperature all of which are of importance when calculating reactivity. They may be neglected in the point reactor model especially for the present study where small oscillations at low power were undertaken for the oscillator series of experiments and noise measurements were made at steady state low power during the second series of experiments.

The chief limitation of the point reactor model is its inability to describe spatially dependent dynamic effects. These effects can be described as changes in spatial distribution (i.e. flux tilting) during transients. They could be regarded as being caused by time lags in propagating the effects of localised perturbations. These effects are of great importance in large reactors. Even in small reactors the point model becomes inadequate for large deviations from criticality. More discussion on the latter points continues in the section devoted to the space dependent transfer function.

At this stage it must be pointed out that nuclear fission and neutron diffusion are discrete processes and that the point reactor model, diffusion and transport theory are approximations to the stochastic processes actually taking place. These have been shown by Thie 1963[13] and Keepin 1965[12].

Six distinct groups of delayed neutron are generally used in reactor dynamic studies[12]. A two group equivalent set is often used for many dynamic control system tests, mainly to save on equipment when computer simulation models are being used.

2.1(2) Equilibrium and Criticality

Considering the kinetic equations 2.1 and 2.2 if β_i, λ_i and ℓ are considered constant the point reactor model consists of m + 1 linked first order differential equations incorporating two specific functions $\rho(t)$ and $S(t)$

In general ρ is a function of n and the system is non-linear. When considering heterogeneous reactors the various

contributions to and methods of reactivity feedback are the constituents that cause the non-linearity in ρ.

In the absence of feedback, i.e. a zero power state, $\rho(t)$ becomes an explicit function of time, the equations and the system becoming linear.

Considering the steady state (all time derivatives disappear).

Summing equation 2.2. over i and adding to equation 2.1.:

$$\frac{d}{dt}\left(n + \Sigma_i C_i\right) = \frac{\rho}{\ell} n + S \qquad \ldots.2.3$$

Steady state implies that:

$$\rho = \frac{-\ell S}{n} \qquad \ldots.2.4$$

Equilibrium conditions could be satisfied for a time dependent source with a constant $n = n_o$ if $\rho(t)$ and $S(t)$ were exactly proportional, but for complete equilibrium ρ and S must be constants namely ρ_o and S_o.

$$\therefore \quad \rho_o = \frac{-\ell S_o}{n_o} \qquad \ldots.2.5$$

the reactor is then in subcritical equilibrium ($\rho_o < 0$, $k < 1$).

Shut down power level is:

$$n_o = -\frac{\ell S_o}{\rho_o} = \frac{\ell S_o}{|\rho_o|} \qquad \ldots.2.6$$

N.B. precursor equilibrium density is:

$$C_{io} = \frac{\beta_i n_o}{\lambda_i \ell} \qquad \ldots.2.7$$

Criticality. In the strictest sense when defined as $k \neq 1$ ($\rho = o$) it is a non-equilibrium situation since in the presence of a source it is divergent, indeed if the source is withdrawn there is always a small supply of neutrons from extraneous sources, i.e. spontaneous fission, cosmic rays. In fact a reactor operating at steady power is always very slightly sub-critical, though the reactivity is extremely small. If the magnitude of reactivity at power is much smaller than that at shutdown the source terms may be ignored in calculations thus at high power equations 2.1 and 2.2 with $S = 0$ describe the kinetic behaviour.

2.2. Frequency Response and Transfer Function

For a subcritical reactor ($\rho = \rho_o$) in steady state with a source S_o (equation 2.5):

$$n_o = \frac{-\ell S_o}{n_o} \qquad \ldots.2.5$$

If the source magnitude is varied sinusoidally and if ρ_o remains constant $n(t)$ will oscillate sinusoidally about the level n_o (N.B. this is a linear system).

If the reactor system is considered as 'black box' or circuit element, the ratio of the Laplace transforms of the output and input to the black box is defined as the Transfer Function.

If $H(p)$ is defined as the system transfer function, for a linear system the frequency response is completely characterised by the magnitude and phase of $H(jw_o)$ where the forcing function is a sine wave input of angular frequency w_o ($p = jw_o$).

N.B. Any arbitrary periodic input can be represented as a Fourier series and using the principle of superposition each harmonic component can be transformed into a corresponding output component and the frequency response can be used to derive the response to any input wave form.

2.2(1) Point Reactor Response to an Oscillating Source

Let $n = n_o + \delta n$

$C_i = C_{io} + \delta C_i$

$S = S_o + \delta S$

$\rho = \rho_o$

As before the equilibrium conditions are (equations 2.5 and 2.6).

$$C_{io} = \frac{\beta_i n_o}{\lambda_i \ell} \quad \text{and} \quad n_o = \frac{-\ell S_o}{\rho_o}$$

Substituting into equations 2.1 and 2.2:

$$\frac{d}{dt}\ \delta_n = \frac{\rho_o - \beta}{\ell}\ \delta_n + \Sigma_i\ \lambda_i\ C_i + \delta S \qquad \ldots.2.8$$

$$\frac{d}{dt}\ \delta C_i = \frac{\beta_i}{\ell}\ \delta_n - \lambda_i\ \delta C_i \qquad \ldots.2.9$$

Using the transforms:

$$\delta N(p) = \int_o^\infty \delta n(t) e^{-pt}\, dt$$

$$\delta T_i(p) = \int_o^\infty \delta C_i(t) e^{-pt}\, dt$$

and $$\delta S(p) = \int_o^\infty \delta S(t) e^{-pt}\, dt$$

and solving the transformed equations:

$$\delta N(p) = \frac{\ell \left[\delta n(o) + \Sigma_i \frac{\lambda_i \, \delta C_i(o)}{p + \lambda_i} + \delta S(p) \right]}{\ell p + \beta - \rho_o - \Sigma_i \frac{\beta_i \lambda_i}{p + \lambda_i}} \qquad \ldots.2.10$$

Steady state part of response:

$$\delta N(p) = \frac{\ell \, \delta S(p)}{\ell p + \beta - p_o - \Sigma_i \frac{\beta_i \lambda_i}{p + \lambda_i}} \qquad \ldots.2.11$$

$$\therefore \frac{\delta N(p)}{\delta S(p)} = I(p) = \frac{\ell}{\ell p + \beta - \rho_o - \Sigma_i \frac{\beta_i \lambda_i}{\rho + \lambda_i}} \qquad \ldots.2.12$$

This is the Laplace impulse response.

Frequency response for a change in δn due to a change in $\delta p = \sin wt$ is given by the magnitude and phase of $I(jw)$.

Equation 2.12 is not restricted to small fluctuations.

2.2(2) Point Reactor Response to a Reactivity Oscillator

Oscillating neutron absorbers have been used in measurements of reactor dynamic parameters and neutron absorption cross sections[15, 16, 17, 18, 19].

Proceeding as in section 2.2(1).

Let $n = n_o + \delta n$

$C_i = C_{io} + \delta C_i$

$\rho = \rho_o + \delta\rho$

$S = S_o$

$$C_{io} = \frac{\beta_i n_o}{\lambda_i \ell}$$

$$S_o = \frac{-\rho_o n_o}{\ell}$$

Substituting these into equations 2.1 and 2.2:

$$\frac{d}{dt}\ \delta n = \frac{\rho_o - \beta}{\ell}\ \delta n + \Sigma_i\ \lambda_i\ \delta C_i + \frac{n_o}{\ell}\ \delta\rho + \frac{1}{\ell}\ \delta\rho\ \delta n \quad \ldots\ldots 2.13$$

$$\frac{d}{dt}\ \delta C_i = \frac{\beta_i}{\ell}\ \delta n - \lambda_i\ \delta C_i \quad \ldots\ldots 2.14$$

These equations are similar to those of 2.8 and 2.9 in the previous section except that the oscillating source δS is replaced by:

$$\frac{n_o}{\ell}\ \delta\rho + \frac{1}{\ell}\ \delta\rho\ \delta n$$

Assuming sufficiently small oscillations that $/\delta n/ \ll n_o$ i.e. $\delta\rho\ \delta n$ is negligible, equation 2.13 is then a linear differential equation with constant coefficients.

Using the Laplace transforms:

$$\delta N(p) = \int_o^\infty \delta n(t) e^{-pt} dt$$

$$\delta T_i(p) = \int_o^\infty \delta C_i(t) e^{-pt} dt$$

$$\delta R(p) = \int_o^\infty \delta\rho(t) e^{-pt} dt$$

The Laplace transform of the steady state portion of the response is given by:

$$\delta N(p) = \frac{n_o\ \delta R(p)}{\ell p + \beta - \rho_o - \Sigma_i \frac{\beta_i\ \lambda_i}{p + \lambda_i}} \quad \ldots\ldots 2.15$$

The reactivity transfer function is:

$$G(p) = \frac{\delta N(p)}{\delta R(p)} = \frac{n_o}{\ell} I(p) = \frac{n_o}{\ell p + \beta - \rho_o - \Sigma_i \frac{\beta_i \lambda_i}{p + \lambda_i}} \quad \ldots.2.16$$

N.B. See equation 2.12

The reactivity transfer function is n_o/ℓ times the source transfer function equation 2.12, section 2.2(1), providing that the resulting power oscillation is small.

The frequency response for a fluctuation in δn due to a small reactivity oscillation is given by the magnitude and phase of $G(jw)$, where $p = jw$

$\therefore$ if $\delta p = A \sin wt$ 2.17

Then $\delta n = A/G(jw)/\sin(wt + \emptyset)$ 2.18

Where $G(jw) = /G(jw)/e^{j\emptyset}$ 2.19

Examining $G(p)$

$$G(p) = \frac{n_o}{\ell p + \beta - \rho_o - \Sigma_i \frac{\beta_i \lambda_i}{p + \lambda_i}} = \frac{n_o}{(\ell + \Sigma_i \frac{\beta_i}{p + \lambda_i})p - \rho_o} \quad \ldots.2.20$$

If the numerator and denominator of equation 2.20 are multiplied by $\prod_i (p + \lambda_i)$ where the product $\prod_i$ extends from $i = 1$ to $i = m$ then $G(p)$ becomes a ratio of two polynomials of degree m and m + 1 respectively. There are m zeroes at $p = -\lambda_i$, and m + 1 poles on the real axis at $p = \dot{w}_i$ (the m = 1 roots). If $\rho_o = 0$ there is a pole at the origin corresponding to equilibrium operation at an arbitrary power level, the other poles being on the negative axis.

For very small ρ and provided that $\rho_o \neq 0$

$$G(p) \triangleq - \frac{n_o}{\rho_o} = \frac{n_o}{/\rho_o/} \qquad \ldots.2.21$$

If $\rho_o = 0$ then for very small ρ

$$G(p) \simeq \frac{n_o}{(\ell + \Sigma_i \frac{\beta_i}{\lambda_i})p} \simeq \frac{n_o}{\ell' p} \qquad \ldots.2.22$$

Where $\ell' p = (\ell + \Sigma_i \frac{\beta_i}{\lambda_i})p$

For very large p

$$G(p) \simeq \frac{n_o}{\ell p} \qquad \ldots.2.23$$

ℓ is very small there is an intermediate range $/p/ \gg \max \lambda_i$

where

$$G(p) \simeq \frac{n_o}{\beta - \rho_o} \qquad \ldots.2.24$$

For one group of delayed neutrons

$$G(p) = \frac{n_o}{(\ell + \frac{\beta}{p + \lambda})p - \rho_o} \qquad \ldots.2.25$$

$$= \frac{n_o(p + \lambda)}{\ell p^2 + (\beta + \lambda\ell - \rho_o)p - \lambda\rho_o} \qquad \ldots.2.26$$

The denominator has two real roots one always negative the other with the same sign as ρ_o

Equation 2.26 could be expressed as:

$$G(p) = \frac{n_o(p + \lambda)}{\ell(p - w_1)(p - w_2)} \qquad \ldots.2.27$$

Where w_1 and w_2 are the roots.

For a critical reactor:

$$G(p) = \frac{n_o}{(\ell + \Sigma_i \frac{\beta_i}{p + \lambda_i})p} \qquad \text{....2.28}$$

Considering one group:

$$G(p) = \frac{n_o(p + \lambda)}{\ell p(p + \lambda + \beta/\ell)} \qquad \text{....2.29}$$

Equation 2.29 has poles at $p = w_1 = 0$ and $p = w_2 = -(\lambda + \beta/\ell)$.

Since $\lambda \ll \beta/\ell$, G(p) could be written as:

$$G(p) \simeq \frac{n_o(p + \lambda)}{\ell p(p + \beta/\ell)} \qquad \text{....2.30}$$

Equations 2.16, 2.28 and 2.29 are termed the zero power transfer functions because the equilibrium power n_o has been assumed small enough for reactivity feedbacks to be negligible. In using G(p) for a critical reactor ($\rho_o = 0$) infers that n_o is large enough for S_o the source to be neglected. Fig. 1 gives the magnitude and phase plots for U^{235} showing also the effect of various values of neutron generation time ℓ, the values being taken from Keepin[12]. Keepin[12] gives transfer function plots for six fission species U^{235}, U^{238}, Pu^{239}, Pu^{240}, U^{233} and Th^{232} systems. From these plots the transfer functions for mixed isotope systems may be estimated by using interpolation between the limiting pure isotope curves. This interpolation would require weighting according to fission rate and delayed yield of each fissioning isotope in the system. For accurate calculations further weighting to account for the average effectiveness in producing fission of the delayed neutrons relative to prompt neutrons for each

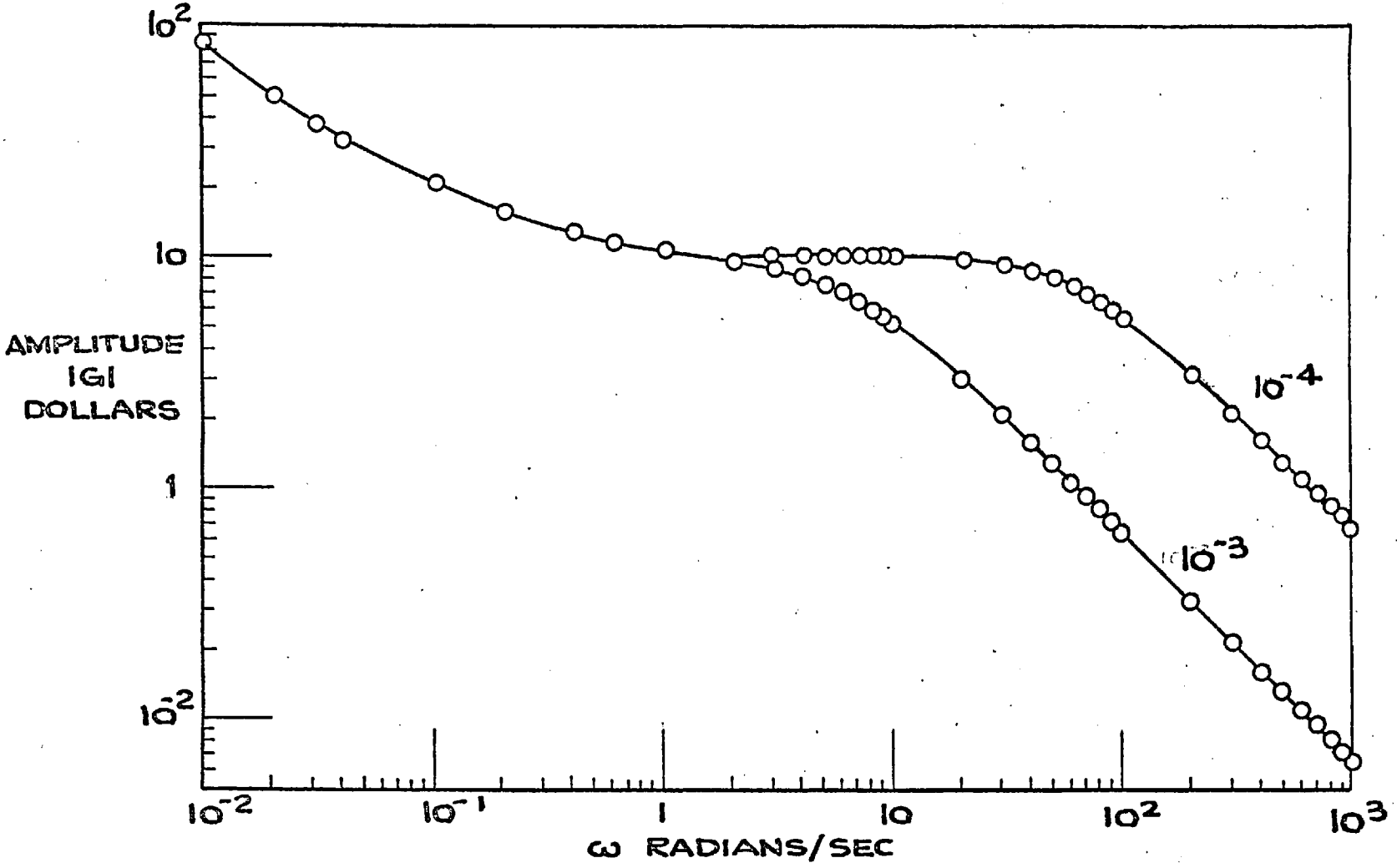

FIG. 1 : REACTOR TRANSFER FUNCTION AMPLITUDE RESPONSE FOR U^{235} VALUES CALCULATED BY DIGITAL COMPUTER TABULATED IN APPENDIX 3.

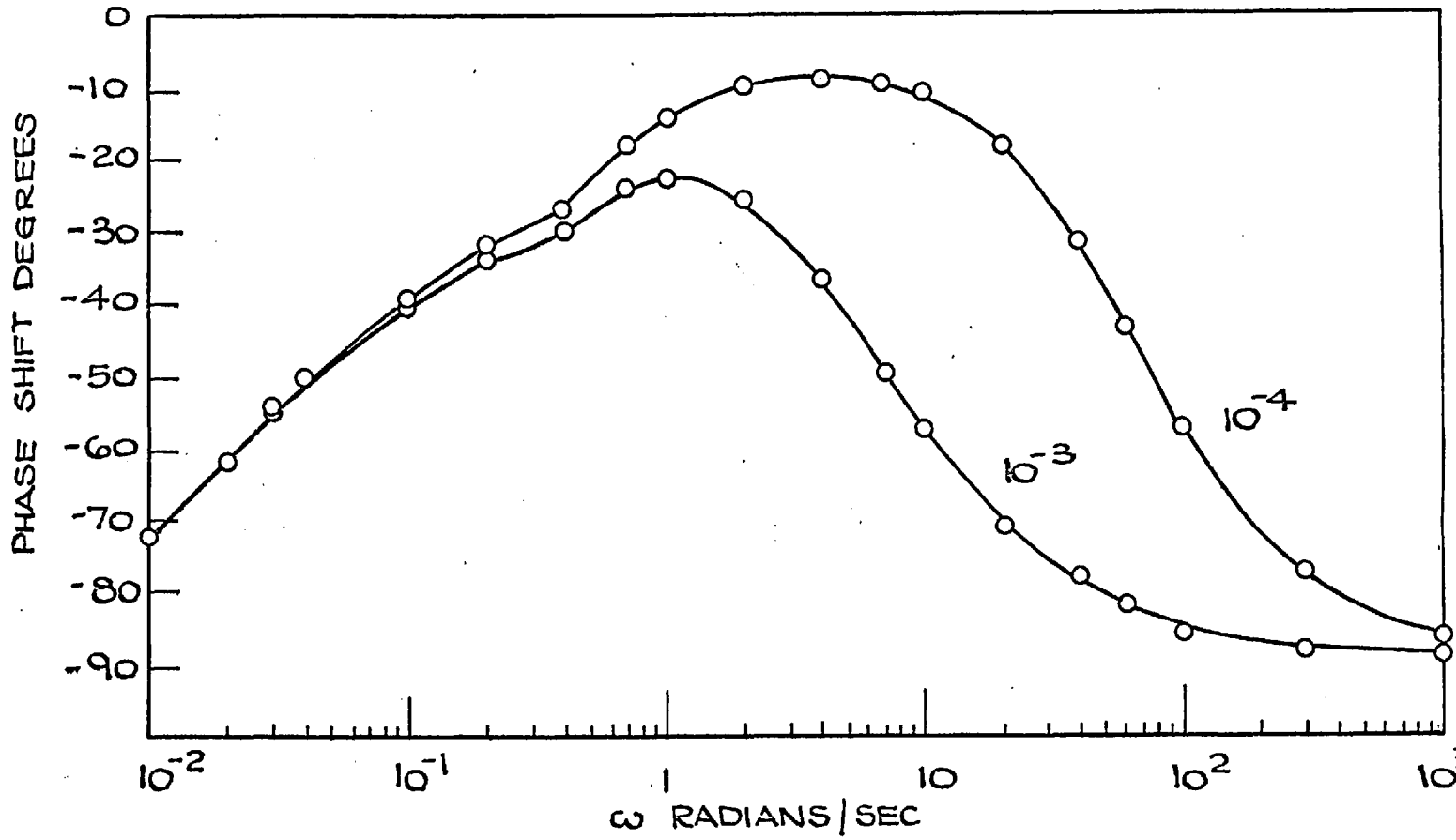

FIG. 1: REACTOR TRANSFER FUNCTION PHASE SHIFT RESPONSE FOR U^{235} VALUES CALCULATED BY DIGITAL COMPUTER TABULATED IN APPENDIX 3.

fission isotope. This would involve adjoint flux calculations requiring details of energy and spatial distribution of delayed and prompt neutrons for a given system.

2.2(3) Frequency Response for a Critical Reactor

One Group Approximation

Considering the equation 2.30 for small ℓ it becomes:

$$G(p) \simeq \frac{n_o(p + \lambda)}{\beta p} \qquad \ldots.2.31$$

As the frequency increases the amplitude remain constant with a limiting value n_o/β see Fig. 2.

This approximation can be used in stability studies since the non-roll off at high frequencies would be of secondary importance to other elements, i.e. reactivity feedbacks controllers etc., which in a realistic model would predominate due to their much larger time constants.

For $/p/ \leqq \lambda$

$$G(p) \simeq \frac{n_o \lambda}{\beta p} = \frac{n_o}{\ell' p} \qquad \ldots.2.32$$

This gives the low frequency asymptote.

For $/\rho/ \geqq \lambda$

$$G(p) \simeq \frac{n_o}{\ell p + \beta} \qquad \ldots.2.33$$

See Fig. 3.

For total response see Fig. 4.

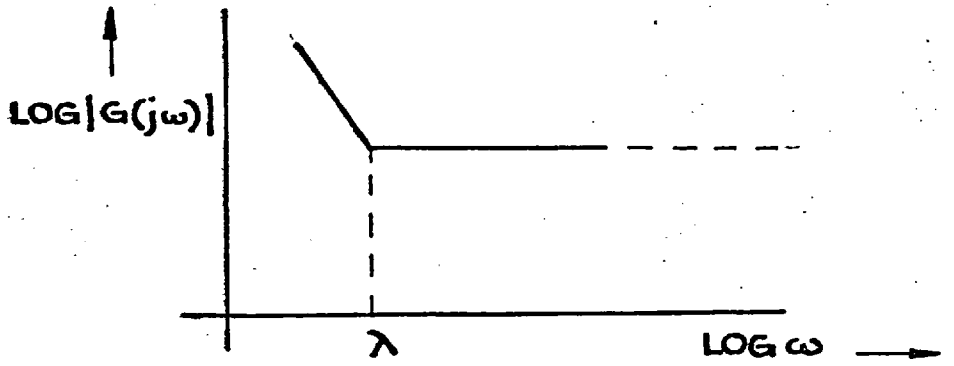

FIG. 2: FREQUENCY RESPONSE FOR SMALL ℓ

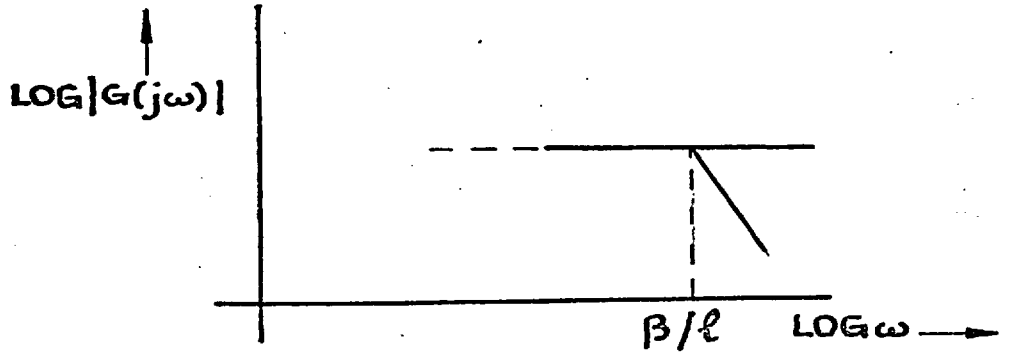

FIG. 3: FREQUENCY RESPONSE FOR $|\rho| \geq \lambda$

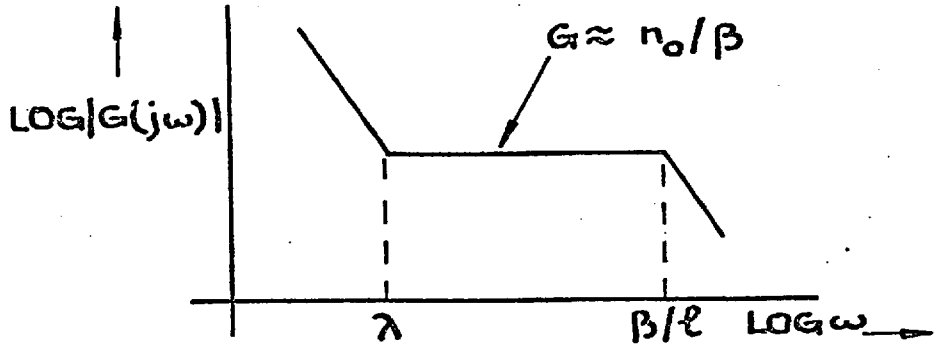

FIG. 4: TOTAL FREQUENCY RESPONSE.

The upper frequency range is the case for no delayed neutrons. From Fig. 1 it can be seen that the plateau is a function of ℓ, this can of course be demonstrated from the former theory.

2.2(4) Source-Sustained Subcritical System

The low frequency behaviour is different from that of the previous section equation 2.21. The amplitude reaches a constant at low frequency with a corresponding zero phase angle see Keepin[12].

2.2(5) Subcritical System

If considering equation 2.20 if $\rho_o > 0$ the physical meaning of the equation is lost since a positive ρ_o would imply a negative source. A transfer function for a source free supercritical system could be derived by using an oscillation superimposed upon an exponential rise with a stable period.

i.e. $n = n_o(1 + A)e^{pt}$

$C_i = C_{io}(1 + A)e^{pt}$

For details of the evaluation reference is made to Keepin[12].

This type of transfer function is of importance when considering control system design for nuclear rockets[4].

The latter two sections 2.2(4) and 2.2(5) on sub and supercritical system transfer functions are beyond the scope of this study, they are included for completeness and information.

2.3. Space Dependency

The space independent reactor kinetic equations (1) and (2) section 2.1(1) Chapter 2 describe satisfactorily the lehaviour of many reactor systems particularly for small, tightly coupled, reactors in which the spatial neutron distribution is relatively insensitive to local material property changes.

The basic point reactor kinetic equations have proved to be inappropriate for the transient analysis of larger power reactors. There are, of course, errors in the prediction of total power arising from the use of incorrect spatial flux distributions in obtaining average reactor properties.

Many authors including Keepin[12] have shown how a general reactor transient can be treated as a superposition of spatial modes. The higher modes die out after a local transient disturbance and the fundamental or asymptotic flux shape being reached usually within a few prompt neutron lifetimes. Delayed neutrons do sustain the higher modes for longer times but they are usually of an intensity low enough to be ignored. One exception is a rod drop experiment. The point kinetic equations effectively assume that the fundamental flux mode remains constant throughout the transient. In the case of large spatially located reactivity disturbances the flux shape can change shape during the transient duration time, e.g. spatial flux tilting under induced by xenon spatial distribution or the slow withdrawal of a poison rod which can produce flux shape changes as well as an overall increase in flux level.

The changes in flux shape would affect, as stated in Chapter 1, the three most important kinetic parameters reactivity, prompt neutron lifetime and delayed neutron fraction. If the

changes induced due to flux shape changes during a transient are significant then both space and time dependence must be accounted for in the reactor kinetic equations.

It is not the intention of this work to provide a comprehensive and detailed analysis of the theory for space and time dependent reactor kinetic theory. It was intended to investigate whether or not the U.L.R. CONSORT would exhibit any space dependency.

Procedures exist for evaluating and synthesising space and time dependent reactor kinetic equations ranging from mathematical solutions to extremely practical approaches where attempts are made to construct three-dimensional models for solution on digital, analogue and hybrid computers.

A common mathematical approach consists of expanding the neutron flux, any sources and the delayed neutron precursor density in terms of an orthogonal set of eigen functions, i.e. space dependent flux modes (harmonics). This method involves the solution of the wave equation:

$$\nabla^2\phi(r) + B^2\phi(r) = 0 \qquad \text{.....(2.34)}$$

These functions vanish at the outer boundary of the reactor, thus comprising a complete set of eigenfunctions ϕ_ν and corresponding eigenvalues B_ν. Keepin[12], page 167, outlines an application of the 'harmonic method' to space-time kinetic behaviour in inhomogeneous reactor systems reference Garabedian[20]. This type of expansion leads to an infinite system of second order differential equations with an infinite number of unknowns which result from the substitution of the terms of the spatial eigenfunctions into the reactor kinetic equations. To obtain a solution the

expansion is considered up to n harmonies which results in a system of n coupled differential equations (there does arise the question of the truncation at the n'th mode.

Since there are n linear differential equations with constant coefficients the solutions should be of the form e^{wt} substitution of this leads to a characteristic equation whose roots are the values w. These roots, as in the point kinetic equations Keepin[12] are all negative except for the case of a critical reactor when one root is zero or in the case of a supercritical reactor where one of the roots is positive. This method is restricted to a one energy group treatment for systems where the geometry is simple and the slowing down of neutrons is uniform and no non-linear feedbacks exist.

Keepin[12] reports that a straightforward practical approach to non-separable space-time kinetics was suggested by Henry[21]. This method treated the neutron flux as a product $\phi(r, t)\ A(t)$ of a shape function $\phi\ (r, t)$, the time and space being non-separable and an amplitude function $A(t)$ of time alone. Once the shape function was determined $A(t)$ the amplitude function could be calculated using conventional kinetic equations. ρ, β^* and ℓ are given by integrals involving $\phi(r, t)$ and its adjoint. The method relies upon the fact that the flux shape adjusts to changing reactor conditions within a few prompt neutron lifetimes so that the instantaneous flux shape can be approximated by the asymptotic shape appropriate to the reactor conditions at a particular instant. This implies that $\phi(r, t)$ can be calculated at a time t or $t + \delta t$ using normal stationary flux calculation methods, these are then used to calculate ρ, β^* and ℓ. Thus a series of discrete

values of flux shape, ρ, β^* and ℓ at various times are calculated, the conventional kinetic equations could then be used to calculate A(t) leading to the product $\phi(r, t).A(t)$ being the desired approximation to the non-separable space-time behaviour of $\Phi(r, t)$.

The former method though not rigorous led to the use of analogue computers where the reactor was represented by a number of regions characterised by an average flux and an average temperature distribution. The reactivity was then calculated at each average temperature using the known flux shape for the region. Power series were then found for the flux levels and reactivity in terms of the region average temperature.

The author in the past worked on a preliminary three-dimensional digital computer model named STAB which effectively split the reactor core into a number of regions, each region being represented by a point so that a three-dimensional dot matrix represented the reactor core. Point kinetic and temperature equations with region averaged properties are applied to each point in the core model. Care had to be exercised at the boundaries of each region to ensure continuity of the various parameters. The whole study was carried out on an IBM 7090 digital computer.

The latter comments were included to highlight the importance of space-time kinetics for large reactors and the use of computer simulations and the specification of suitable spatial models.

A book covering many of the recently developed theories of space-time nuclear kinetics has been written by Stacey[22]. It emphasises the basic theory and discusses various computational methods of solution ranging from modal and nodal approaches to

variational techniques and their application to the development of space-time synthesis approximations. The work also includes numerous references to recent work in the field.

It is of interest to briefly review several recent contributions to the study of space-time kinetics using oscillators.

Loewe[23] applied two group reactor kinetic equations to analyse space dependent effects due to forced oscillations from a reactivity absorber. A digital computer program called SDTF was written to study the case of a symmetrical slab geometry. This program was used to investigate two basic reactors, one using natural uranium heavy water moderated and reflected and the other enriched uranium light water moderated and reflected. The reactors were investigated under conditions of no temperature-reactivity feedback. These reactors only served as examples and were not intended to be typical. The computer data shows that when the detector and oscillator are close together there is a resonanace in phase angle versus frequency at very high frequencies and that for the cases examined the location in the resonance occurs at a frequency determined by the neutron lifetime. The author noted that the space dependent effects seemed to be relatively insensitive to core structure, core parameter and to transport effects as permitted by the telegrapher's equation.

A subsequent paper by Saji[24] distinguishes itself from the former and related papers in the sense that a time-dependent flux constructed from the various space modes is explicitly obtained for a forced oscillation thus enabling one to discuss neutron wave propagation in the time domain. The work clarifies some of the ambiguities that arise such as the rate of convergence of the

modal expansion, the effect of delayed neutrons on the excitation of higher space modes and the physical reasons why higher space modes are excited at higher frequencies. The method developed was applied to the analysis of the NORA reactor for which the zero power space dependent reactor transfer function had been determined by Haugset[25].

The author concludes that space dependency is unavoidable if the input frequency is higher than $\frac{1}{10}$ of the eigenvalues of the first higher space mode and that in this region the frequency approaches the eigenvalues of several higher space modes. Additional space modes are excited corresponding to the increase of frequency. The influence of higher space modes is expected to die out when the frequency is lowered.

In these studies the oscillator was placed in the centre of the core and the detector placed at successive increased radii, similar to the actual experimental work carried out on the NORA reactor by Hansson[26].

This paper also pointed out the poor agreement between predicted data and experimental data when the oscillator and detector were close together and attributes it to local heterogeneous effects.

Reference is made to a paper by Cohn[27] which develops a method by which static techniques can be used to calculate source transfer functions in a multi-group, multi-dimensional approximation. The flux is resolved into steady and fluctuating components, the time dependent neutron equations being satisfied by the fluctuating part alone. If the external source and the flux response are assumed sinusoidal the original time dependent equations transform

into a set of complex equations dependent upon space and frequency but independent of time. The equation can be separated into real and imaginary parts and the resulting equations can be solved using static techniques to yield real and imaginary components of the complex flux thus giving gain and phase shift as a function of a particular frequency. It is interesting to note that the CRAM [8] code was applied to the problem, this code was in fact used in the design of the oscillator for the present reported experiments. The CRAM [8] code was used to obtain the space dependent gain and phase shift for the afore-mentioned NORA reactor with a good level of agreement. The author's motivation for using CRAM was to demonstrate the use of an existing code to calculate transfer functions.

A final reference is made to a Ph.D. thesis by Kylstra[28] which investigated the spatially dependent transfer function of nuclear systems using cross correlation methods. This study utilised the time-dependent Fermi age and diffusion theories for a single region isotropic homogeneous medium. The fluctuation of the thermal density at any point in an assembly was related to the variation of fast neutron source intensity.

Theoretical curves were calculated for both multiplying and non-multiplying media and compared with a lumped parameter transfer function.

The results indicated that the lumped parameter model predicts the correct behaviour of the nuclear system only if the output detector was located a specific distance from the source, location of the detector did not give accurate results using a lumped parameter model.

The author performed experiments on light and heavy water assemblies to measure the spatially dependent transfer function between two detectors. The input to the system was provided by a neutron generator switched on and off in a pseudo random manner.

The transfer function was obtained using cross correlation techniques, i.e. computing the ratio of the cross power spectra for two different runs with one of the detectors being moved for the second run. This method eliminates the effects of source spectra and of the measuring system.

A comparison of experimental and theoretical transfer functions produced no conclusive evidence as to the validity of the theoretical model. It was claimed that the disagreement was mainly due to a reflection of neutrons from the surroundings, that the light water experiment should have accounted for a distributed source rather than a point source and that the small size of the heavy water system plus its nearness to other structures contributed to the disagreement.

A survey of some recent work in the field of non-separable space and time reactor kinetics was included in this section to demonstrate both the need for and varied interest in the subject.

Limitations were placed upon the actual experiments carried out in CONSORT. It was not possible to locate the detector relative to the oscillator at different separation distances within the actual core. Permission was given for a second access tube to be inserted on the 270° face of the core, see Fig. 5 Chapter 3. By using the fact that the detector and oscillator

could then be positioned at different vertical positions relative to each other it was hoped that a spatial dependency, if any, could be investigated for CONSORT. Fig. 25 Chapter 4 shows the relative position of the oscillator and detector used in the series of experiments.

CHAPTER 3

Experimental and Equipment Details

The experimental equipment, including the University of London Reactor Consort (U.L.R.) and the oscillator/reactor/detector systems studied, are described in this chapter. Details of the measuring system and calibration procedures undertaken are included in the description.

The series of experiments described range from preliminary experiments to predict and measure the maximum permissable reactivity perturbation to the design and construction of the oscillator and its use in the kinetic experiments.

During the experiments observations were made of the conventional reactor instrumentation wherever appropriate and possible so that comparisons could be made between the readings and those made on the specific experimental instruments.

3.1. The University of London Reactor Consort (U.L.R.)[29]

The reactor is based upon the well known swimming pool type, being moderated, reflected, cooled and partially shielded by purified light water. It combines the principal advantages of the swimming pool and enclosed-tank types of reactor by providing the accessibility and ease of fuel handling of the former while retaining the compact layout of the latter. It has the good safety features of small excess reactivity with a compact core and a negative temperature coefficient.

The core is approximately a 0.6 metre cube positioned in an open topped cylindrical aluminium vessel containing purified light water. Surrounding the core is an octagonal concrete biological shield. Instrument tubes, beam tubes, a thermal column and large area irradiation facilities penetrate the shield, the core being positioned at the centre of these facilities. At the centre of the core and on the centre of the 270° core face are two aluminium tubes, internal diameter 27 mm. which are available for 'in-core' experiments, (see Fig. 5).

A top platform mounted across the entire shield provides access for fuel handling, maintenance and experimentation. The water shield in the vertical direction is supplemented by concrete filled trolleys which cover the reactor vessel.

The core is made up of U.K.A.E.A. standard M.T.R. type fuel elements. A 300 mC Americium-beryllium neutron source emitting 7.5×10^{5} n/sec is secured in a pocket fixed to the side of the centre tube at mid-core height.

The reactivity of the reactor is varied by the vertical movement of the blade type absorbers (control rods) A, B and F (Fig. 5) where A and B are coarse rods controlling 1.5% of reactivity each and F is the fine rod controlling 0.5% of reactivity. There is, in addition, a safety rod, S, normally held in the 'up' position. Each rod has a total distance of travel of 61 cm., rod position being indicated on the control panel in the control room.

A BF_3 proportional counter feeding an accurate scaler is used for monitoring the source and the low power range (<0.5 watts). An RC6EB ionisation chamber is used to cover the remainder of the power range to 100 KW, this forms part of a

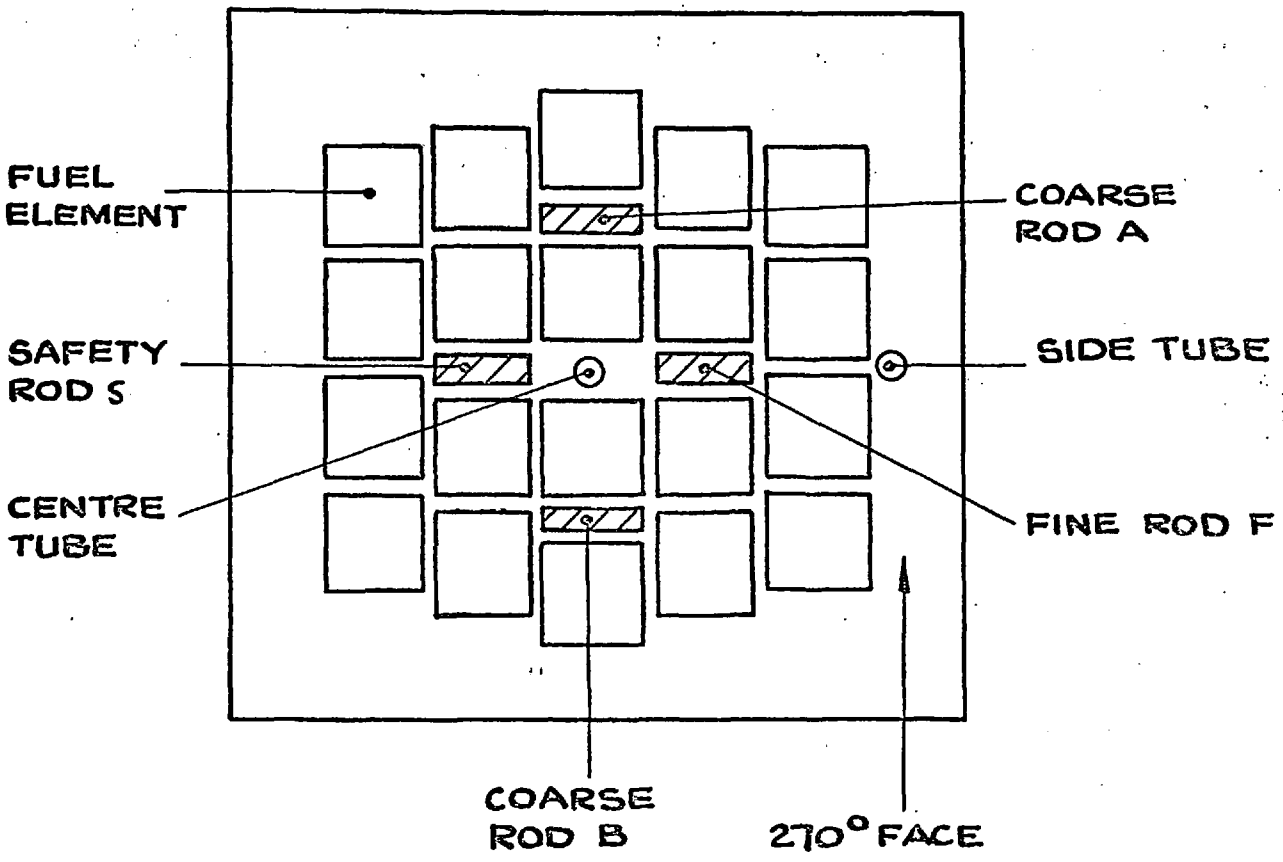

FIG.5: DIAGRAM OF CORE PLAN VIEW INDICATING CONTROL RODS AND ACCESS TUBES.

logarithmic channel. The two instruments have an overlap range (approximately 10 mW to 1 W). There are three other channels of instrumentation, one a linear DC and two shut down channels using ion chambers.

When operating at full power, 100 KW, a thermal neutron flux ϕ_n of 10^{12} n/cm/sec is present at the centre of the core accompanied by a gamma flux ϕ_γ of 10^7 R/hr (composed of prompt gammas during operation and delayed gammas from the decay of fission products). Measurements have indicated that this gamma flux falls to approximately 10^4 R/hr fifteen hours after shut down from a normal 8 hour shift operation at full power. The operational history of the reactor shows that there is a steady build up of fission products, since due to its experimental role, the core is only partially dismantled during a prolonged shut down period the core is very rarely free from gamma background.

More general details of the University reactor are given in Appendix 1.

It is interesting to note, at this stage, that although the University Reactor was designed for research experimentation and as an irradiation facility, some quite difficult access problems were encountered when the design of an in-core oscillator was undertaken, particularly when operation at full power was considered for future experimentation. This would entail running the reactor with the top biloogical shield closed making access more difficult. These points will become more apparent in the succeeding sections.

3.2. Neutron Detectors

Standard 'off the shelf' detectors supplied by 20th Century Electronics Ltd., England were used during the experiments. These detectors had not been specifically optimised for noise measurements in the presence of a gamma background though they were used for the noise measurements conducted in the second series of experiments. The specific detectors used were:

(1) P7/22, B^{10} coated pulse counter, stainless steel construction.

(2) 12EB40, BF_3 (filled) proportional counter, copper construction.

(3) RC6EB, B^{10} coated ionisation chamber.

Their neutronic and gamma sensitivities are tabulated in Fig. 6 and compared to those used in Roux's[30] study of optimised chambers.

The RC6EB having a diameter of 8.89 cm. could not be used either in the reactor core or the containment vessel.

Though small enough to be used in the core or the containment vessel the P7/22 could not be used in the centre of the core, due to its high absorption the core could not then be made critical.

The 12EB40 (copper construction) could be used in the core under critical operation though it was not designed specifically for use in the high fluxes or for prolonged periods of irradiation.

Two additional chambers, suitable for high flux long irradiation measurements, were ordered from 20th Century but were not available for any experimentation.

3.3. Design of the Sinusoidal Reactivity Absorber

Preliminary discussions with the reactor manager and the operating staff resulted in a decision concerning the permissible

	RC6EB	RC7EB	P7/22 stainless steel	12EB40	RSN76A[30]	RSN76A[30] (modified)
Neutron Sensitivity S_n ($\times 10^{-14}$ amp per nv)	2.0	2.75	0.9	8.0	7.2	2.7
Gamma Sensitivity S ($\times 10^{-11}$ amp per R/hr)	0.72	0.54	3.1	2.4	3.3	0.65

Fig. 6. Neutron and Gamma Sensitivities of Detectors used in Oscillator and Noise Experiments

reactivity worth of the oscillator. It was agreed that the mechanism required to oscillate the reactivity would involve a static and an oscillatory reactivity worth. The maximum reactivity investment in the total mechanism should not exceed 0.12% and the fluctuation range 0.06 to 0.12.%

It was agreed that a series of preliminary tests be carried out to determine the area of Cadmium (Cd) absorber that would be required to achieve the previous reactivity oscillation. To prevent the accidental release of reactivity the equipment had to be designed so as to prevent the accidental removal of all the mechanisms when the reactor was operating. This is discussed in more detail in succeeding sections of this chapter.

3.3(1). Preliminary Tests

3.3(1)(i). A digital computer program to solve the multi-group diffusion equations was available within the Nuclear Power Section. This program CRAM[8] was developed by the U.K.A.E.A. The program was used to obtain an estimate of the effect on reactivity of placing an absorber near the outer surface of the University reactor core. The CRAM program is a 2-dimensional multi-group finite difference calculation to solve the diffusion equation. The 3rd dimension is represented by an infinite prism. The program operates on a grid of mesh points.

A one dimensional CRAM run was made to determine an effective height for the core (allowing for the water above and below the core, the core support plate and the top and bottom of the fuel elements). This was to be used in an axial buckling factor necessary for use when a 2-dimensional run was made since

having infinity on the axial direction would infer no leakage. The axial buckling derived from the 1-dimensional run would compensate for the no leakage condition for a normal 2-dimensional run.

An effective core height of 72 cm. was obtained from the first computer run.

The second computer run was made assuming that an absorber 10 cm. wide by 72 cm. high and 0.6 cm. thick was placed 0.6 cm. away from one face of the reactor core. The resulting value of k was 1.016643.

A third computer run was made differing from the second run in that no absorber was placed near the core the resulting value of k was 1.024781. The insertion of the absorber caused the reactivity to change by 0.008138.

Bearing in mind the assumptions that were made in the input data to the program (i.e. axial buckling, radial flux distribution etc.) it was decided to treat the results obtained as an absorber area of 720 sq.cm. corresponding to a 0.0082 change in k with an error band lying between $\pm$ 5 to $\pm$ 10%.

Due to the upper levels placed upon the oscillator reactivity for reactor safety it was necessary to calculate the absorber area that would correspond to a change in reactivity of .06% in k or 0.0006 in k. This is an order of magnitude down from the value obtained for the second of the computer runs, thus the area of absorber could be assumed down by a similar order of magnitude. For the same width of absorber as in the second computer run i.e. 10 cm. the height of the new absorber to give 0.0006 in k would be approximately 6.0 cm.

Assuming a cosine flux distribution in the axial direction this smaller area would lie in the region of the peak axial flux rather than distributed as a 10 cm. strip up the entire height of the core. To accommodate this a weighting factor relating ϕmax^2 to $\phi mean^2$ was used:

$$\frac{(\phi max)^2}{(\phi mean)^2} = \frac{1}{0.5} \qquad \ldots\ldots(3.1)$$

Using this weighting factor:

$$\frac{0.0082 \cdot (x)}{720} \cdot \frac{1}{0.5} = 0.0006$$

Where 0.0082 is the reactivity change due to an absorber area of 720 cm., 0.0006 is the permitted change in k and x is the unknown area.

$\therefore$ $x = 26.34$ sq.cm.

The value used being 26 $\pm$ 10% sq.cm.

3.3(1)(ii). Experimental tests with Cadmium foils in the reactor

To substantiate the calculations it was deemed necessary to carry out tests placing various areas of Cadmium absorber at different positions in the core and near one outer face.

The latter tests could only be carried out by the insertion of an additional aluminium tube mounted vertically in the water and close to the 270° core face.

A tube of similar dimensions to the existing centre tube was made together with especially designed locating and clamping devices. This tube had to be the subject of careful testing since the flooding of a tube can cause safety hazards. This tube is now a permanent addition to the reactor as described earlier in

this chapter. See Fig. 7 for details of tubes and experimental configuration.

The various areas of Cd to be used were taped in turn to one of three positions for a length of aluminium rod. One position corresponding to the centre of the core the other two being equidistant above and below the centre position. See Fig. 7.

The procedure adopted was to balance the reactor with the cadmium foil in position, then to remove the rod carrying the foil as quickly as possible from the core, the corresponding rise in power against time was measured on the control room instruments. The corresponding reactivity was obtained from a stable doubling time curve versus reactivity supplied by the reactor operating staff. See Fig. 7(a).

The tests were repeated for various foils in the various positions. Graphs of reactivity versus cadmium surface area are given on Fig. 8.

These results must be treated as a design guide, there was always the possibility that the exact orientation of the Cd foil on the aluminium rod relative to the core could vary between tests. To achieve a central registration in the tube loose bearing guides were used. In addition the speed of removal from the core was variable though it was removed by an experienced member of the reactor operating staff. The doubling time was measured over as wide a range as was permissible for safe reactor operation.

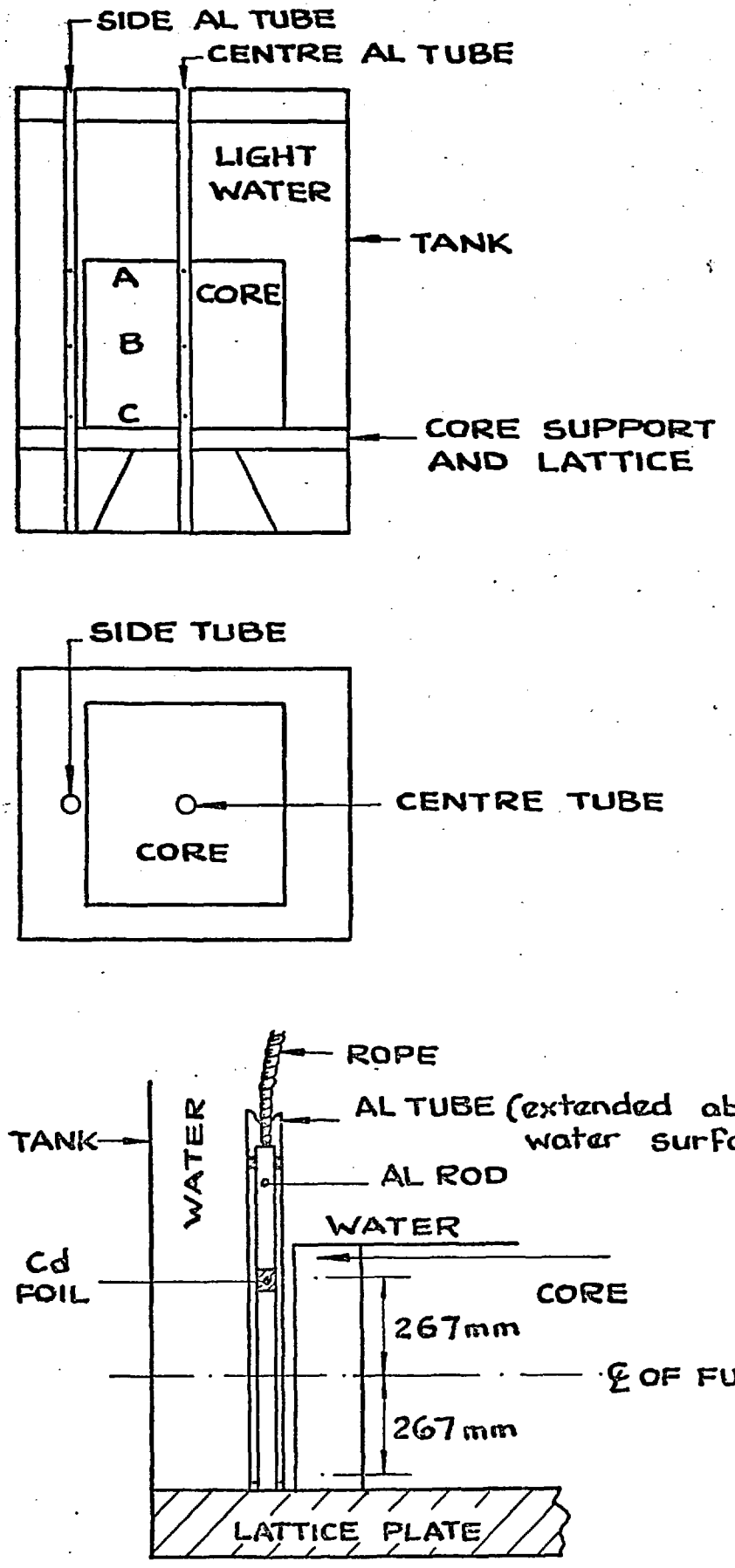

FIG.7: SCHEMATIC SHOWING POSITIONS OF ACCESS TUBES, DETAILS OF ACTUAL Cd FOIL HOLDER AND RELATIVE POSITIONS.

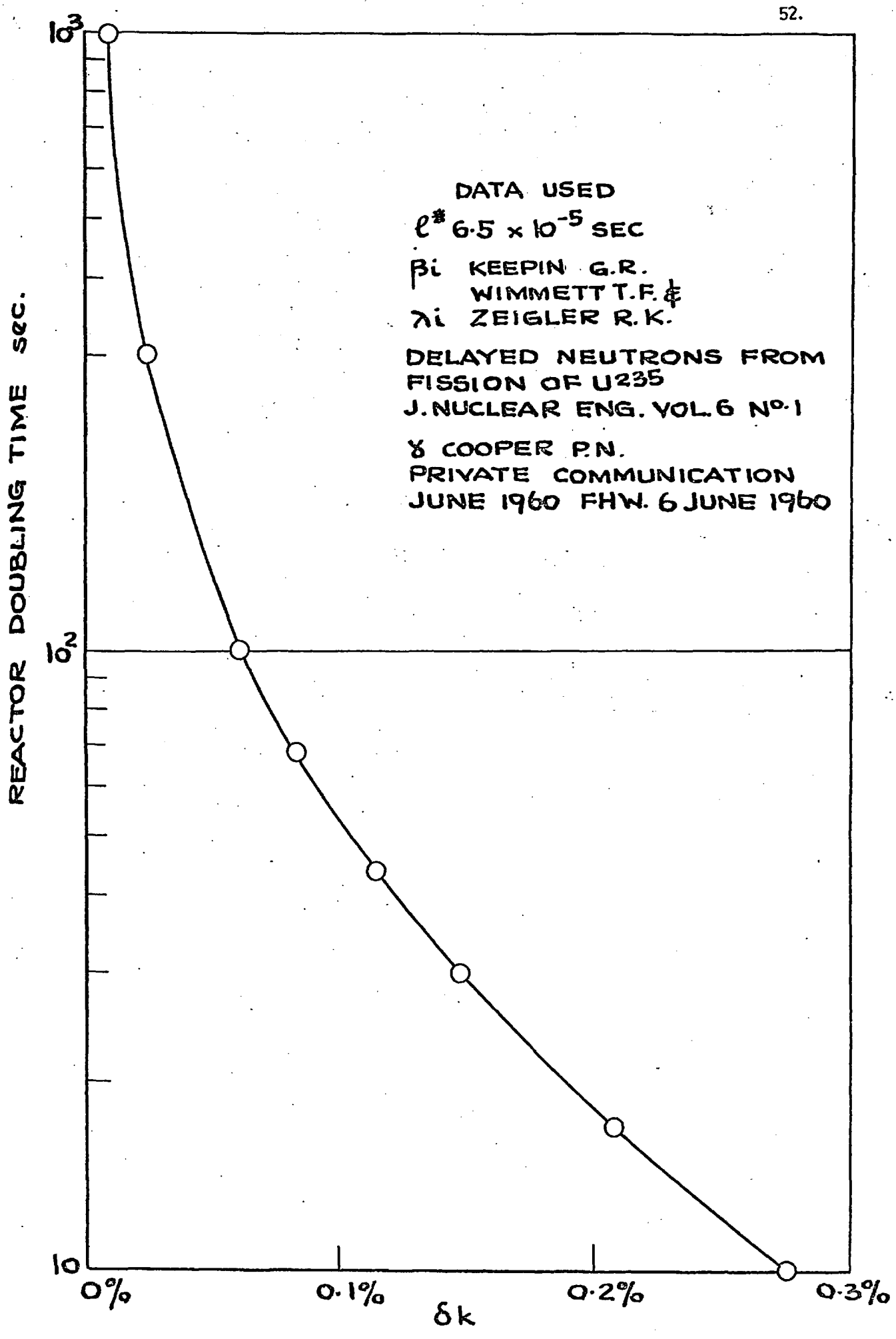

FIG. 7(a) : STABLE DOUBLING TIME vs REACTIVITY

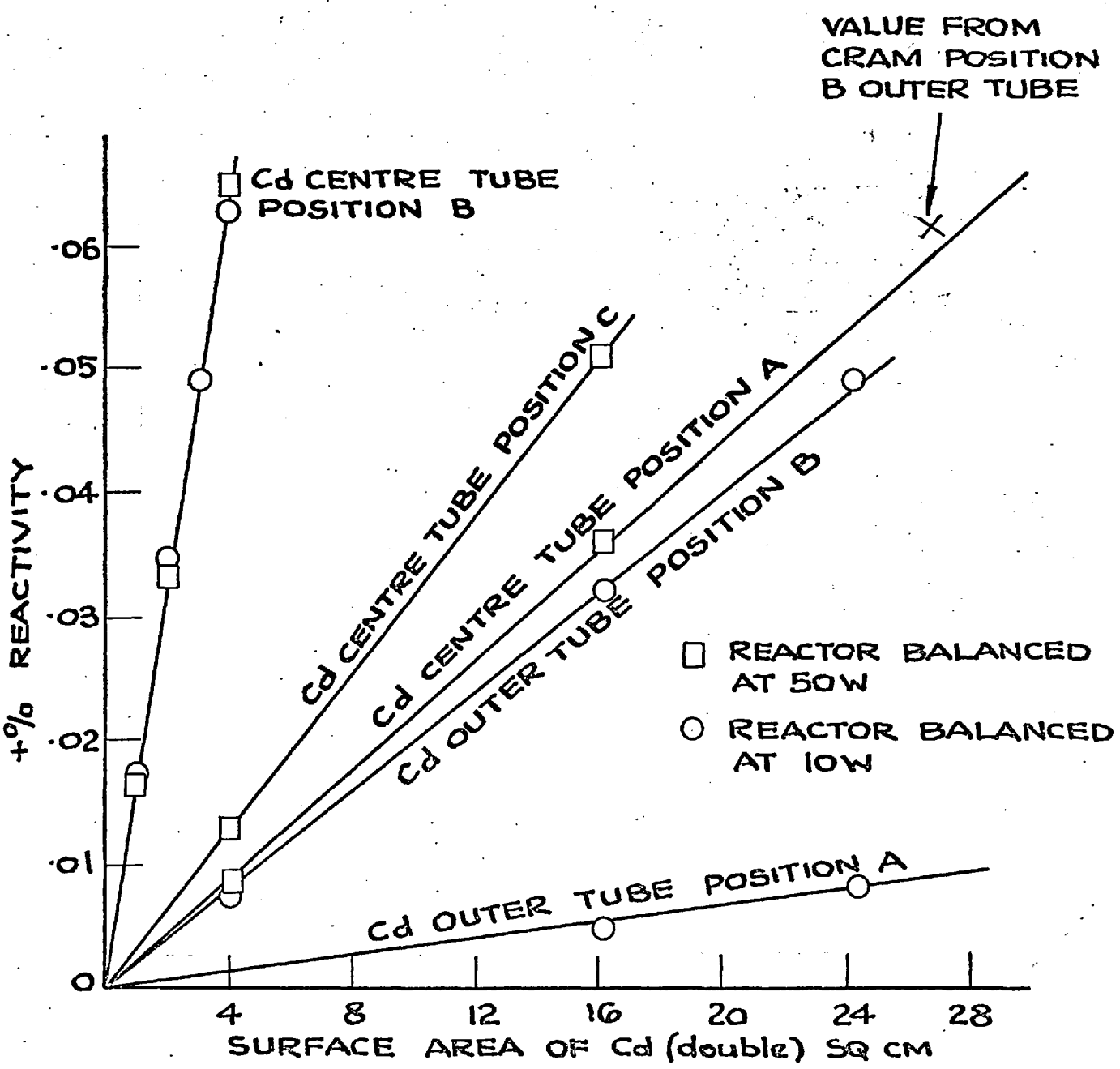

FIG. 8 : REACTIVITY vs Cd AREAS FOR DIFFERENT CORE POSITIONS .

The value of reactivity and area predicted by the CRAM run is indicated on Fig. 8.

Extrapolating the curve for various areas of Cadmium foil placed at the centre of the outer tube gives a value of 30.4 sq. cm. for a reactivity change of 0.06% which compares with the CRAM value of 26.34 sq.cm. for the same reactivity change.

Fig. 8 shows that the maximum area of Cadmium permitted for the oscillator will be determined by its reactivity effect when placed in the centre of the core in the centre access tube.

After discussions with the reactor staff and a comparison with tests carried out independently by the reactor staff a factor of 0.016% change in reactivity per sq.cm. for Cadmium placed at the centre of the core was a design criterion for the oscillator.

3.3(2) Design, Construction and Testing of the Reactivity Oscillator

3.3(2)(1) Design Parameters

Certain basic design parameters were chosen based upon the results from previous tests and the computer calculated transfer function for a U^{235} reactor system, see Fig. 1 chapter 2 section 2.2(2).

(1) Maximum permissible reactivity variation 0.03% in k.

(2) Frequency range $10^{-2} \leq W \leq 10^{3}$ cps

(This includes the range of greatest practical interest[12]).

(3) Maximum external diameter of the oscillator and housing 25.4 mm.

This limit was imposed by the size of the core access tubes I.D. 27 mm.

A decision was made to utilise an electrical drive system, the motor chosen being a $\frac{1}{4}$ HP parvalux shunt wound d.c. motor.

Difficulties were envisaged with the actual drive mechanism since the oscillator would be operating in various positions at the bottom of a 27 mm. internal diameter aluminium tube approximately 305 - 380 mm. from the top of the reactor containment vessel. Since the oscillator would eventually be used for experiments at full power the drive mechanism had also to be capable of operating with the top concrete biological shield closed.

3.3(2)(2) Oscillator Drive System

A gear box plus a Bowden Cable drive was first considered but was rejected due to the following reasons:

(1) It was not possible to get a single gear box to cover the entire speed range.

(2) The problems involved in considering the backlash due to the gears.

(3) The hysteresis of the Bowden Cable complicated by a restriction upon the sharpest bend permitted for a Bowden Cable sufficiently strong enough to drive the total assembly.

Points (1) and (2) could have been overcome by the purchase of an expensive variable speed high quality gear box.

It is appropriate at this stage to point out that one of the aims of this study was to provide a low cost, reliable and easy method to operate a student experiment.

Tests were carried out on toothed belts and pulleys. As a result of these tests a system of toothed belts and pulleys was chosen the use of this type of drive had the advantage that

backlash was almost non-existent, the belts were guaranteed not to stretch at higher speeds and loads than they would ever be subjected to in this study. In addition the pulleys and belts were of such dimensions that they could fit beneath the reactor top shield for eventual high power experiments.

A schematic of the drive system is shown on Fig. 9 and a photograph of the actual system is shown on Fig. 10.

The intermediate belt drive shown on the schematic layout Fig. 9 and photograph Fig. 10 is supported by a bracket clamped to the upper edge of the reactor containment tank. The support clamp is movable and allows the intermediate pulley support mechanism to pivot. This latter movement is necessary when belts and pulleys were changed to achieve the necessary speed range.

3.3(2)(3) Drive Support System to be inserted in Reactor Access Tubes

At this point in the design process an assessment was made of the type of support system to be placed within the reactor access tubes.

The clearance between the top of the reactor and the roof of the reactor building prevented a one piece mechanism from being used. Whatever design was carried out it would have to be sectionalised. Since the experiments were to be carried out at different heights relative to the core in both reactor access tubes the use of a sectional support and drive system would facilitate the location of the oscillator. Fig. 11 is a positional schematic for the oscillator detector system. e.g. On Fig. 11 one test would be carried out with the oscillator at a position of maximum flux B' and the detector at position B, the position would then be reversed.

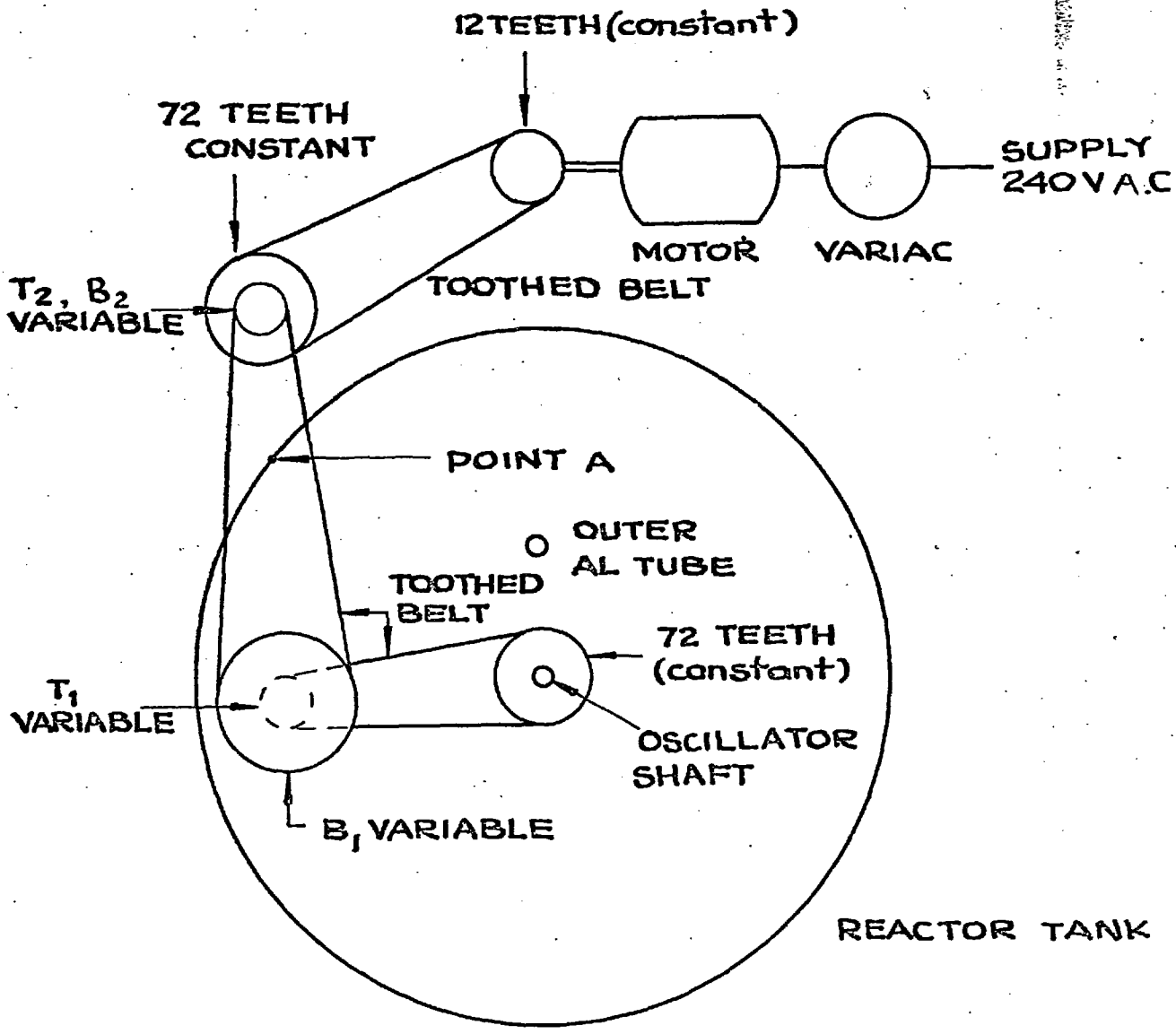

T_2, T_1, B_1 ARE PULLEYS THAT ARE CHANGED TO GIVE FULL SPEED RANGE.

FIG. 9: SCHEMATIC OF OSCILLATOR TOOTHED BELT DRIVE SYSTEM.

Fig. 10. Actual Belt and Pulley Drive System.

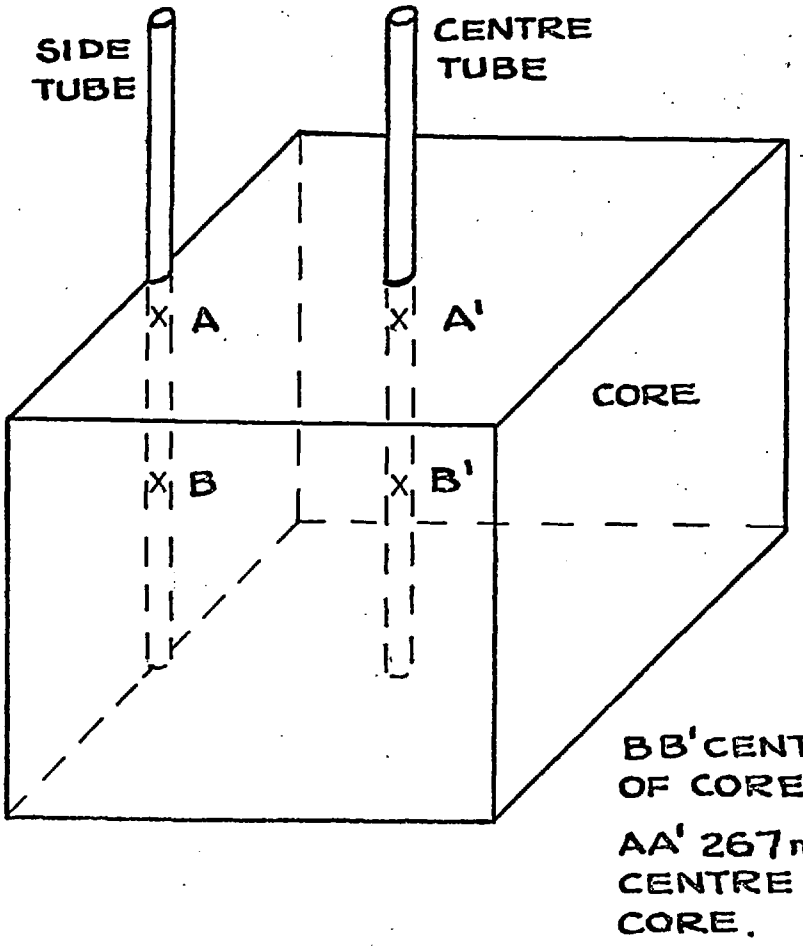

FIG. 11: SCHEMATIC OF OSCILLATOR / DETECTOR SYSTEM.

Bearing in mind the type of drive required from the electric motor a design was produced that basically consisted of a rotating shaft concentric with an outer tube, this outer tube to be a good fit in the existing centre and side reactor access tubes. Bearings would be placed at suitable distances between the outer stationary tube and the inner concentric rotating shaft. The materials to be used being reactor grade aluminium, stainless steel and nylon wherever appropriate. The system was designed to be sectional to facilitate its insertion into the two reactor access tubes. Each section would be joined together with a nylon coupling that would also act as a support guide between the outer tube and the access tube of the reactor. The outer tube could not be made too tight a fit in the reactor tube for reasons of insertion and removal especially since there was no guarantee as to the trueness of the bore of the existing reactor access tubes.

The details of the actual oscillator are discussed later in this section. At this stage in the design it is sufficient to note that it would consist of a rotating and stationary part in some form of window. Thus the outer stationary part of the drive assembly would be the location of the stationary part of the actual oscillator. This implied that the outer stationary drive assembly tube should remain stationary relative to the central rotating shaft and the reactor core. To achieve this it was necessary that the outer concentric tube be clamped securely to the top cruciform structure of the reactor vessel. This would, in addition, prevent the removal of the total mechanism when the reactor was operating in a critical condition. Fig. 12 gives a schematic sketch of the reactor drive assembly. A fully detailed design drawing is given in Appendix 2.

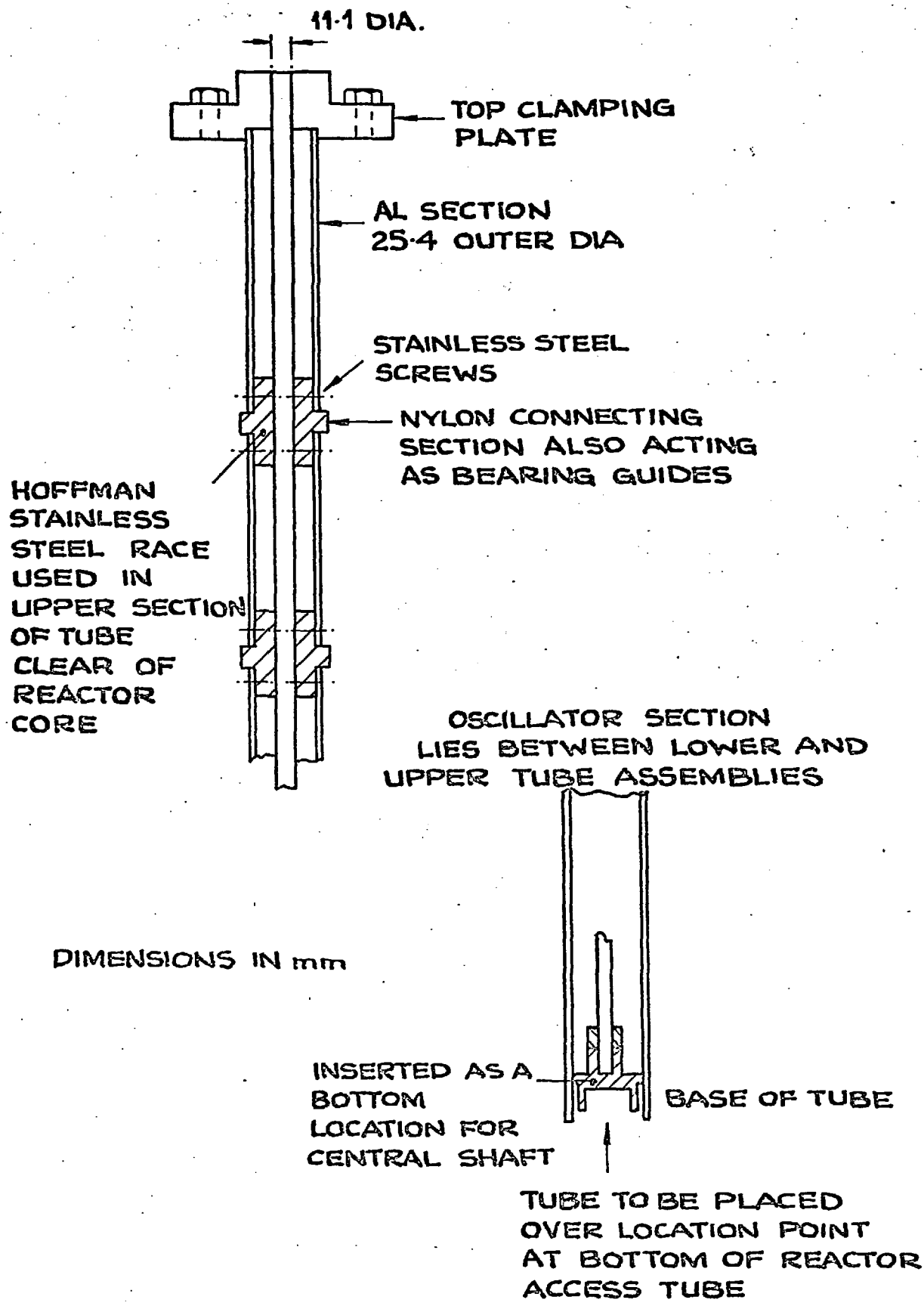

FIG. 12: SCHEMATIC OF TUBE DRIVE ASSEMBLY FOR OSCILLATOR.

Though the outer tube of the assembly was deemed rigid enough for the bottom to move relative to the top when the oscillator was rotating at maximum speed a location unit was placed at the bottom of the reactor access tubes. This consisted of a simple plug that had an expandable central section activated by turning thus forcing the device against the inside bore of the reactor access tube. Care had to be taken not to damage the tube internally.

3.3(2)(4) Oscillator Section Design

Assuming a maximum reactivity investment in the oscillator of 0.12% in k and the result from the preliminary reactivity experiments of 0.016% reactivity per sq.cm. for Cadmium absorber placed at the centre of the reactor core, the total area of

$$\text{Cadmium} = \frac{0.12}{0.016}$$

$$= 7.46 \text{ sq.cm.} \qquad \ldots.3.2$$

The maximum outer diameter of any assembly was 35.4 mm. being that of the outer drive tube.

The principle aim of the oscillator design was to achieve as pure a sine wave fluctuation in reactivity as was physically possible within the physical limits of the access space. Previous workers had recorded the presence of harmonics due to asymmetry of their sine wave oscillators[31, 32].

After various alternatives ranging from an eccentric rotor and stator to a rotating system using vanes it was decided to use a rotating inner cylinder, suitably shaped, passing a system of windows.

A system consisting of a complete sinusoidal shape of cadmium wrapped around a rotor with a stationary shield of cadmium extending for half the circumference of an outer stationary cylinder, i.e. stator, was considered. See Fig. 13(a). It was felt that this type of design could possibly present a different absorption effect due to self-shielding since the arrangement is not symmetrical.

The decision was made to have a double sine wave per revolution to reduce the asymmetry and self-shielding effect, see Fig. 13(b). One advantage of the two cycles per revolution was that the maximum speed of rotation of the total assembly would be reduced for a given upper frequency limit.

The detailed oscillator design is shown on the drawing in Appendix 2, its physical size being determined by the total area permitted of 7.46 sq.cm. and the physical dimensions of the reactor access tube, it was in fact constructed as another section to be inserted in the total reactor drive assembly.

The physical dimensions of the oscillator are given in the drawings shown in Appendix 2 but a brief resume is included at this point to explain the slight difference between the actual measurements used and the ones suggested from the preliminary experimental tests.

The outer tube or stator would be the 25.4 mm. O.D. aluminium drive tube the I.D. of this being 23.6 mm. The diameter of the inner rotor was chosen to be 22.2 mm. since it was felt that for the speeds concerned an annular gap of approximately 0.51 mm. was sufficient to avoid any fouling between rotor and stator.

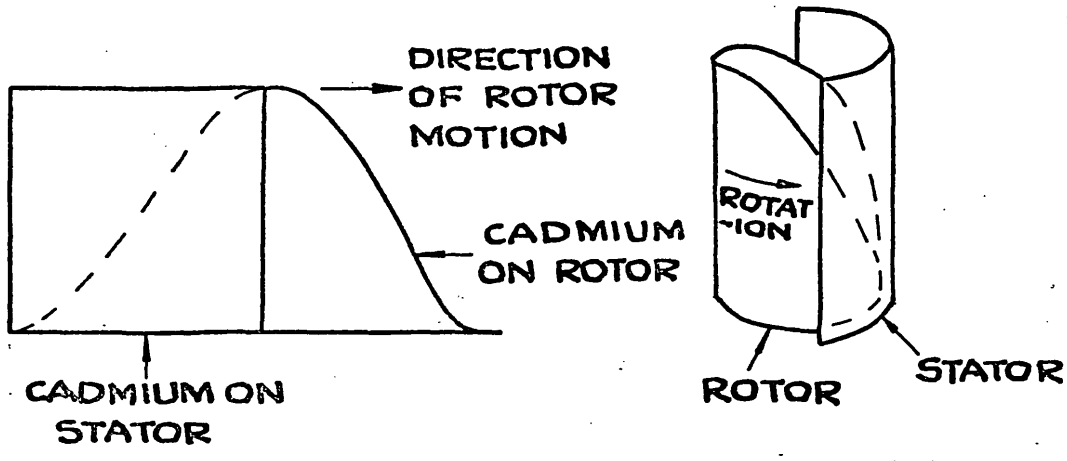

FIG 13.(a): SINGLE SINE WAVE OSCILLATOR.

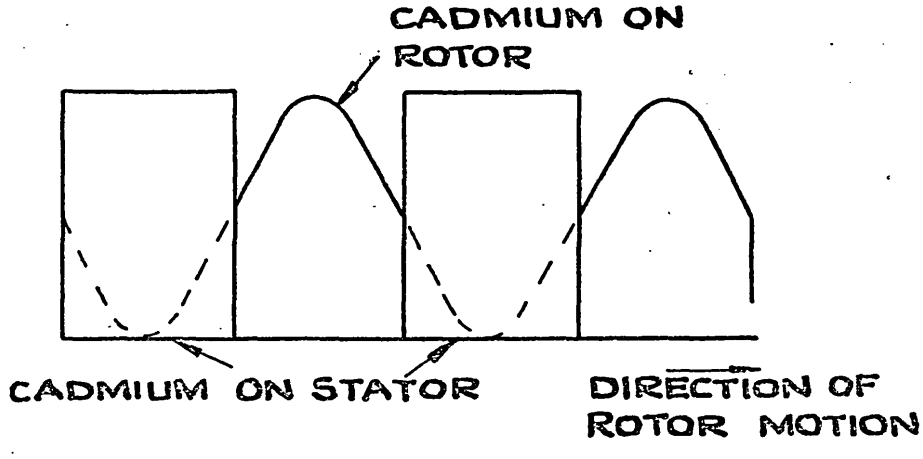

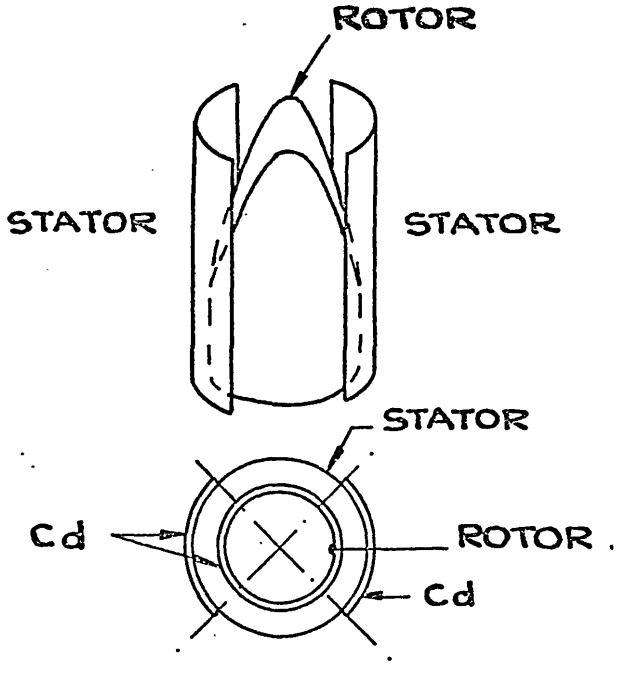

FIG. 13 (b): DOUBLE SINE WAVE OSCILLATOR.

Based upon the area of 7.46 sq.cm. of Cadmium predicted from the preliminary tests and assuming that at high speeds the rotor and stator of the oscillator would at the worst present a swept out continuous cylinder of absorber, the calculated height of sine wave was 10.80 mm. for a diameter of 22.2 mm. for the rotor.

At this stage some consideration was given to the task of actually cutting an accurate two cycle sine wave of cadmium. The final method chosen was to make a former of mild steel, see Fig. 14 for a schematic. This former was to have a 45^{o} slope machined across it, the cadmium was then swaged around the former or mandrill and then the cadmium was machined on a mill to match the former 45^{o} slope, the cadmium when opened would then be in the shape of a single sine wave. The process was repeated to obtain two sine waves.

There was allowance for a small band of cadmium to be left on the bottom of the sine wave since this would facilitate its alignment when it was placed upon the oscillator rotor.

The cadmium former used had a diameter of 11.1 mm. which when two sine waves were made together corresponded to a diameter of 22.2 mm.

The 45^{o} slope necessary to give the desired sine wave gave a sine wave of 11.1 mm. nominal height which was larger than the value of 10.8 mm. calculated from the preliminary reactivity tests. This difference was deemed acceptable from the point of view of the reactor operating staff.

The two sine waves were then checked on a travelling microscope to check their accuracy and found to be within the limits of assessment against calculated figures. This procedure

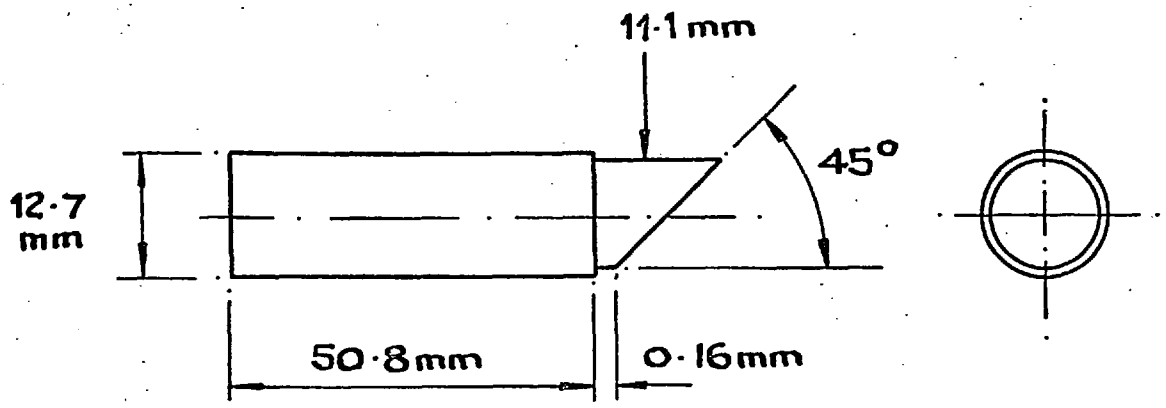

FIG. 14: CADMIUM FORMER.

was only adopted as an initial check since the final measurements had to be made when the oscillator was placed inside the reactor.

Whilst the overall in core assembly was being constructed tests were carried out on the drive system of belts and pulleys. These tests showed that for the drive spans considered there was excessive whip on the belt drives if the system was driven much greater than 3000 rpm measured at the oscillator drive shaft. For 2 cycles per revolution this corresponded to a frequency of 100 cps. For this value of frequency the reactor transfer function has satisfactorily tended to the upper asymptotic value (see Fig. 1, chapt. 2). Thus it was decided to limit the upper frequency to 100 cps hence the speed to approximately 3000 rpm. To cover the design frequency range 0.01 cps to 100 cps it was found necessary to change three of the pulleys and the position on the tank in the system twice to provide three overlapping ranges. This overlap was necessary so that any errors could be investigaged and normalised if necessary. The pulley arrangements and speed ranges are given in Fig. 15.

3.3(2)(5) Oscillator Input Trigger and Speed Measurement

To determine the input and output amplitude and phase relationship it was necessary to have some reference level and trigger.

Since the input amplitude of the oscillator would remain constant providing accurate measurements were taken in a static and dynamic mode, there would be no necessity to have a monitoring system for the input amplitude, especially since it is more common to normalise the transfer function for evaluation and use.

Fig. 15. Typical Pully Arrangements and their Appropriate Speed Ranges

See Fig. 9 for symbol references.

Motor shaft	12 teeth (constant)
Oscillator shaft	72 teeth (")
Position B_2 (on reactor tank)	72 teeth (")

Position T_2, T, B, having 12, 72 and 18 teeth respectively gives a speed range 2.78 to 85.7 r.p.m. for a variac setting of 100% and 0.31 to 9.5 r.p.m. with a variac setting of 10%.

Various other combinations of pulleys with different number of teeth and the use of an additional 2 to 1 gear box on the motor shaft covered the permitted frequency range.

Assuming a constant input reactivity amplitude, a light operated pulse system was developed that would trigger a pulse once every revolution of the pulley drive system on the oscillator drive shaft. A hole was drilled close to the periphery of the oscillator drive shaft and a light trigger system mounted either side. The photo transistor and its associated circuitry is shown on Fig. 16(b) together with a diagramatic sketch of the arrangement used in the experiments Fig. 16(a).

The size of hole in the pulley was of 0.5 a degree of angular rotation, this size being necessary to trigger a pulse over the entire speed range. This placed the accuracy of measurement within $\pm$ 0.5 degree though to allow for the response time of the photo transistor and its associated trigger circuitry this should read $\pm$ 0.5 degree $\pm$ 0.25 degree.

The circuit and arrangement proved reliable over the complete speed range utilised in the experiments.

The hole in the oscillator pulley was arranged mechanically to be in alignment with the mean position and start of a sine wave for the oscillator rotor so that a reference start position was available. The relative difference between the output wave form and the trigger pulse would then provide a measure of the phase difference between the reactivity input and the measured neutron flux output.

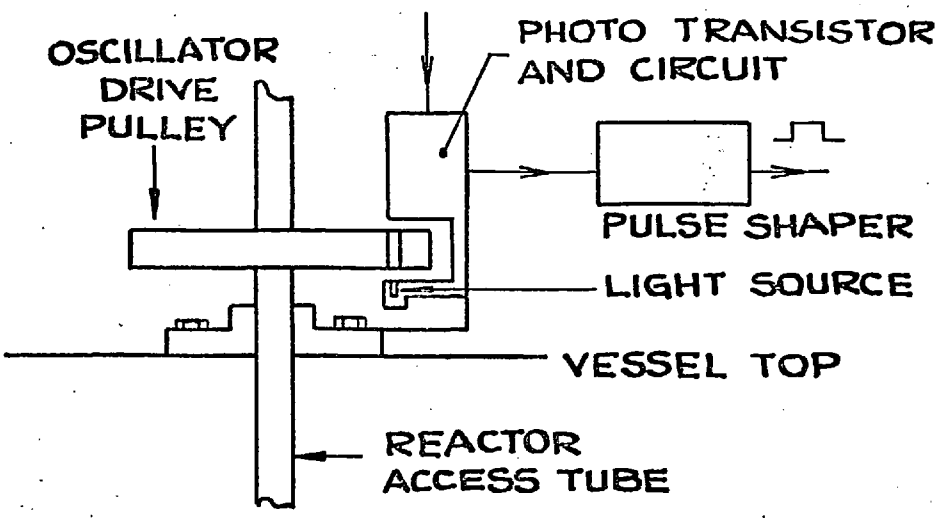

FIG. 16 (a): PULSER DIAGRAMATIC INSTALLATION.

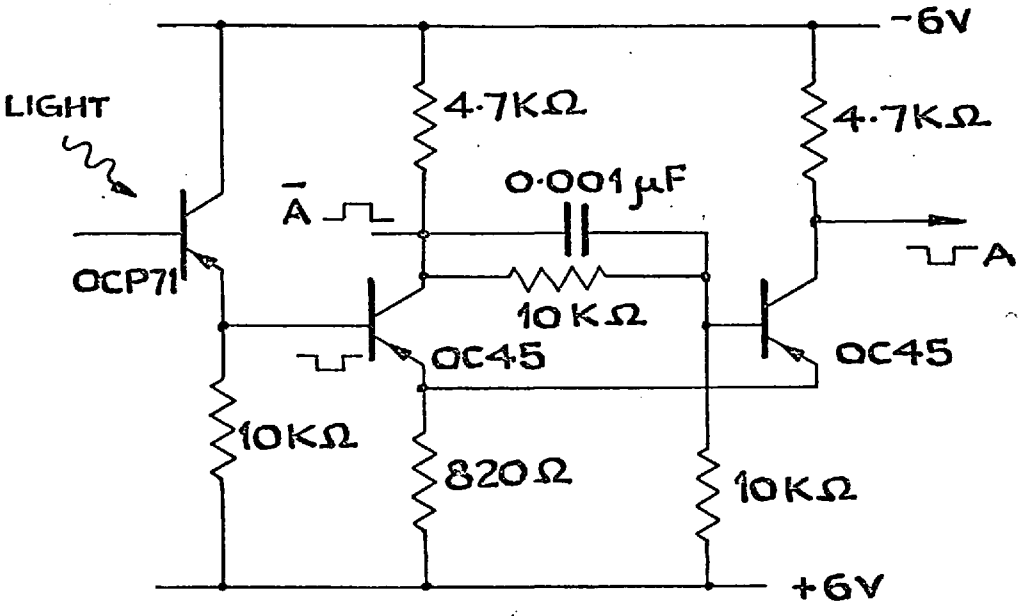

FIG. 16 (b): PHOTO TRANSISTOR CIRCUIT.

3.4. The Electronic Measuring System

A block diagram of the oscillator experiment is given in Fig. 17.

The detectors used were encased in polythene to shield the casing from the reactor structure in order to minimise any stray earth loop that might arise. The cable connecting the detectors to the amplifiers was of a low noise type, having a capacitance of 0.1 pF per mm. run. The weight of the chamber kept the cable taut when the chamber was lowered into the reactor and the position of the chamber relative to the core was measured by the cable. A safety line was also attached to the chamber for obvious reasons. All cables were kept as short as possible to minimise noise pick up.

The Kiethley amplifier was of low noise, high gain with a bandwidth flat from 0 to 100 cycles per second, this adequately covering the frequency range envisaged.

Both the Dana amplifiers are of low noise, variable gain and bandwidth type.

The pulse trigger channel utilised a standard Harwell 2000 series pulse shaper and a similar Dana amplifier to that used in the detector channel.

Both channel signals amplified by the Dana amplifiers were available for either on-line or off-line analysis.

A photograph of the equipment is given on Fig. 18.

3.4(1) Speed Measurement

During the actual experimental runs use was made of a clock pulse generator and a standard 2000 series counter. The

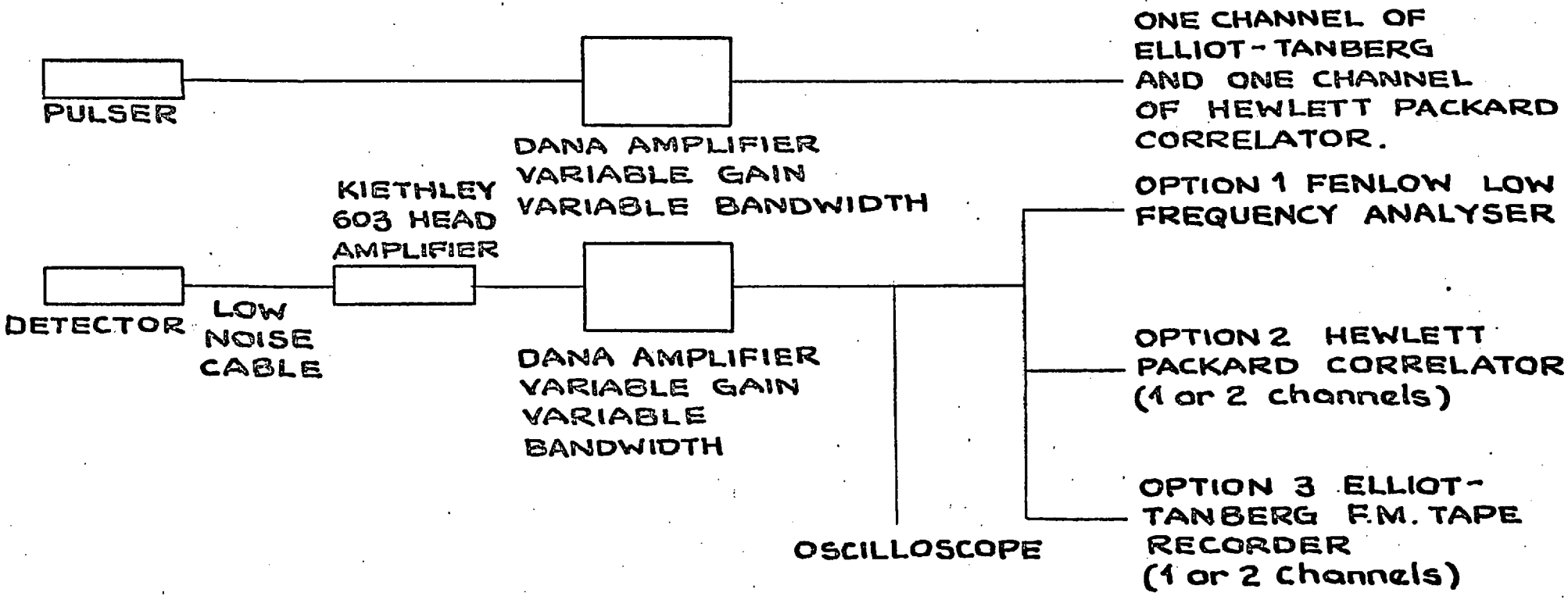

FIG. 17: OSCILLATOR DATA ACQUISITION SYSTEM.

Fig. 18. Electronic Measuring System.

pulse from the pulser on the oscillator drive pulley was used to trigger this count system, the resulting cycle time being indicated digitally.

At the same time a stop watch check was kept on the actual oscillator pulley rotation, this being of particular use when very slow rotations were being undertaken, i.e. of the order of several minutes per revolution.

The speed of the actual drive motor was checked both on and off load using a standard tacho-generator.

It was decided that since the results were to be finally analysed using an IBM 1800 data acquisition and reduction system the final frequency would be obtained by using a digital clock triggered off by the pulse obtained from the oscillator drive shaft. Using this method would mean that both the phase and frequency measurements were made from the one reference point.

3.5. Calibration Methods

Since the 12EB40 counter was designed for use in a pulse mode its operation as an ionisation chamber was investigated with the equipment shown in Fig. 19.

The chamber was placed in one of the beam tubes situated in the reactor graphite thermal column where it was exposed to a neutron flux of $\simeq 10^6$ nv. The resulting saturation curve for the chamber is shown on Fig. 20. The detector was then calibrated for its neutron (S_n) and gamma (S_γ) sensitivities given in table Fig. 6 which includes some of the results from Roux's[30] study of optimised chambers. Cross calibration against a standard gamma sensitive ionisation chamber (I G 1) placed near a strong Cobalt^{60}

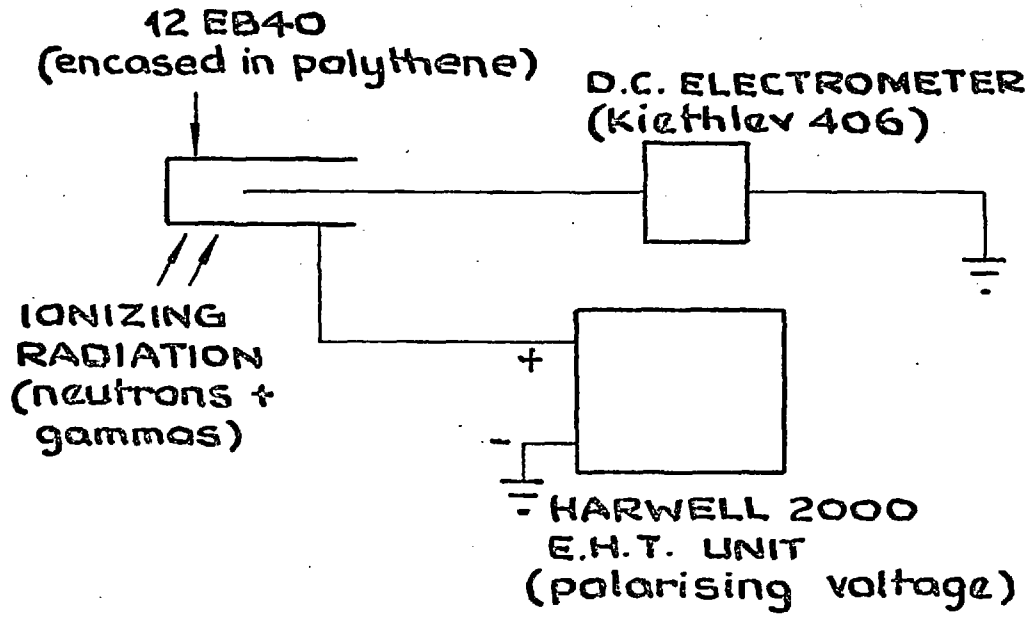

FIG. 19: CONTINOUS CURRENT OPERATION OF 12EB40 COUNTER.

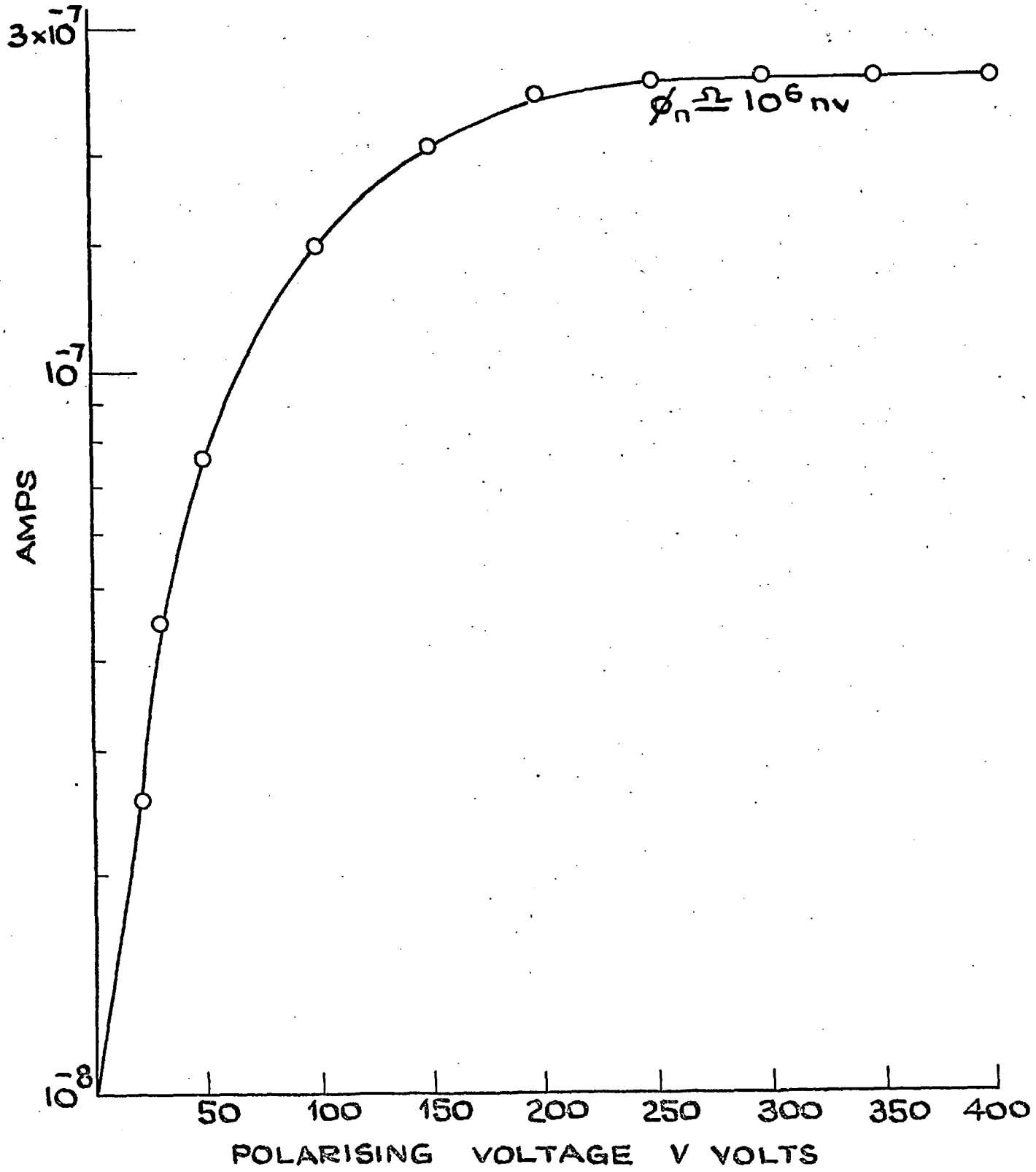

FIG. 20: PLOT OF IONISATION CURRENT VS POLARISING VOLTAGE FOR 12 EB40 PULSE COUNTER OPERATING IN CONTINUOUS CURRENT MODE.

source gave values of S_γ and exposure to a thermal neutron flux in the reactor (where $\phi \gg \phi_\gamma$) and cross-calibration with an RC6EB chamber gave values of S_n. Errors of $\pm$ 10% were expected due to local flux depression effects.

The frequency response of the Kiethley amplifier was checked and found to be correct to its specified bandwidth. This amplifier proved to be the limiting bandwidth factor in the total measuring system. Fig. 17, checked on the frequency analyser option (1) Fig. 17.

Subsequent noise analysis was carried out later in the study using a modified Winfrith head amplifier designed by Fowler[33].

The Dana amplifiers, the Elliott-Tanberg F.M. tape recorder, the Fenlow Low Frequency Spectrum Analyser and the Hewlett-Packard Correlator were tested for bandwidth and noise and found to be within specification.

Inaccuracies due to electronic equipment have, of course, to be expected. These range from noise pick up and generation (in cables and amplifiers) to variations in gain, bandwidth and distortion due to magnetic tape flutter distortion and speed variations.

Based upon the specifications of the various instruments and experience an error band of $\pm$ 2$\frac{1}{2}$% would seem reasonable.

CHAPTER 4

Experimental Tests, Results and Analysis

4.1. Static Tests

It was necessary that the total reactivity invested in the mechanism should be determined and its variation as a function of angular position, the latter determination being absolutely necessary so that both the accuracy of the designed sine wave variation and the possible presence of harmonics could be determined.

Accurate measurements of reactivity versus control rod position had been made previously and a rod calibration curve produced as shown in Fig. 21 (this had been obtained using doubling time techniques).

4.1(1) Measuring System

4.1(1)(1) Rod Movement

It was decided to make measurements of a vernier type on the actual rod driving tape. This was possible since the drive tape moves in horizontal grooves and a permanent reference could be made on the reactor vessel structure. Using this technique a measurement accuracy of $\pm$ 0.25 mm. was possible.

4.1(1)(2) Angular Rotation of Oscillator

The large pulley on the oscillator drive shaft was accurately marked in one degree steps and a correspondingly marked small arc of 15 degree pitch was mounted on the stationary part of the oscillator assembly, again a vernier type measurement being possible. Before measurements of angular rotation could be made an alignment test was necessary so that a zero start position

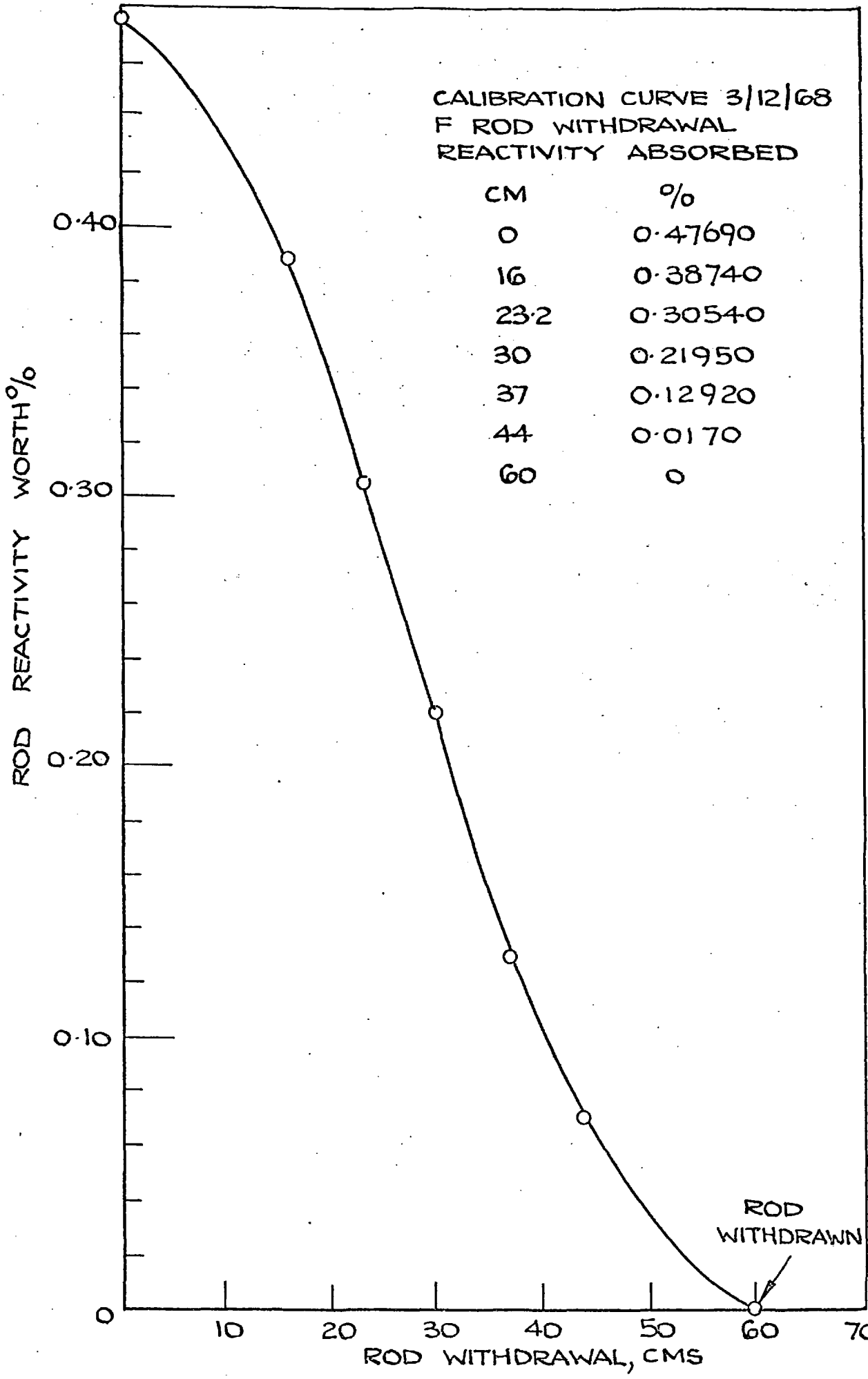

FIG. 21: FINE CONTROL ROD CALIBRATION CURVE

between the actual sine wave oscillator assembly in the reactor core and the pulley mounted on the drive shaft. Measurement accuracy was to within ± 1 degree.

4.1(2) Preliminary Static Test

Test Conditions

Reactor power	–	Balanced at 8 watts.
Oscillator	–	At centre of core in centre access tube.
Safety rod	–	Fully withdrawn.
Rod A	–	" "
Rod B	–	44 cm. withdrawn.
Rod F	–	Balance position 31.5 cm.

The balance position of the fine rod F at 31.5 cm. indicates from the calibration curve Fig. 21 a total reactivity investment of 0.1950% in k. This figure is greater than the agreed figure of 0.120% though it must be pointed out that this latter figure was a maximum for the actual oscillator assembly in the reactor core. The additional 0.0750% was a fact due to the total assembly necessary to permit a mechanically safe and adequate drive system. No objection to this increased figure was raised by the reactor operating staff since the mechanism was securely clamped against removal and even accidental flooding of the tube would have not caused an unsafe reactor conditions. It should be pointed out at this stage that stringent precautions were necessary since one of the main aims was to provide a student experiment.

With regard to the balance position of the reactor with the fine rod F at 31.5 cm. Fig. 21 and knowing the expected reactivity swing of approximately 0.03% it should be noted that the reactivity swing lies within the linear part of the calibration curve.

After various slow rotations had been made a maximum reactivity investment of 0.1950% and a minimum reactivity investment of 0.1615% was measured giving a swing of 0.0335% in reactivity which corresponds to a value predicted from experimental measurements made using Cd foils and physical design limitations, as discussed in Chapter 3.

A comparison of the upper design limits, the results of preliminary tests combined with an understanding of the physical design limits and actual static test results are given in Fig. 22.

Though there is a difference between the allowable and the actual reactivity variations it must be borne in mind that 0.06% was a desired and acceptable upper limit. When consideration is given to the oscillator assembly used, see Fig. 13(b), it is apparent that the maximum and minimum area of Cd absorber varies between two levels lying in the range 50 to 100% of the total area presented by the swept out cylinder. The maximum variation is a direct function of the maximum permitted reactivity investment. For the physical dimensions of the assembly the maximum variation was calculated to be 0.09 to 0.12%, these calculations involved the use of reactivity per unit area obtained from the preliminary foil experiments. To achieve a desired swing of 0.06% in k the total reactivity investment would have had to exceed 0.20% the absolute limit set by the reactor operating staff.

	Design Limits	Predicted Values from Preliminary Foil Tests and Physical Design Limits	Static Tests. on Actual Equipment
Absolute Maximum Reactivity Investment %	0.20	Drive assembly not available	0.1950
Oscillator assembly maximum investment %	0.120	0.12	0.119
Oscillator reactivity variation %	0.06	0.03	0.0335

Fig. 22. Comparison of predicted and actual reactivity variations for the sinusoidal oscillator assemblies.

4.1(3) Static Test

With the reactor state as given in section 4.1(2) a complete test was made by rotating the oscillator shaft manually at 15^{o} degree intervals. At each interval the reactor was re-balanced at 8.0 watts by moving the fine control rod F, this movement being measured on the actual rod drive tape. In addition the rod movement was recorded on the actual control room rod position indicator to investigate whether or not that instrument could be used in a future student experiment. The corresponding reactivity reading for each rod position was calculated using the fine rod calibration curve previously obtained by doubling time measurements.

The experiment run was carried out for several complete rotations in forward and reverse directions. The run was repeated the next day with the reactor balanced again under the same conditions.

The results of the tests are shown in Fig. 23. Values for a single run in one direction are only plotted since the values for reversed rotation and the run on a consecutive day were too close to the points plotted, i.e. they were within the expected experimental tolerances.

The oscillation envelope determined by plotting the control room rod position indicator against angular rotation is given in Fig. 24. This was plotted to indicate whether or not the normal control room instrumentation would be adequate for student measurements. The relative position could only be measured to the nearest 0.1 digit, this, as can be seen, shows up on Fig. 24. No further

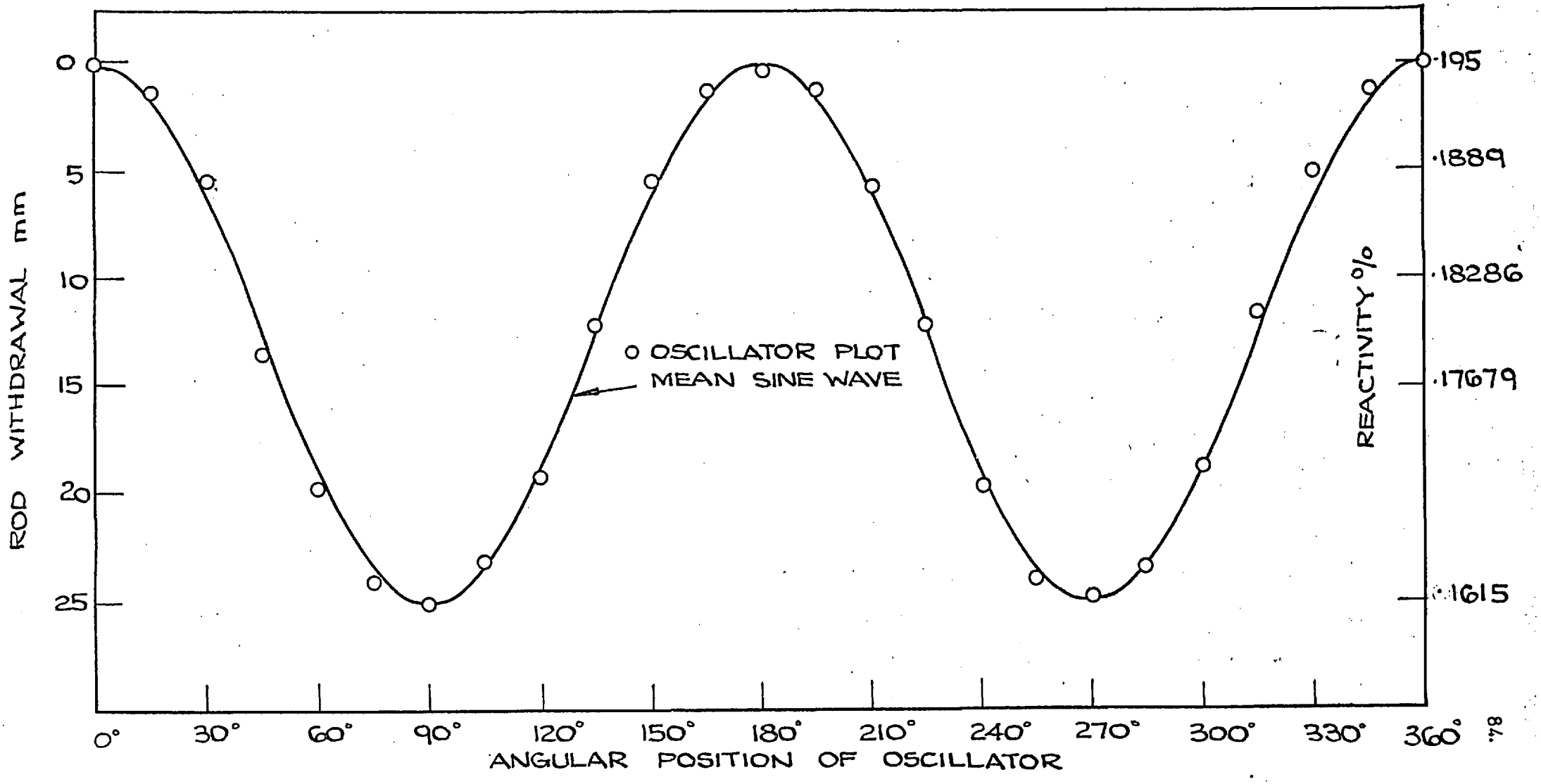

FIG. 23: OSCILLATOR STATIC TEST.

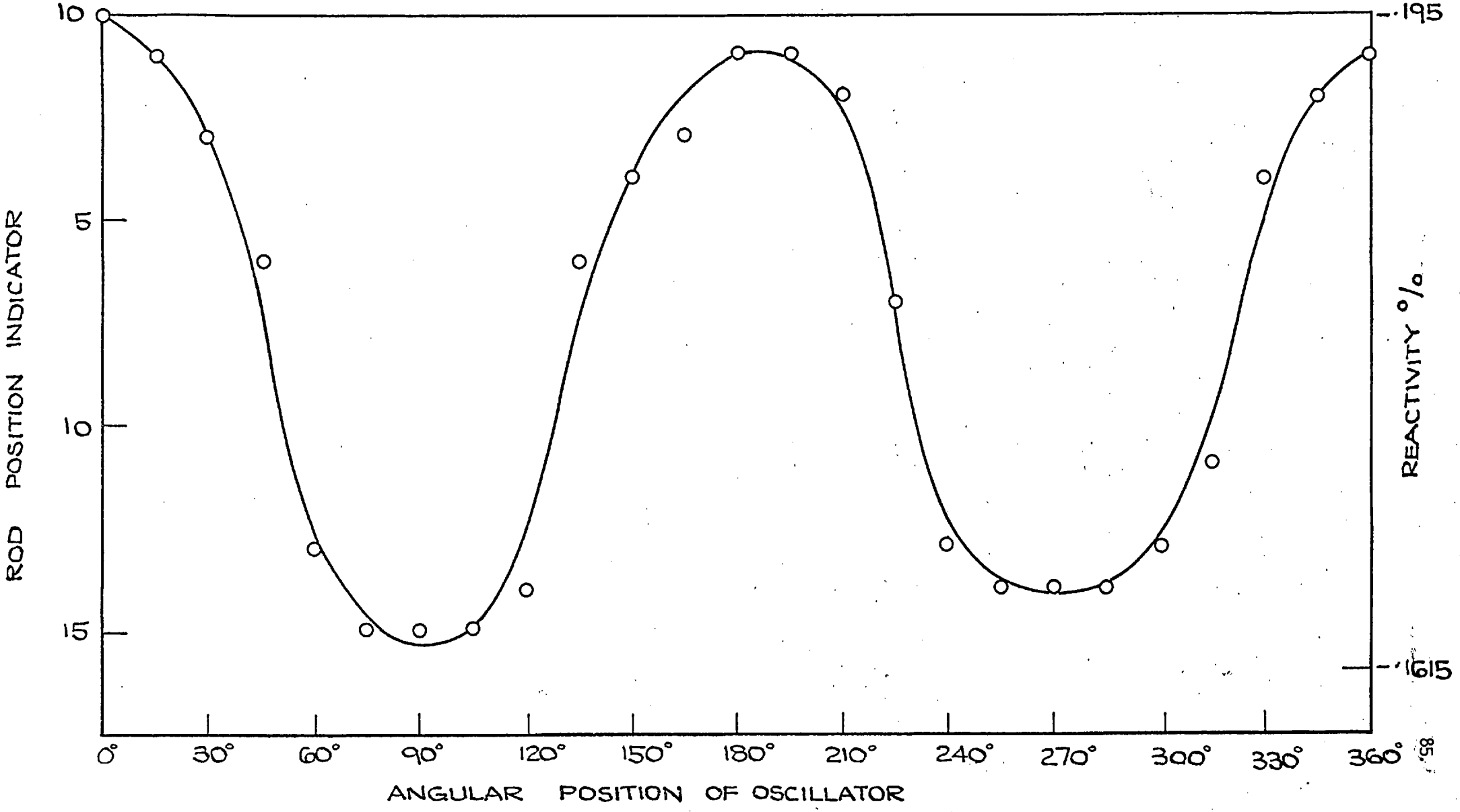

FIG. 24: OSCILLATOR STATIC TEST (VALUES MEASURED ON REACTOR CONTROL ROOM INSTRUMENTS)

use was made of this method of measurement due to the crudeness of the measurements. From the purely operational point of view the indication was within operational requirement especially since the instrument gave only an indication of the rod position to an operator.

4.2. Dynamic Tests with Reactivity Oscillator

A series of experiments were carried out covering the frequency range 0.01 c.p.s. to 100 c.p.s., this frequency range being achieved by using three different pully arrangements combined with the use of a variac on the driving motor. These ranges overlapped by a considerable margin so that continuity could be preserved over the whole frequency band. With respect to the use of a variac as a control it should be pointed out that a motor with a suitably flat torque, speed curve was chosen so that at the lowest speeds utilised, sufficient torque was available to avoid any friction effects. The motor was in fact rotating quite rapidly even at the low frequency end of the spectrum.

The various oscillator/detector positions are shown on Fig. 25.

For each of the experiments indicated on Fig. 25 measurements were made driving the oscillator in the reverse direction, this provided a check on linearity and meant that the exact zero phase over point could be more accurately determined since systematic errors due to direction of rotation would be subtractive.

Before discussing the actual reading and analysis methods finally used, it is of interest to study the results shown in Appendix 4. One of the aims of the study was to investigate the

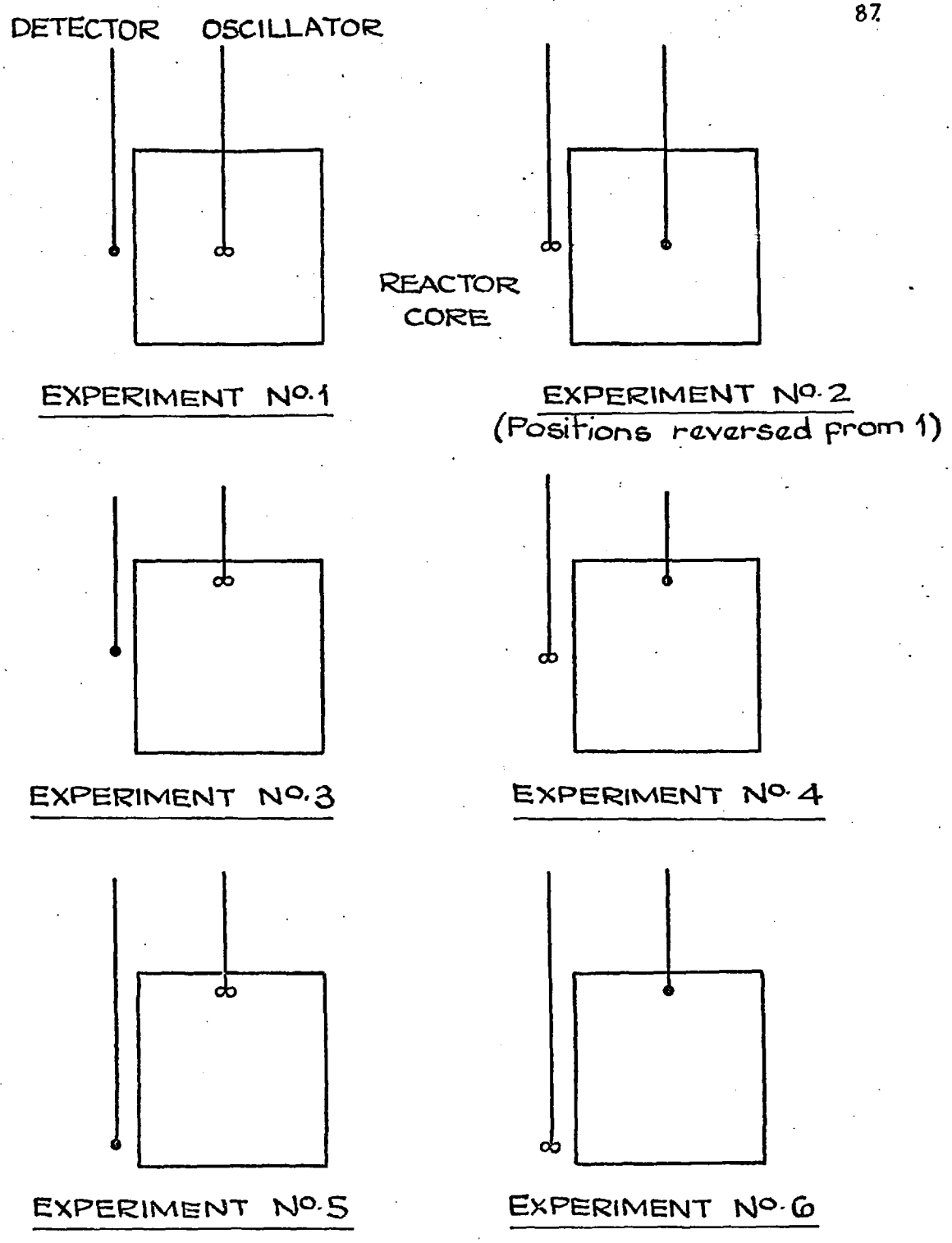

FIG. 25: OSCILLATOR / DETECTOR SYSTEMS

provision of an undergraduate and postgraduate experiment. To achieve this objective it was considered necessary that the use of existing measuring equipment be made wherever possible. A 400 channel multi-channel analyser was available, this was used as a measurement device connected to the output of the neutron detector. The start of the reading was initiated by the trigger pulse from the pulser on the oscillator shaft, thus the relative phase between the input and output could be measured. The results are given in Appendix 4 with a list of the reasons why the method was not used in the main experiments. All the experiments were conducted using the 12EB40 chamber with the reactor balanced at 8 watts.

The measuring system described in Fig. 12 Chapter 3 was used throughout the series of experiments.

The two signals were simultaneously recorded on the two track FM tape recorder at various speeds, dependent upon the oscillation speeds, and played on line into the Hewlett Packard correlator. This latter recording was done mainly so that a visual indication could be seen. The College's correlator had no print out facilities or computer attachment. The results were therefore replayed on another Hewlett Packard correlator that had print out facilities and an on-line mini-computer. This latter facility was sited at the company's main works near Edinburgh. This facility was used for the noise experiments described later in this report but the computer installation was unavailable for the on-line evaluation of the transfer function data. The correlator was therefore used to display the cross correlation of

the input and output channels and a paper tape output was obtained that could at a later date be played into a computer.

For each setting of the speed range utilised in the experiments a tape recording was made of sufficient length that auto and cross correlation functions could be obtained.

The Fenlow low frequency spectrum analyser and oscilloscope Fig. 12 Chapter were used as on-line monitoring guides, for later noise experiments results were directly obtained on the low frequency analyser.

When a particular run was deemed satisfactory using the on-line correlator and the afore mentioned instruments, the data was stored permanently on the two tracks of the F.M. tape recorder.

Observations were made on the control room instrumentation during the experimental runs, particularly when the reactor was oscillated at very low frequencies. The reactor operators were asked not to trim the reactor during the runs unless absolutely necessary. In fact no trimming was required even during the very low frequency runs. It is interesting to note that the reactor was oscillated at 0.00349 cycles per second for a run lasting for 45 minutes during which time no reactor trim was necessary.

Traces were obtained on the reactor control room power chart recorder particularly for the lower frequency runs. An example of the recording is given in the results, section 4.4 of this chapter.

4.3. Analysis

Although it would appear that adequate on and off-line analysis methods existed, as described in the previous section 4.2, the author felt that problems were present with the suggested analysis routes. The existing reactor centre on-line correlator had no attached mini-computer nor any print out facilities, due at that time to the unavailability of interfaces.

The correlator computer installation at the Hewlett Packard company headquarters was a demonstration installation and would not necessarily always be available although, in fact, the noise experimental results (described later in this study) and some limited transfer function experimental results were analysed on the system, fig. 26.

It was finally decided that the results should be analysed on an I.B.M. 1800 data acquisition system that existed in the medical electronics section at Imperial College. Certain additional software had to be written to fully utilise the system and its peripherals for the presentation and analysis of the results from the oscillator experiments. A block diagram of the system is given in Fig. 27. The output from the two channels of the F.M. tape recorder are translated via the multiplexer and an analogue to digital converter into digital form. The I.B.M. 1800 computer uses fast fourier transforms to perform the necessary calculations to provide auto and cross correlation, power spectral densities etc. The output from the computer is normally transferred to a 7 track industrial magnetic tape unit thence to a plotter or cathode ray tube (C.R.T.) display.

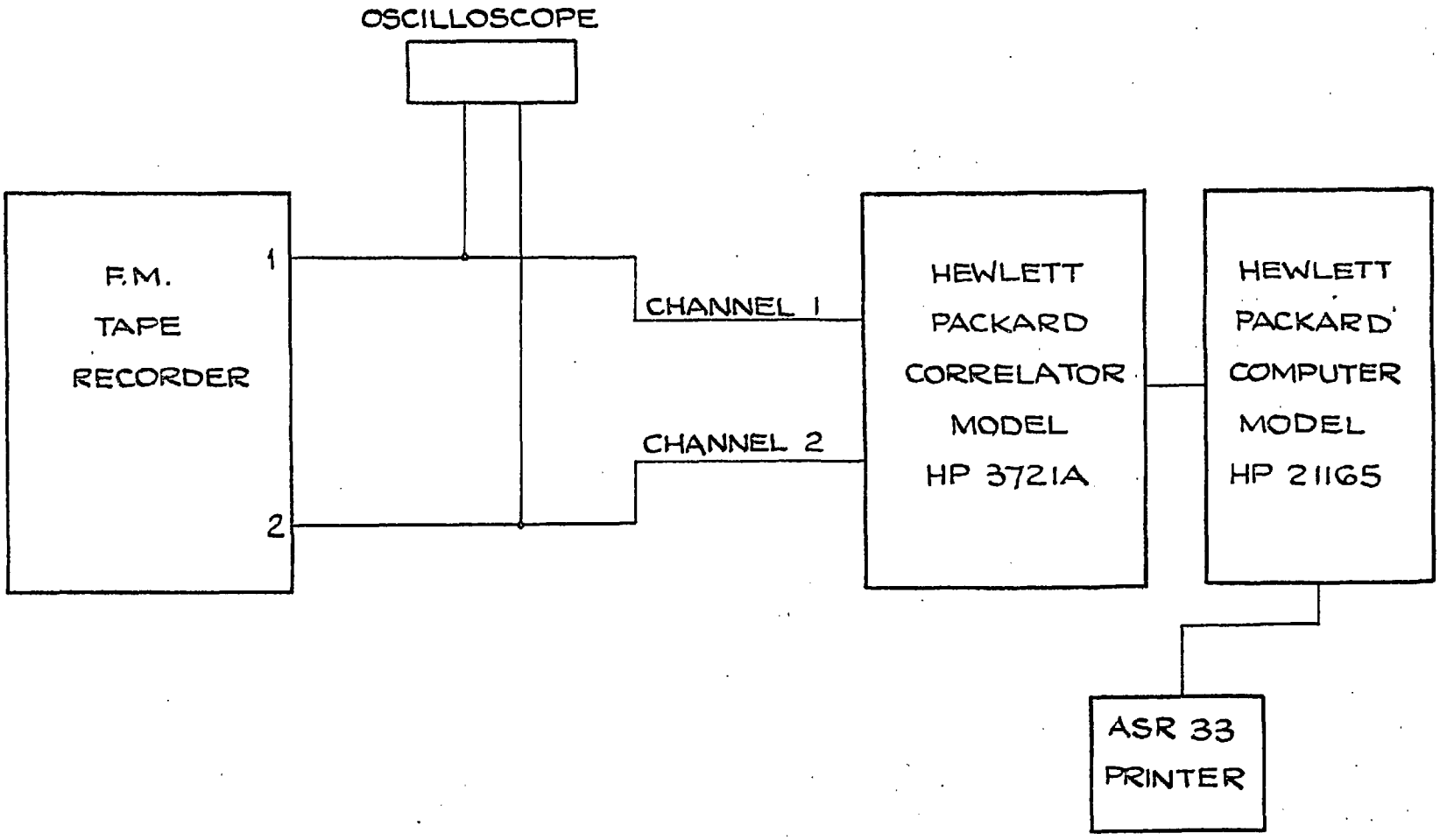

FIG. 26: OFF LINE: CORRELATION ANALYSIS.

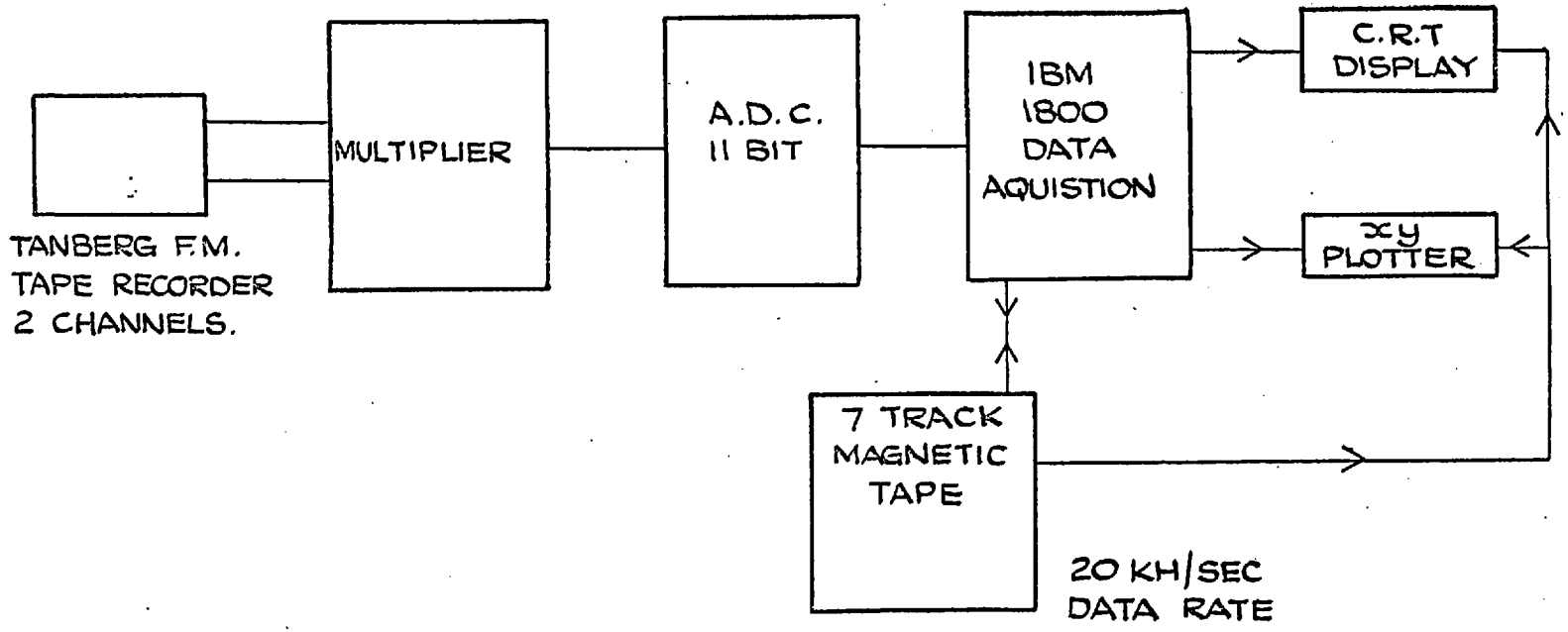

FIG. 27: DATA AQUISITION SYSTEM.

If required, direct communication between the computer, the C.R.T. and x y plotter is available. Two forms of x y plotting were available, analogue or digital, the latter using an I.B.M. Calcomp drum plotter.

4.4. Results

Experiment No. 1

Fig. 28 gives the reactor transfer function amplitude response for the U.L.R. Reactor determined from experiment no. 1 Fig. 25 Chapter 4 Section 4.2. Points are plotted for forward and reverse rotation of the oscillator over the frequency range 0.0219 to 746.0 radian per second. Fig. 29 gives the corresponding phase shift response for experiment no. 1, the points plotted being the mean of the forward and reverse rotations wherever appropriate. Figs. 30 and 31 show the comparison between data plotted from Keepin[12] for U^{235} and the experimentally obtained points for the amplitude and phase responses. Fig. 32 is the experimental data obtained for Fig. 28 replotted in terms of gain in decibels versus frequency in cycles per second, this representation being the more common form of transfer function presentation for control system design and synthesis. The slope of the high frequency part of the plot has an asymptotic value of 19.4 dbs/decade which compares favourably with a predicted theoretical value of 20 dbs/decade. Further comment is made upon values obtained from these results in Chapter 5. Fig. 33 and Fig. 34 repeat the plots of Fig. 28 and Fig. 29 respectively within the error bands indicated, a detailed analysis of these error bands being given in Chapter 5.

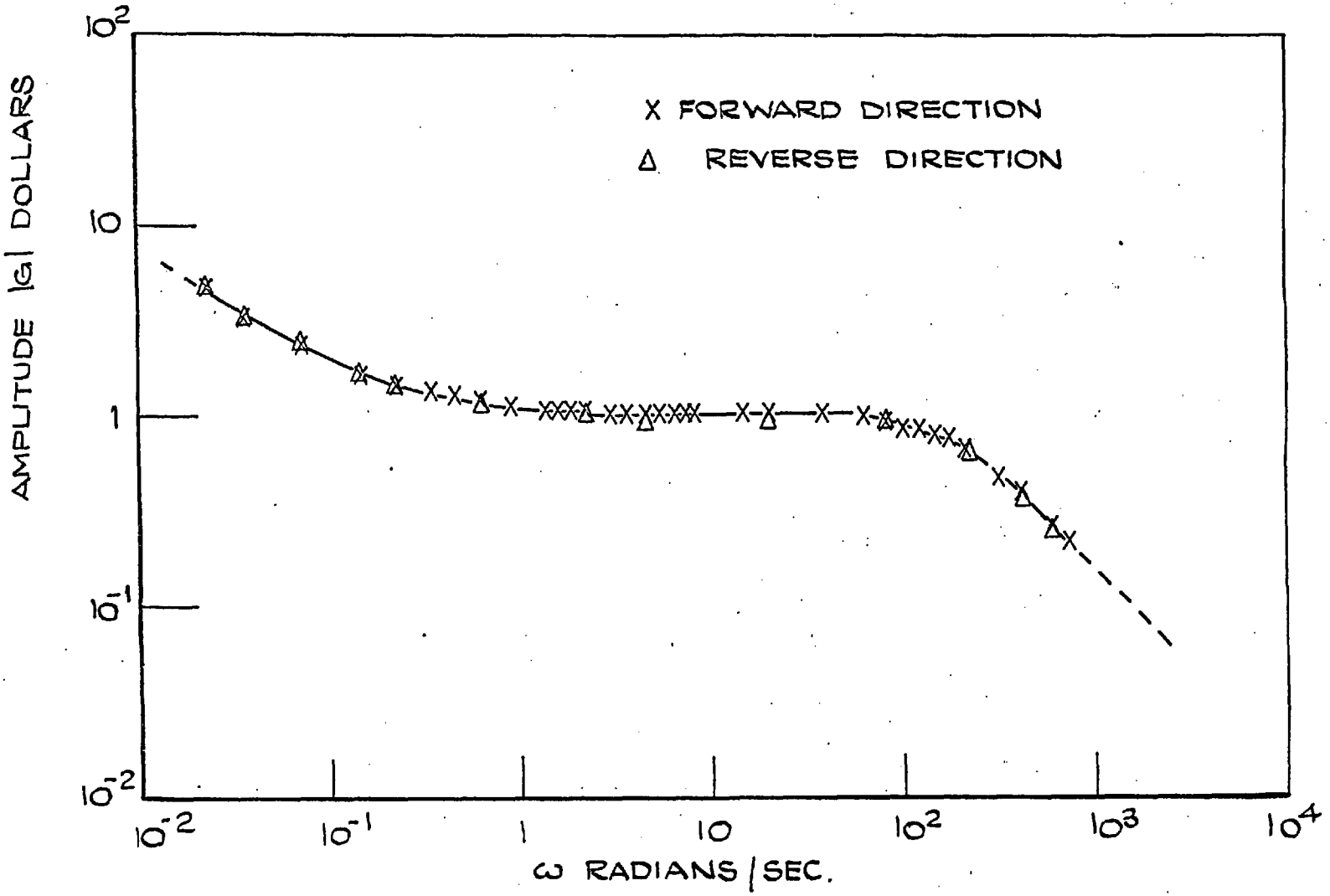

FIG. 28: U.L.R. CONSORT REACTOR TRANSFER FUNCTION AMPLITUDE RESPONSE OSCILLATOR EXPERIMENTAL POINTS.

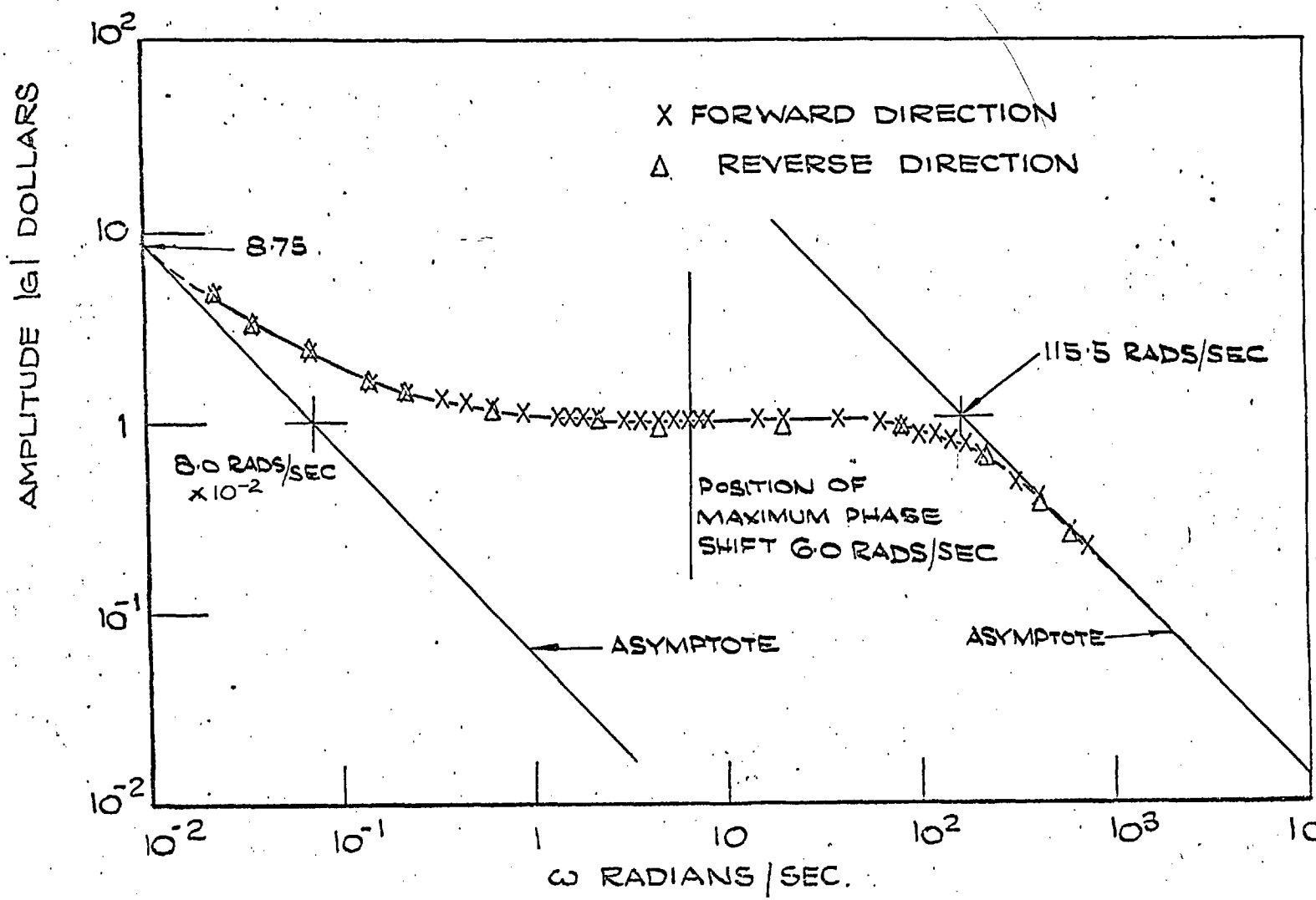

FIG. 28(a) U.L.R. CONSORT REACTOR TRANSFER FUNCTION AMPLITUDE RESPONSE OSCILLATOR EXPERIMENTAL POINTS.

D76

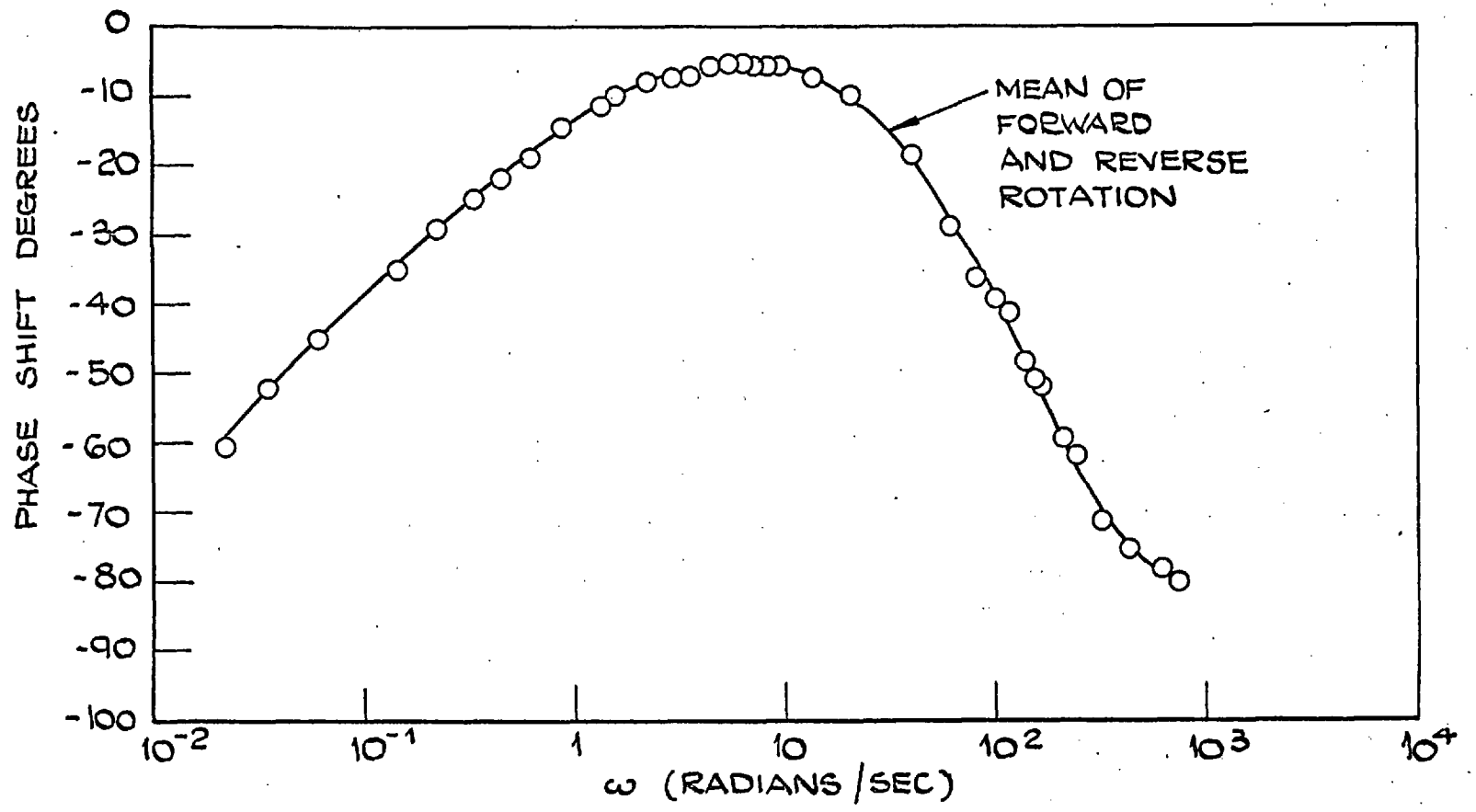

FIG. 29: U.L.R. CONSORT REACTOR TRANSFER FUNCTION PHASE SHIFT RESPONSE OSCILLATOR EXPERIMENTAL POINTS.

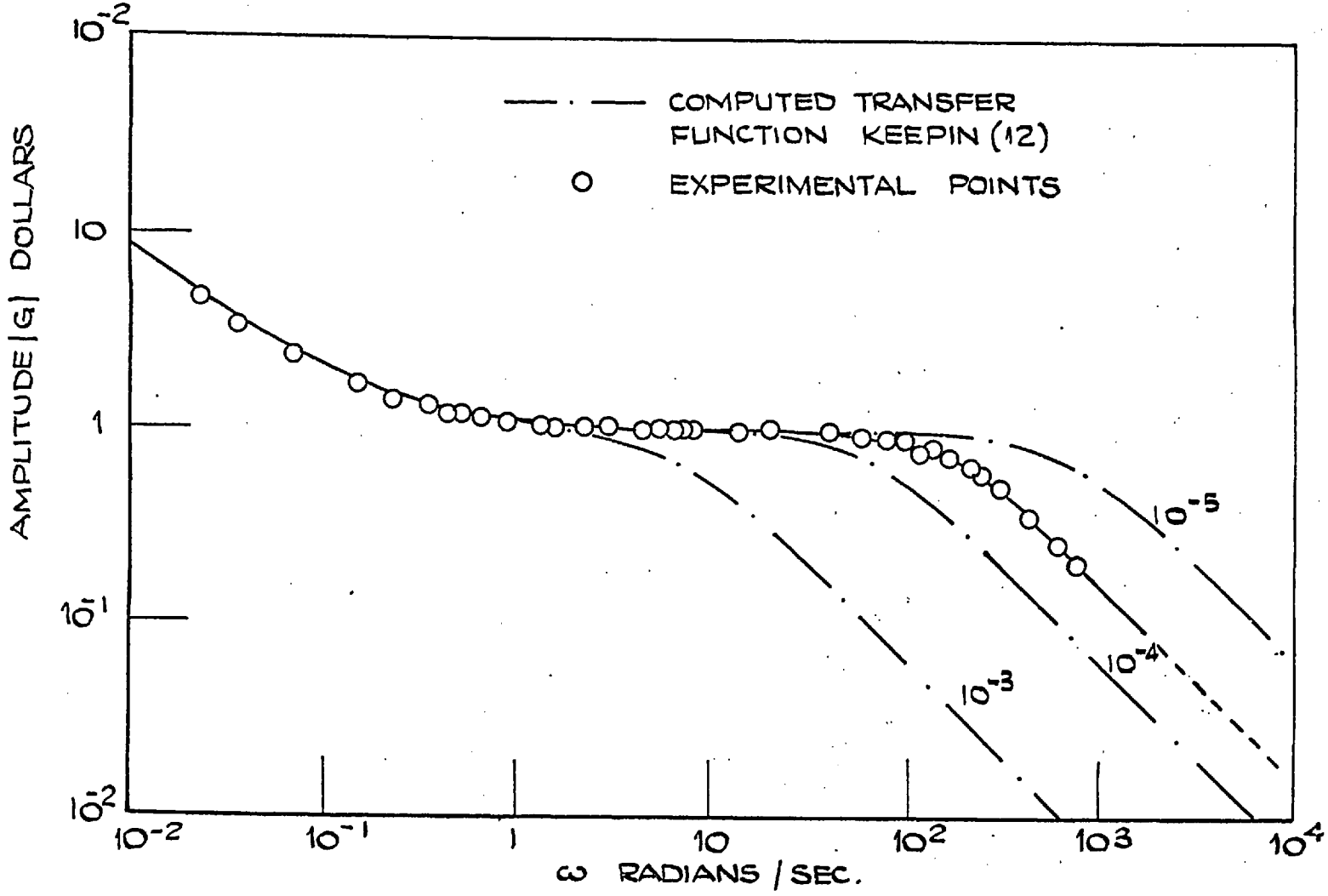

FIG. 30: REACTOR TRANSFER FUNCTION AMPLITUDE RESPONSE FOR U^{235} SYSTEM CALCULATED ($\ell = 10^{-3}, 10^{-4}$ & 10^{-5}) AND EXPERIMENTAL POINTS.

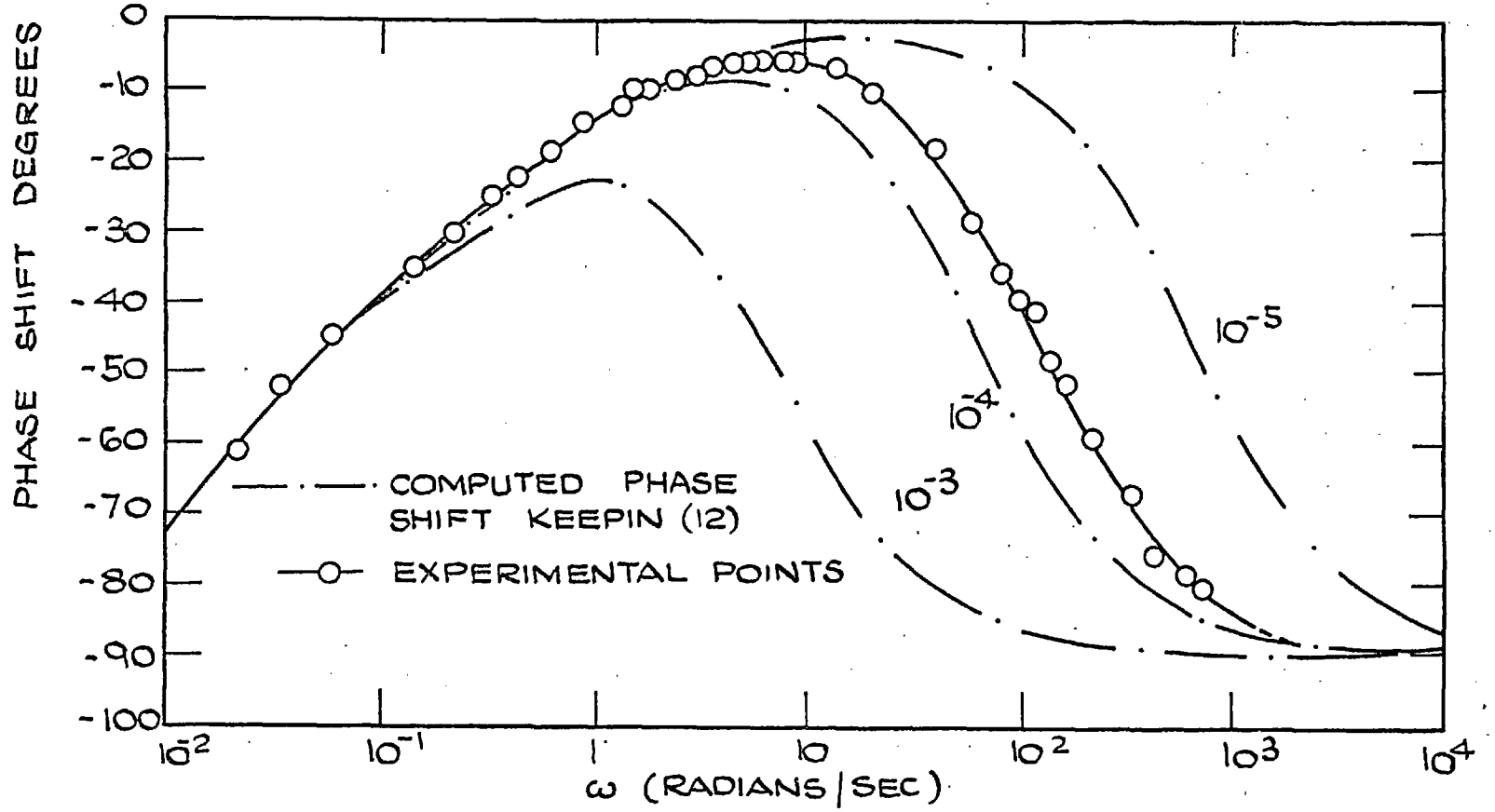

FIG. 31. REACTOR TRANSFER FUNCTION PHASE SHIFT RESPONSE FOR U^{235} SYSTEM CALCULATED ($\ell = 10^{-3}, 10^{-4}$ & 10^{-5}) AND EXPERIMENTAL POINTS.

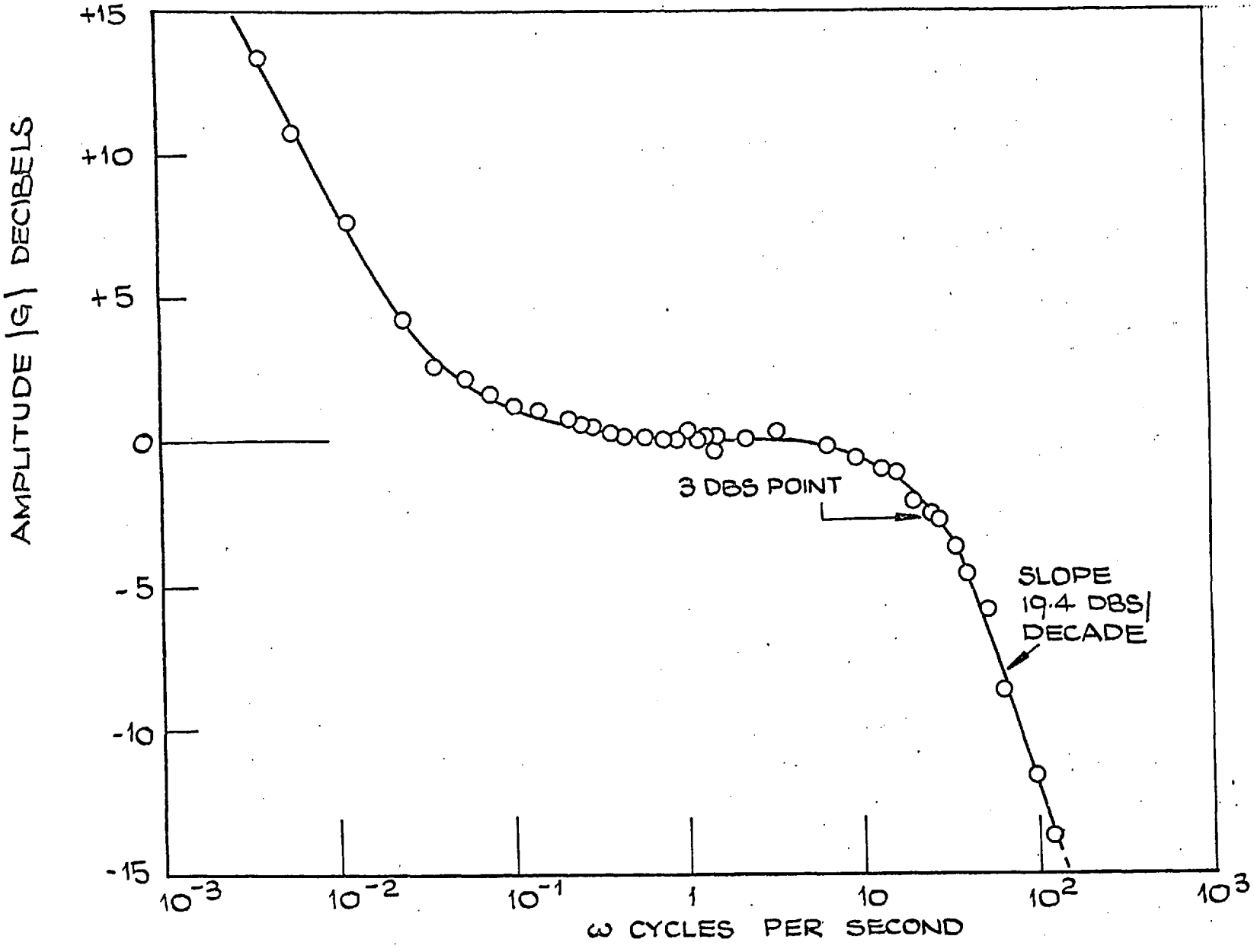

FIG. 32: U.L.R. CONSORT REACTOR TRANSFER FUNCTION AMPLITUDE RESPONSE OSCILLATOR EXPERIMENTAL POINTS.

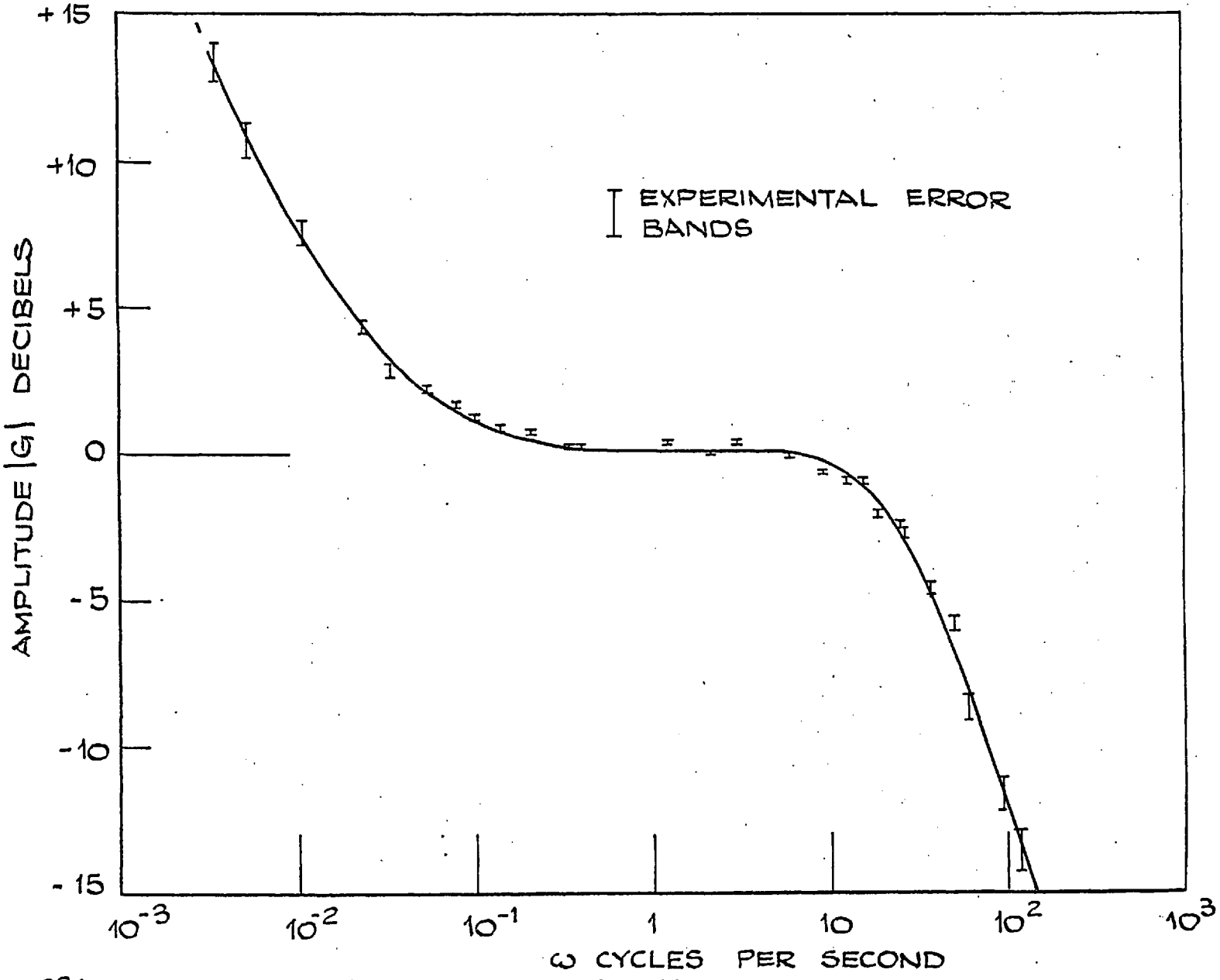

FIG. 33: U.L.R. CONSORT REACTOR TRANSFER FUNCTION AMPLITUDE RESPONSE OSCILLATOR EXPERIMENTS ERROR BANDS.

'66

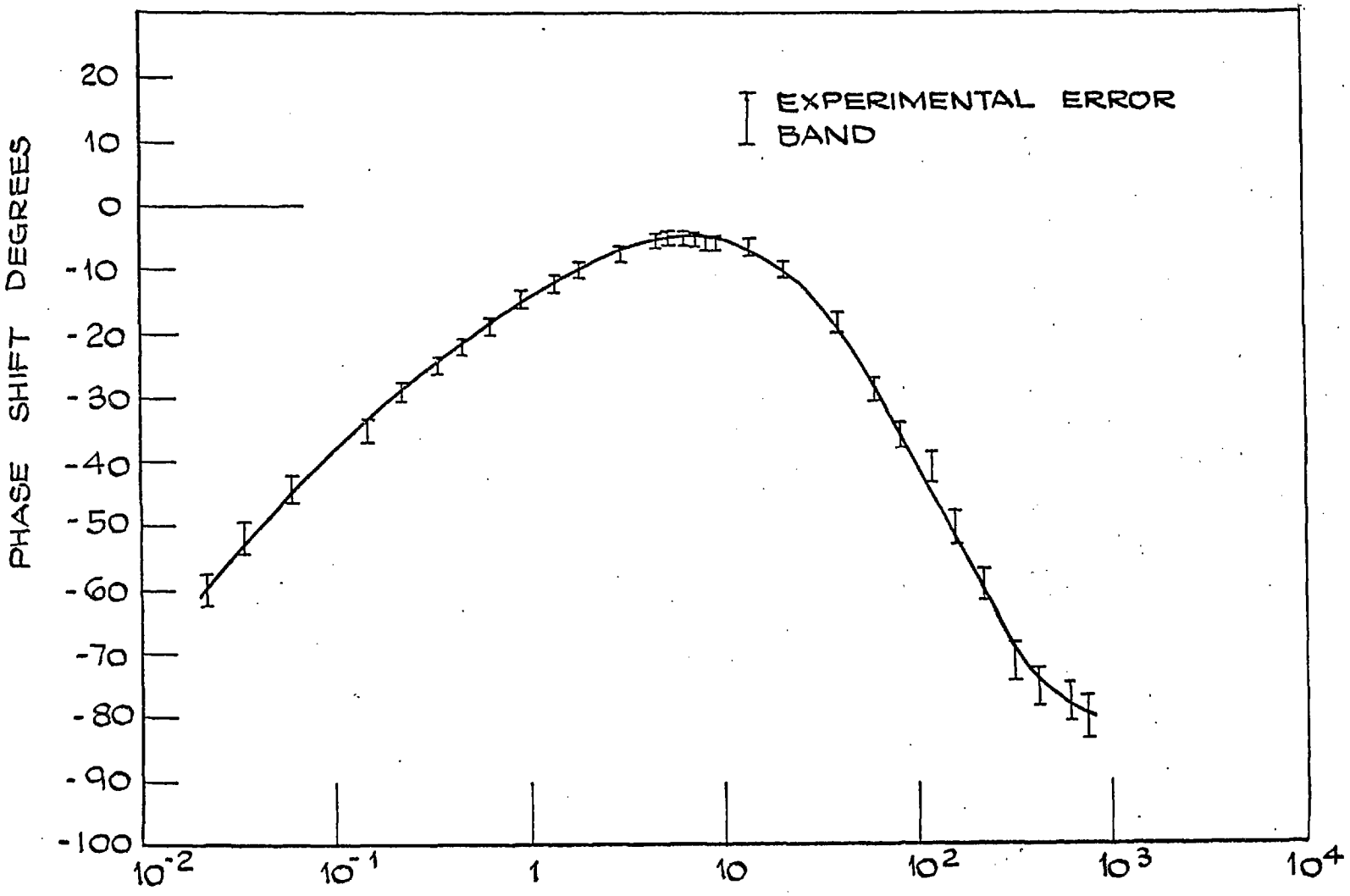

FIG. 34: U.L.R. CONSORT REACTOR TRANSFER FUNCTION PHASE SHIFT RESPONSE OSCILLATOR EXPERIMENTAL POINTS ERROR BANDS.

The results obtained for experiments no. 3 to no. 6 are not plotted since they lie within the error bands specified on Fig. 33 and Fig. 34. These latter results were made in areas of the reactor configuration where the signal to noise ratio of the neutron flux decreased hence more random fluctuations were apparent on the waveforms; pictures of these waveforms are shown in subsequent figures. The use of correlation techniques within the IBM 1800 data acquisition and manipulation system Fig. 27, Chapter 4, section 4.3, meant that the noisy part of the waveform could be correlated out of the calculation.

It is of interest to note at this stage that the number of cycles of information recorded on the FM tape recorder per experimental frequency point was made sufficiently large for adequate correlation to be undertaken. A discussion of the non-variation between different oscillator detector positions in the reactor is given in Chapter 5.

Fig. 35 (a) and (b) are typical x y plotter records derived on-line from the IBM 1800 data acquisition system. Point A on each trace indicates the point at which the oscillator trigger pulse commenced the detector output, giving the phase relationship between output and input. The traces indicate block sizes and within these blocks upto twenty thousand samples could be made, should this be deemed necessary. Since two cycles per revolution of the oscillator shaft between trigger pulses was a fundamental physical fact of the experimental equipment a maximum of ten thousand samples per cycle was the upper limit. In practice it was only necessary to ensure that the individual number of samples per recording was within the

experimental accuracy. In fact the number of samples taken was dictated mainly by the speed of rotation or frequency.

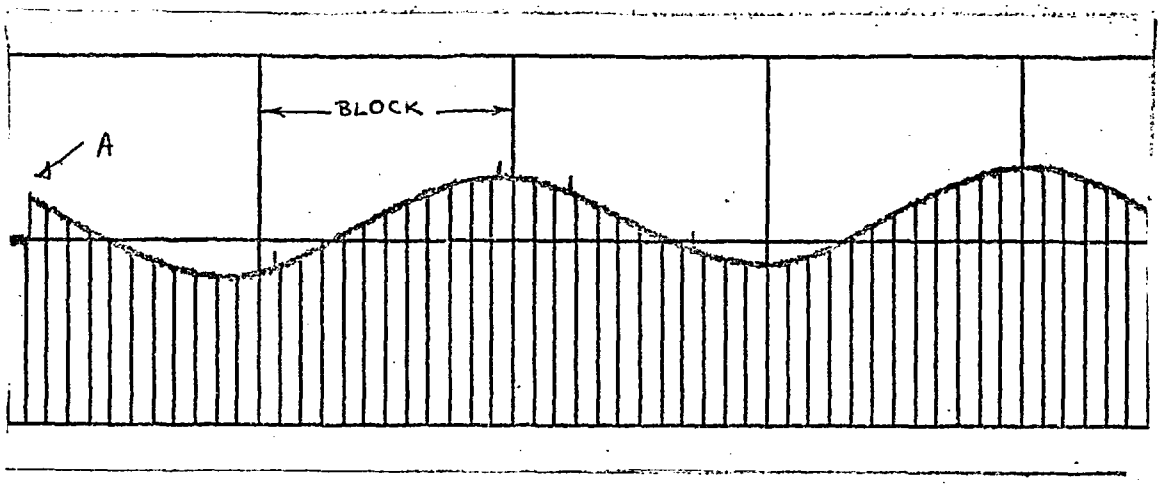

Fig. 35(a). Frequency 3.49×10^{-3} C/S
Amplitude 2.3V
Reactor state 8 watts critical

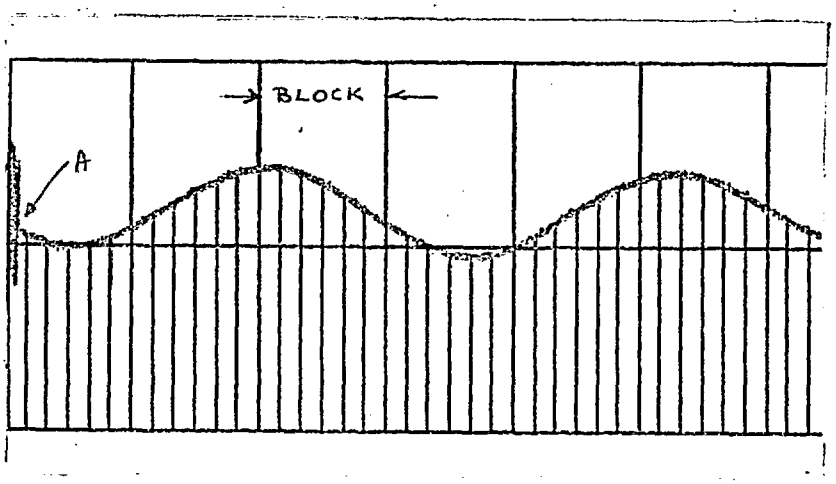

Fig. 35(b). Frequency 5.32×10^{-3} C/S
Amplitude 1.69V
Reactor state 8 watts critical

Fig. 35(a) and (b). Typical outputs on x y recorder from IBM 1800 data acquisition system. Both runs are for experiment no. 1. Fig. 25, Chapter 4, section 4.2.

The previously verified magnetic tapes produced on the FM tape recorder were replayed on the Hewlett Packard off-line correlator Fig. 26. Unfortunately the computer was not available so that only photographs and a punched paper tape output was available, the latter could be played at some future date when the Hewlett Packard became available.

Fig. 36 gives the reactor response plotted by the correlator in the signal recovery mode. In this mode of operation one channel of the correlator was fed with the trigger pulse from the experimental tape recording, this pulse signifying experimentally the start of a new two cycle operation of the oscillator. This trigger or synchronising pulse tells the correlator where to start each repetition of the detector output wave form (recorded on the other channel of the experimental tape recording). This input is then sampled, these separate samples are stored in separate locations in the correlator main store. Subsequent repetitions of the input waveform are read sequentially, these are then averaged with the previous corresponding sample, this process is repeated. It should be noted that the noise portion of the average will gradually die out since the noise makes a random contribution, positive and negative, to each main store location on successive repetitions. For random noise, the signal to noise voltage ratio is improved in proportion to $\sqrt{N}$ where N is the number of repetitions. Fig. 36 and subsequent figures are included mainly to demonstrate the viability of the method and the use of the correlator. In addition it should be pointed out that a similar principle was used in the runs carried out on the IBM 1800 data acquisition system.

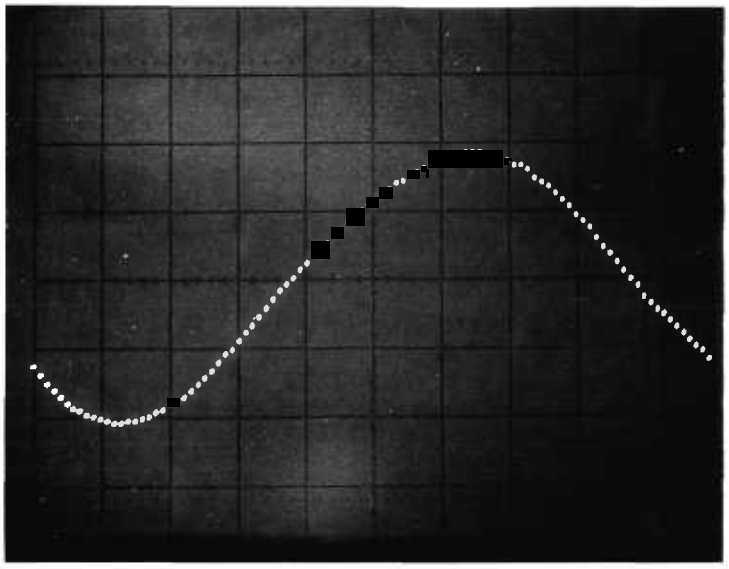

Fig. 36. Signal Recovery: Oscillator Experiment.
Reactor State 8 watts critical.
"X" Axis of display 33.3m$_2$Sec/mm
"Y" Axis of display 0.75V^2/cm
Display background in cm squares
Oscillator frequency 0.98 C/S
Oscillator/detector position - Experiment no. 1.
Fig. 25, Chapter 4, section 4.2.

Fig. 37 involves an inversion of the signal.

Fig. 38 indicates a non-linear effect in the recordings. It is included since it demonstrates the ease with which apparent physical effects can be caused due to the misuse of the equipment. There is no physical reason for the appearance of what is apparently a third harmonic content in the detector output for a linear condition. This effect was due to the fact that one channel of the FM tape recorder had an incorrect setting on the output channel, The output switch should have had a gain setting corresponding to that of the input recording. The result of the error caused a break through from one channel of the recording to the other. Under signal recovery the repetition of the fundamental with a phase shift was apparent. One significant point to note is that in an auto correlation mode there would have been only one fundamental frequency shown thus assisting the identifying of the effect. Of course no phase information would have been obtainable from the auto correlation mode.

Fig. 39(a), (b) and (c) are included to demonstrate the signal recovery mode under conditions where the signal to noise ratio is lower, hence for a given number of repetitions the traces should show more random fluctuations on the funadmental wave shape. A larger number of repetitions, i.e. longer recording would reduce the random fluctuations, this was the method adopted when using the IBM 1800 data acquisition system. Fig. 40 demonstrates the use of auto correlation when the oscillator was in operation. Unfortunately the misuse of the tape recorder output channel is apparent on this recording but the function behaves as expected with the noise correlation leading to the particular basic oscillator frequency.

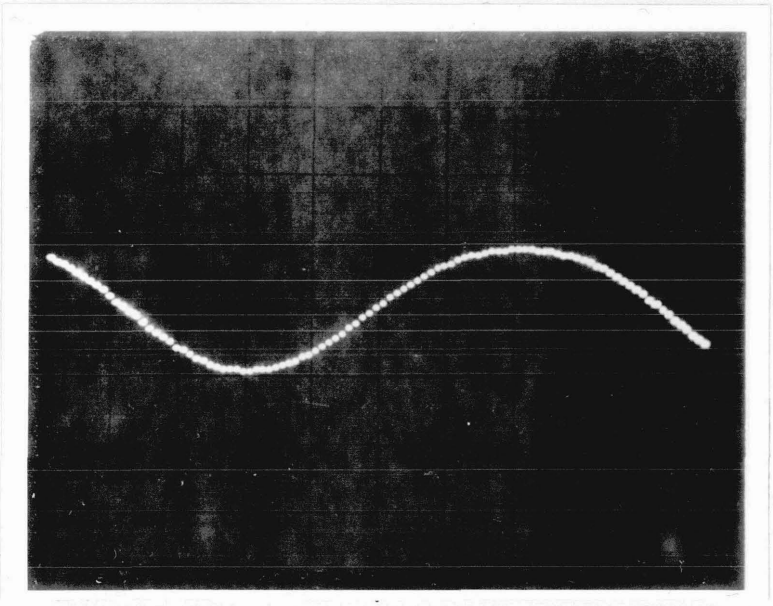

Fig. 37. Signal Recovery: Oscillator Experiment.
Reactor State 8 watts critical
"X" Axis of display 1.0 mSec/mm
"Y" Axis of display $0.5V^2$/cm
Display background in cm squares
Oscillator frequency 26.35 C/S
Oscillator/detector position as for Fig. 36

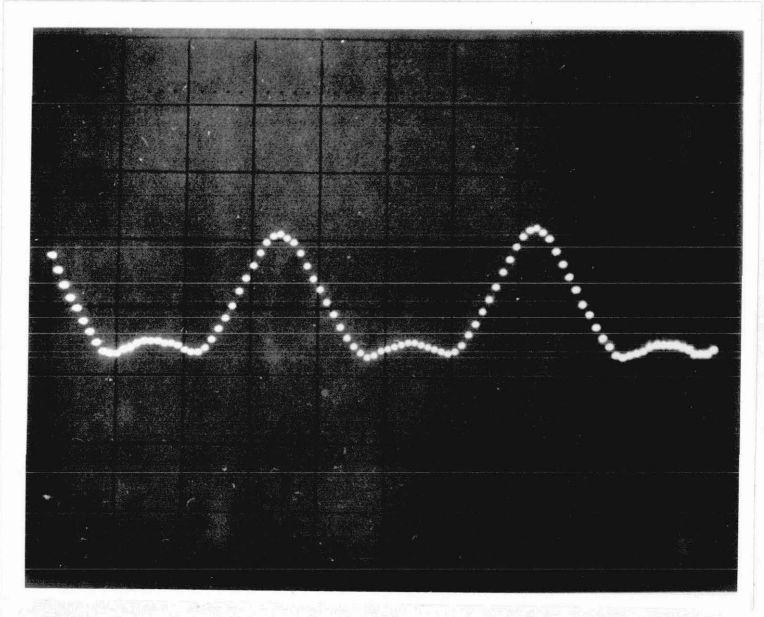

Fig. 38. Signal Recovery: Oscillator Experiment.
Reactor state 8 watts critical
"X" Axis of display 33.3m Sec/mm
"Y" Axis of display 1.0V^2/cm
Display background in cm squares
Oscillator frequency 2.17 C/S
Oscillator/detector position as for Fig. 36.

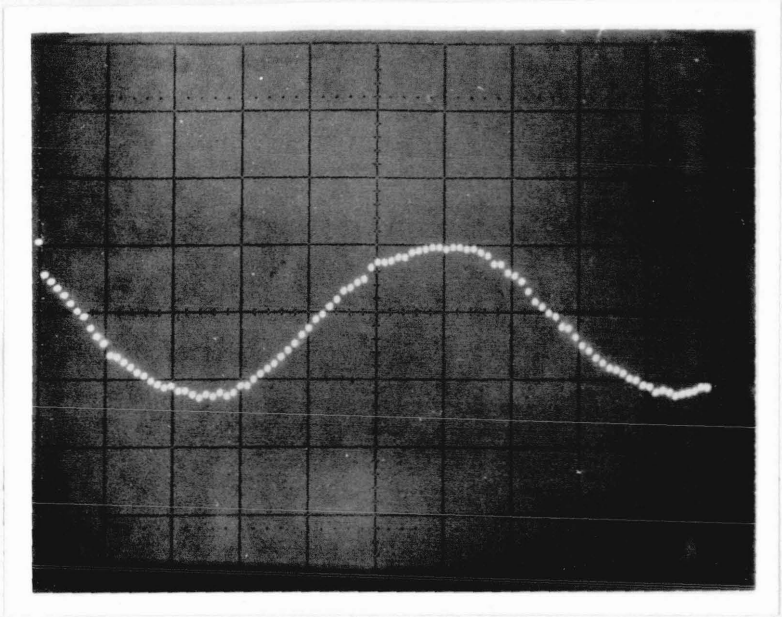

Fig. 39(a). Signal Recovery: Oscillator Experiment
Reactor state 8 watts critical
Oscillator Frequency 1.4 C/S
Oscillator/detector position experiment no. 3.
Fig. 25, Chapter 4, section 4.2.

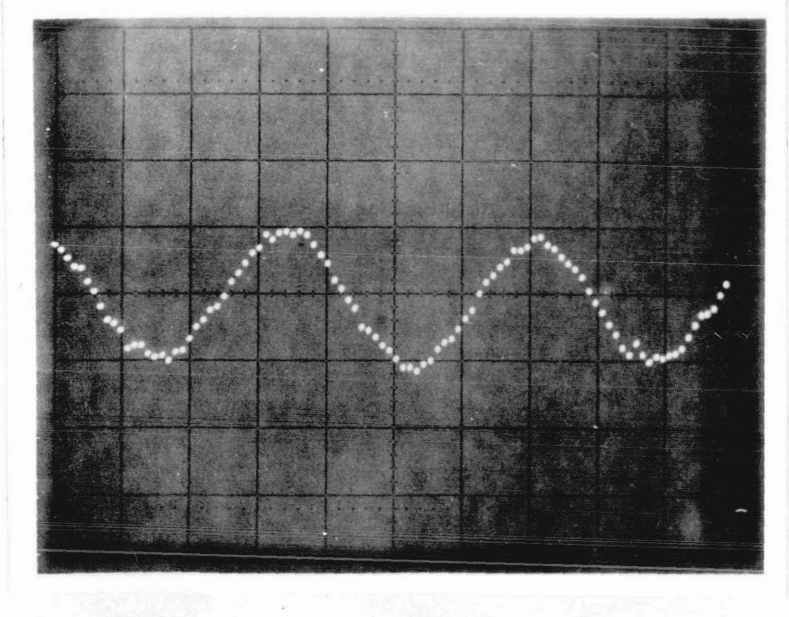

Fig. 39(b). Signal Recovery: Oscillator Experiment.
Reactor state 8 watts critical
Oscillator frequency 0.84 C/S
Oscillator/detector position as in Fig. 39(a).

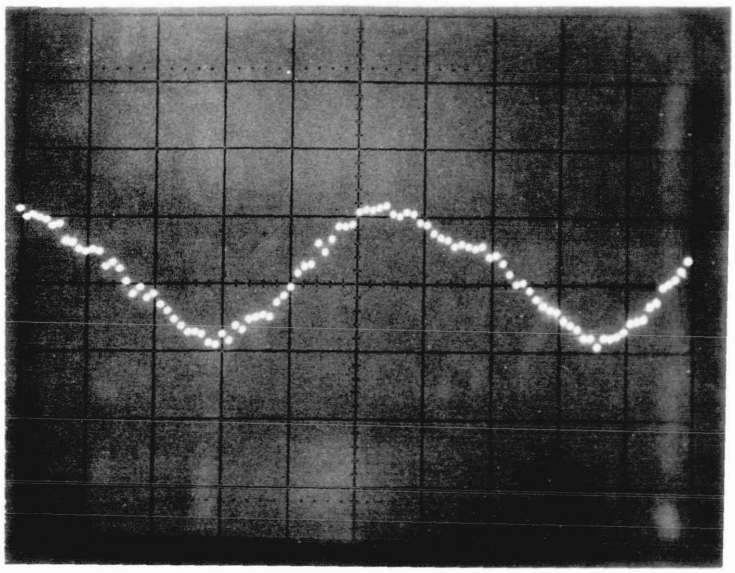

Fig. 39(c). Signal Recovery: Oscillator experiment.
Reactor state 8 watts critical
Oscillator/detector position: experiment no. 3
Fig. 25, Chapter 4, section 4.2.

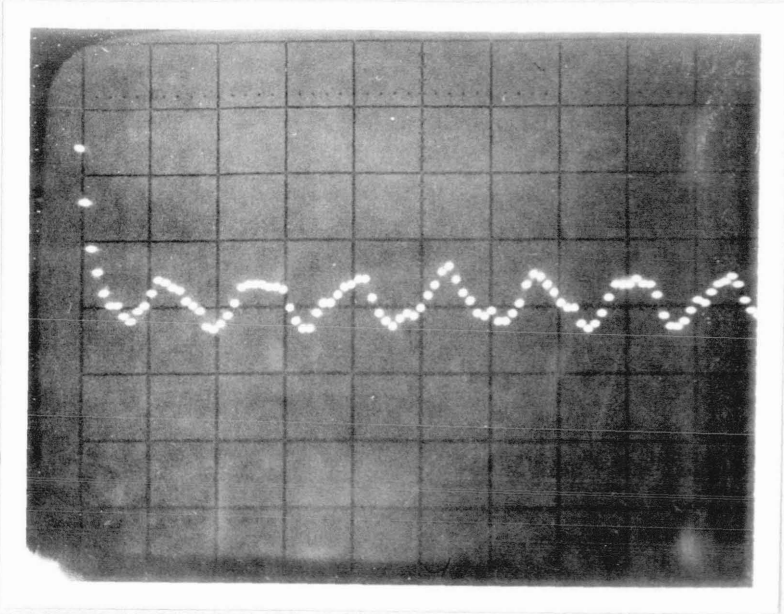

Fig. 40. Auto correlation: Oscillator experiment
Reactor state 8 watts critical
Oscillator frequency 15.5 C/S
Oscillator/detector position: experiment no. 2.
Fig. 25, Chapter 4, section 4.2.

Fig. 41. This is a plot obtained on a standard Calcomp plotter, the data being prepared using a data retrieval package developed on the College IBM 7094 by a former student working on a noise analysis system, R. Shamdasani[34]. The trace is a repeat of traces produced both on the IBM 1800 system and the Hewlett Packard correlator. This method suffered from the fact that the FM experiment magnetic tapes had to be translated into an input form suitable for the IBM 7094, the program then produced an output magnetic tape to drive the Calcomp plotter off-line. In addition the limit on the definition of the points on the Calcomp plot meant that when noisy plots were obtained the inability to define the phase angle sufficiently accurate for the experiment eliminated this method. Nevertheless the method would be of use as an off-line facility for certain limited experiments.

Fig. 42. This is a plot of power taken on the standard control room power indicated chart recorder. No phase or amplitude information is shown. The frequency for the run was 3.49×10^{-3} cycles per second. The trace is included since it demonstrates the steady state behaviour of the reactor under a very slow oscillation.

The complete recording was made during a 45 minute period during which no power trims were made by the reactor operator. Similar traces were obtained for all of the slow oscillatory runs.

FIG 41 DETECTOR OUTPUT SIGNAL RECOVERY

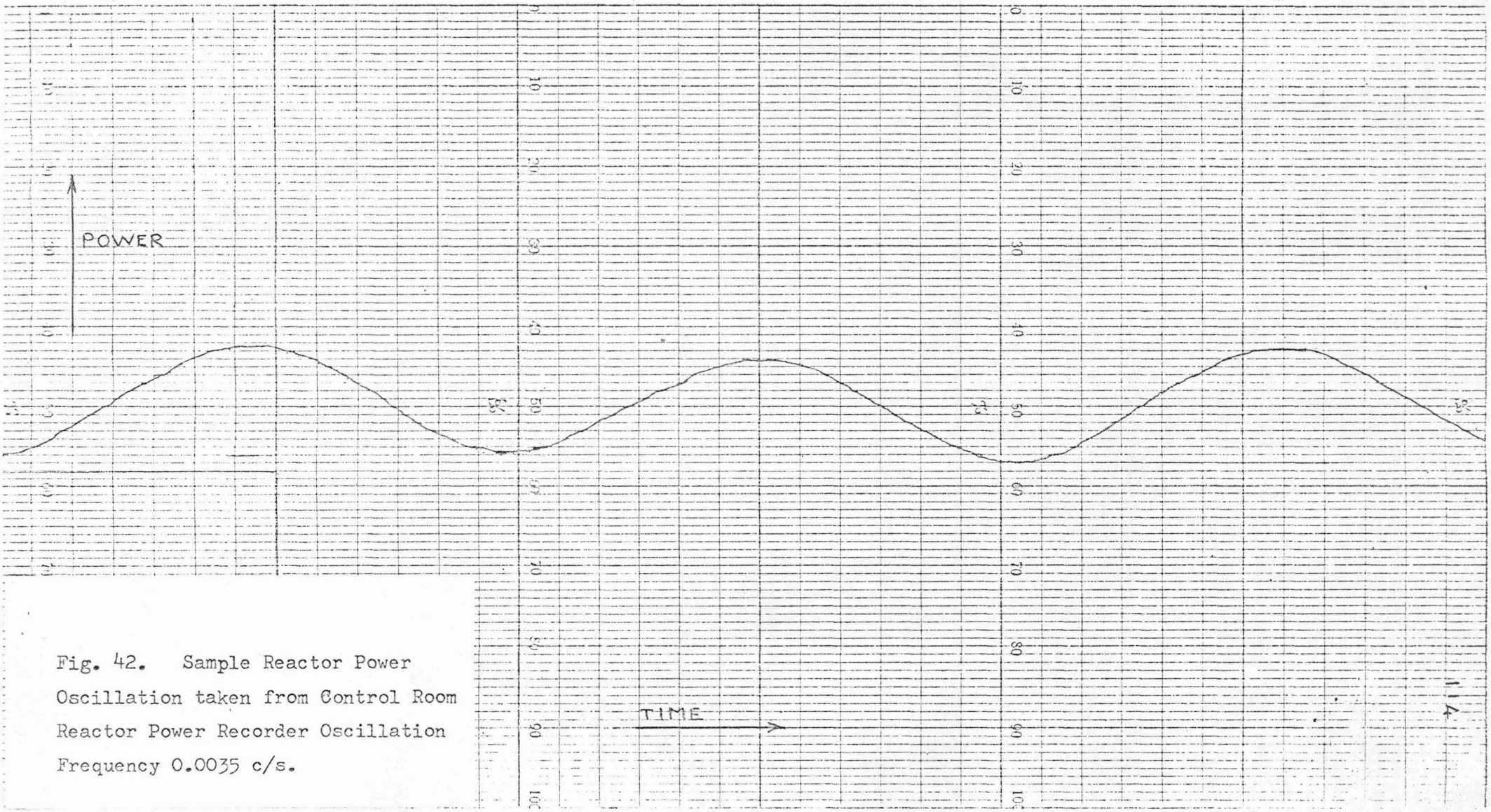

Fig. 42. Sample Reactor Power Oscillation taken from Control Room Reactor Power Recorder Oscillation Frequency 0.0035 c/s.

4.5. Error Analysis

4.5(1) Phase Angle Measurement

In section 3.2(5), Chapter 3, the oscillator angular position and consequent speed measurement was quoted as being $\pm 0.5^{\circ} \pm 0.25^{\circ}$, the former figure being due to the physical limit upon the positioning and size of the light trigger holes in the periphery of the drive assembly and the latter figure being an estimate of the effect of the response of the light trigger and its associated circuitry. A maximum error of $\pm 1.0^{\circ}$ would appear to be reasonable.

In section 3.5, Chapter 3, an error band of $\pm$ 2.5% was estimated for the experimental electronic equipment, this figure being based upon the manufacturers quoted figures and the author's past experience.

The IBM 1800 data acquisition and manipulation system had a quoted error lying within the band $\pm$ 0.05% of the operational variable.

Assuming the maximum phase shift measurement to be 90°, which is the theoretical prediction for a transfer function going from a constant gain expressed in decibels to a 20 dbs/decade gain change, an error summary can be constructed.

Summarising:

Error band due to light trigger and associated circuitry ...	$\pm 1^{\circ}$
Error band due to experiment electronic equipment 2.5% x 90°	± 2.25
Error band due to IBM 1800 data acquisition system ...	$\pm 0.045^{\circ}$
Total RMS error band	$\pm 2.50^{\circ}$
Corresponding percentage error band	2.75%

Bearing in mind the small but important extra errors that can occur due to such things as magnetic tape wow, flutter and stability it was felt that an error band of $\pm$ 5% for the phase measurements was realistic.

4.5(2) Amplitude Measurement

The amplitude or gain data was normalised to one dollar or zero db gain over a frequency range where the output amplitude remained constant, independent of frequency. This range is in effect where the input and output amplitudes are equal in magnitude. This implied that the accuracy with which the initial amplitude was known and the resulting measurement method dominated the error probability.

The reactivity worth of the oscillator was measured in the static test. The actual reactivity was determined using a control rod calibration curve provided by the reactor operating staff.

The actual movement of the control rod as the oscillator was moved through 15 degree steps was measured, using a vernier

type measurement, on the actual metallic tape that drove the control rod. The estimated error in tape measurement was ± 0.25 mm. which corresponded to a ± 1.67% variation in amplitude. Additive to this value is that due to the electronic equipment used during the experiments, namely ± 2.5%. This gave a total of ± 4.17%. Bearing in mind the ± 0.05% maximum error due to the IBM 1800 data acquisition system a value of ± 4.22% maximum error is achieved.

One area of doubt remains in the measurement, that of the rod calibration curve. The reactor staff assessed the maximum error as being ± 0.5%.

Bearing in mind this latter figure it was felt that an error of ± 5% would reasonably represent the amplitude error.

4.5(3) Positional Error

The question of the relative positions of the oscillator/reactor/detector configurations, their reversibility and repeatibility needs to be examined in connection with possible errors systematic or otherwise.

The vertical positions of the oscillator and detector relative to each other and the core are governed by the use of extension tubes that accurately specify the height of the oscillator or detector from the bottom of the reactor access tubes. For example the aim in experiment 1, fig. 25, Chapter 4, section 4.2, was to get the oscillator and detector on the appropriate centre line of the core or as near as possible to the anticipated nuclear centre line. Once the centre line position had been established the repeatibility of the position relative to the core was

dependent solely upon the extension tubes, their location in the bottom of the reactor access tubes and their couplings to the main drive assembly.

On height measurements carried out in a simulation test run earlier in the study, the drive assembly and tubes were mounted outside the reactor vessel using the reactor guard rails as a support. The estimated height measurement error lay within $\pm$ 1 mm. but an assumed error of $\pm$ 2 mm. was felt to be a more than adequate maximum error band. This error was not deemed troublesome since as will be seen in Chapter 6 due to the active length of the detector being 12 cm. and other factors involved in diffusion and migration of neutrons small differences in the height of the oscillator would be insignificant. Any effect would, of course, show up in the amplitude measurements.

Positional errors could be envisaged due to the twist in the oscillator drive shaft when driven at relatively high speeds. These could lead to phase shift measurement errors. From observations on the afore-mentioned test rig and a study of the experimental results no apparent errors were attributable to twist problems. In actual fact the mean of forward and reverse directions phase shifts were taken to eliminate this type of error and those due to backlash.

As with the measurements made with amplitude errors in mind, due to possible vertical errors in the location of the detector and oscillator the results obtained lay within the anticipated $\pm$ 5% error band. No systematic errors could be detected within the error band due to the previous possible positional errors.

CHAPTER 5

REACTOR NOISE

5.1. General Introduction

Over the years there has been an increasing interest shown in the information that can be obtained from the study of inherent or induced statistical fluctuations on original levels, these fluctuations being normally referred to as noise.

The inher ent statistical fluctuations of the neutron density in zero power stationary multiplying systems are well known and have been measured and studied by many workers. These fluctuations are often termed 'pile noise' or 'reactor noise'.

In a reactor operating at effectively zero power the statistical fluctuations on reactor flux are due to stochastic nature of the neutron behaviour. The power level is too insufficient for reactivity feedbacks due to temperature, pressure and density changes to have any significant contribution. Furthermore if there are no externally caused reactivity perturbations due to such things as control rod motion, fuel element vibration due to changing coolant velocity, the reactors behaviour is completely characterised by the source, the neutron chain reaction involving fission, absorption and leakage. This is the reactor condition that was investigated during the series of experiments carried out during the study.

It is of interest to briefly consider the aspects of the noise that emanates from power reactors. Power reactors have many more aspects of dynamic behaviour than those solely described by the neutron kinetic equations. Thus one would expect to find a variety

of different applications of noise analysis for power reactors.

Sources of noise in power reactors could be generalised as:

(1) Those due to the statistical nature of the chain reaction, i.e. zero power reactor noise.

(2) Intrinsic reactivity noise. These cover feedback due to temperature, pressure and density changes which are coupled with the heat removal equipment.

(3) Excitations due to controlled random reactivity, such as that from a control rod. This latter method can be utilised as a driving input to assist analysis.

When a reactor is at power the noise due to the statistical nature of the neutron chain reaction alone may be of insufficient amplitude when compared to the other sources of noise.

Returning to the study in question, that of a zero power reactor transfer function, it should be pointed out that the main aim of the one and two detector experiments carried out in the study was to provide both a check on and a comparison with the zero power transfer function obtained from the oscillator experiments. Additionally it was hoped to investigate whether or not more information on the spatial dependency could be provided from the noise measurements. Bearing in mind the limited aim of the investigation with respect to noise only a brief survey will be made of various noise methods and investigations; the reader is referred to the references for more detailed reading.

During the period that the noise experiments were carried out some collaborative work was undertaken with a research student whose work is published as a thesis Shamdasani[34].

5.2. General Review of Zero Power Reactor Noise Experiments

The inherent fluctuations due to the statistical nature of the fission process is characterised by a 'noise spectrum' which is the means square amplitude of the noise in a given frequency band per unit bandwidth. The spectra could be measured by analysing the neutron fluctuation with tunable band pass filters. Moore[35], an early worker in this field, has shown that the noise spectrum is proportional to the square of the amplitude of the transfer function. Measurements at Argonne[36], on various low power experimental reactors have demonstrated that reactor noise analysis can be used to determine the amplitude versus frequency response of the transfer functions. These measurements are of more interest in the high frequency 'roll-off' portion of the transfer function where $w = \beta^*/\ell$ (i.e. $\overline{\gamma}\beta/\ell$), other experiments could be troublesome at this end of the spectrum due to the attenuation of the response and in the case of an oscillating absorber the need to rotate the assembly at high rotational speeds. The effects of delayed neutrons is usually negligible in this high frequency range and the transfer function is very dependent upon the prompt neutron decay constant α of the system.

An alternative to the use of band pass filter is to use auto and cross-correlation techniques. The former requiring a long time record of the fluctuations for a steady power level, which is then used in an auto correlation calculation Cohn[37] calculated the reactor noise transfer function by assuming that the noise

had arisen from a noise equivalent neutron source, the characteristics of this source being determined from standard random noise theory Wax[38]. Observed noise was then obtained using the source transfer function. This technique effectively said that the equivalent reactor source noise was due to the statistical fluctuations in the rates of neutron absorption and fission. This direct approach by Cohn[37] is limited in its treatment of complex system models. The work has been extended by Cohn[39] to include a two-group single point reactor model and a one-group two zone reactor model.

In the measurement of reactor noise there is, of course, the question of additional noise due to the detection system. For a small chamber efficiency the pile noise and white noise (due to detection system are uncorrelated Keepin[12] and the two can be added directly to obtain the chamber output. Cohn's analysis method permits the direct use of conventional noise theory.

The noise analysis discussed previously provides transfer function amplitude data but no information regarding the transfer function phase shift. The use of cross correlation techniques where the system output is statistically cross-correlated with known random inputs, permits the determination of a complex transfer function (i.e. amplitude and phase) Feyman[40], Hurwitz[41], Hansen[42].

The following is a brief summary of the noise experiments relative to this study it is by no means the complete list of possible noise experiments with their corresponding reactor parameter determination:

(1) The transfer function of the reactor is achievable, though its determination at low frequency (<0.5 c.p.s.) becomes time consuming when compared to the oscillator method.

(2) The ratio β^*/ℓ may be found, hence the prompt neutron decay constant can be determined Cohn[37] this is effectively the delayed critical Rossi-alpha where

$$\alpha_{DC} = \beta^*/\ell \ \text{sec}^{-1} \qquad \ldots\ldots\ldots 5.2(1)$$

(3) For a subcritical reactor the parameter α, since it can be observed experimentally, can be treated as an alternative expression to reactivity ρ when α is related to the value of α_{DC} for the reactor/detector system, it is possible to calibrate control rods in terms of α or $\$$ (dollars).

(4) Space-time dependency of the reactor/detector system may be investigated by the use of reactor noise Sheff[43] and Natelson[44].

For details on more noise experiments and the parameters that can be determined are covered in Keepin[12] or Thie[13].

One great advantage to the use of noise measurements for nuclear reactors is that the reactor can operate in its normal unperturbed mode during the noise measurements. Care must be exercised to achieve a high correlated to uncorrelated events ratio since the signals are in fact inherent fluctuations.

When the reactor is at power the former comments hold true plus the need to be able to separate other noise signals that may be both periodic and aperiodic and have amplitudes in excess of the one of main interest.

In the investigation of spatial dependency the noise measurements offer the advantage of only needing the insertion of detectors into the core, thus reducing the effect of local perturbation to a minimum when compared with oscillator usage. At high power of course the insertion of an oscillator may not be possible though the normal control rods could be moved in a sinusoidal pattern.

5.3. Experiments Carried out on U.L.R. CONSORT

One and two detector noise experiments were conducted on the unperturbed U.L.R. CONSORT under critical and sub-critical operating conditions. The former being undertaken for comparison with the oscillator experiments, the latter undertaken mainly as an interest in control rod calibration.

The U.L.R. due to its full power (100 kw) operational history had a gamma background of about 10^4R/hr. Gamma background does not convey an information concerning the kinetic condition of the reactor particularly at sub-critical operation. The use of two detectors made it possible to exclude a large portion of the contributions due to the gamma background and other uncorrelated signals.

The chambers used in the experiments were those discussed in Chapter 3 section 3.2. The measuring and recording system was that used in the oscillator experiments fig. 17, Chapter 3, section 3.4. the only change being the substitution of the modified Winfrith head amplifier for the Kiethley head amplifier Fowler[33]; this being a low noise, high gain, high input impedance charge sensitive amplifier designed by Fowler[33] and was modified for use in the present experiments as a current sensitive amplifier.

The chambers were operated in a continuous current mode mainly because at power the alternative pulse mode would prove unsuitable due to the high counting rates leading to a pulse pile-up whilst trying to maintain a suitable detector efficiency. For sub-critical operation the continuous mode was again preferred due to the fact that high detection efficiencies would be required for sub-critical operation, this implied the close proximity of the

detectors to the core, the high gamma field causing spurious counts.

For space dependency either pulse or continuous mode could be used though at high fluxes the continuous mode would be necessary.

5.4. Theory

It is not the intention in this report to give any general theories for noise phenomena in Nuclear reactors other than the comments made in section 5.1 and 5.2 of this chapter. Reference is made to the various authors of papers made in these preceding sections of this report. It is felt necessary to cover briefly the basic description of statistical data and its amplification to the transfer function of the reactor.

5.4(1) Statistical Data - Bendat[45]

For stationary and stochastic process four main types of functions are used to describe their basic properties:

(1) Mean square value.

(2) Probability density functions (PDF's).

(3) Auto and cross-correlation functions (ACF's and CCF's).

(4) Auto and cross spectral density functions (APSD and CPSD).

The mean square value provides an estimate of the intensity of the random data. The probability density function provides information concerning the properties of the data in the amplitude domain. The correlation and power spectral density functions give similar information in the time and frequency domain. The latter two functions are best suited for continuous current experiments.

The auto correlation function (ACF) of a waveform is a graph of the similarity between the waveform and a time shifted version of itself as a function of this time shift.

The ACF of a waveform or stochastic variable $x(t)$ is defined as:

$$\text{ACF} = R_{xx}(\tau) = \lim_{T\to\infty} \int_0^T x(t) \cdot x(t+\tau)dt \qquad \text{.....5.4(1)}$$

it can be written as $R_{xx}(\tau) = \overline{x(t) \cdot x(t+\tau)}$

The cross-correlation function (CCF) between two waveforms or stochastic variables $x(t)$ and $y(t)$ is a measure of the similarity between the two waveforms or stochastic variables.

The cross-correlation function is defined as:

$$R_{xy}(\tau) = \overline{x(t+\tau) \cdot y(t)}$$

$$= \lim_{T\to\infty} \frac{1}{T} \int_0^T x(t+\tau) \cdot y(t)dt \qquad \text{.....5.4(2)}$$

Their corresponding P.S.D. functions are:

$$\text{APSD} = S_x(f) = F[R_x(\tau)] = \text{Fourier transform of } R_x(\tau) \qquad \text{.....5.4(3)}$$

$$\text{CPSD} = S_{xy}(f) = F[R_{xy}(\tau)] = \text{Fourier transform of } R_{xy}(\tau) \qquad \text{.....5.4(4)}$$

5.5. The Transfer Function Representation

Cohn[36], Moore[35], Sheff[43], Nieto et al[46] among other workers have contributed considerably to the noise analysis in particular to the Langevin technique. The use of the Langevin technique is described adequately in the former papers.

The theory basically makes use of fluctuating sources in the equations describing the mean variables of the system. In Moore's treatment f(t) is a stochastic function of time considered as an input to a linear system whose observed noise was characterised by y(t) then:

$$Z(D)\ y(t) = f(t) \qquad \ldots\ldots 5.5(1)$$

Where Z(D) is a polynomial in D (the differential operator) of the constant coefficients describing the dynamic behaviour of the system. Equation 5.5(1) is called the Langevin equation of the system, a formal solution is given by Wax[38].

$$y(t) = G(t - t^1)\ f(t^1)\ dt^1 \qquad \ldots\ldots 5.5(2)$$

Where G(t) is the Greens function of the system.

Assuming 'white noise' properties for the input function f(t) Moore arrives at:

$$\text{APSD of } y(t) = K./H(w)/^2 \qquad \ldots\ldots 5.5(3)$$

Where H(w) is the transfer function of the reactor system. Sheff extended the treatment to cover the space dependence of reactor noise in one and two detector experiments assuming a one group diffusion equation. He derives the auto and cross-correlation functions and their corresponding spectral density functions of the detector readings for various reactor/detector configurations.

To summarise this work, deviations from the space independent or point reactor containing a point detector, shows up in the rates of 'roll-off' of the high frequency ($w^2 > \alpha^2$) portion of the spectral density functions. These results have been confirmed by Natelson and Osborne[44]. These latter workers concluded that the success of space and energy independence theory in the analysis of reactors is limited to a class of thermal reactors in which the migration length M is large enough with respect to the overall reactor size R i.e. $\frac{M}{R} \ll 1$.

5.6. Results

Figs. 43 and 44 show the critical APSD function for the 12EBCO chamber placed at the centre of the core showing the effects of uncorrelated background events and a correlated APSD, this latter curve was determined by Shamdasani. On the same graphs the oscillator determined transfer function is given. All the results were normalised to Odb's in the flat portion of the curve. The corrected or correlated APSD points have been fitted with a third order polynomial. Figs. 45, 46 and 47 are the figures showing APSD correlated and uncorrelated at various points in the core, as detected jointly with Shamdasani.

They were determined using the P7/22 chamber in the centre access tube at the centre of the core, position A and at the top of the core of the core position C and with the 12EB40 chamber at the centre of the core. The correlated portion of the ASPD function shown on Figs. 43, 44 and 47 was typical of the correlated ASPD functions obtained for all three detectors, the latter one being the large diameter RC6EB, see Chapter 3 section 3.2, which could not

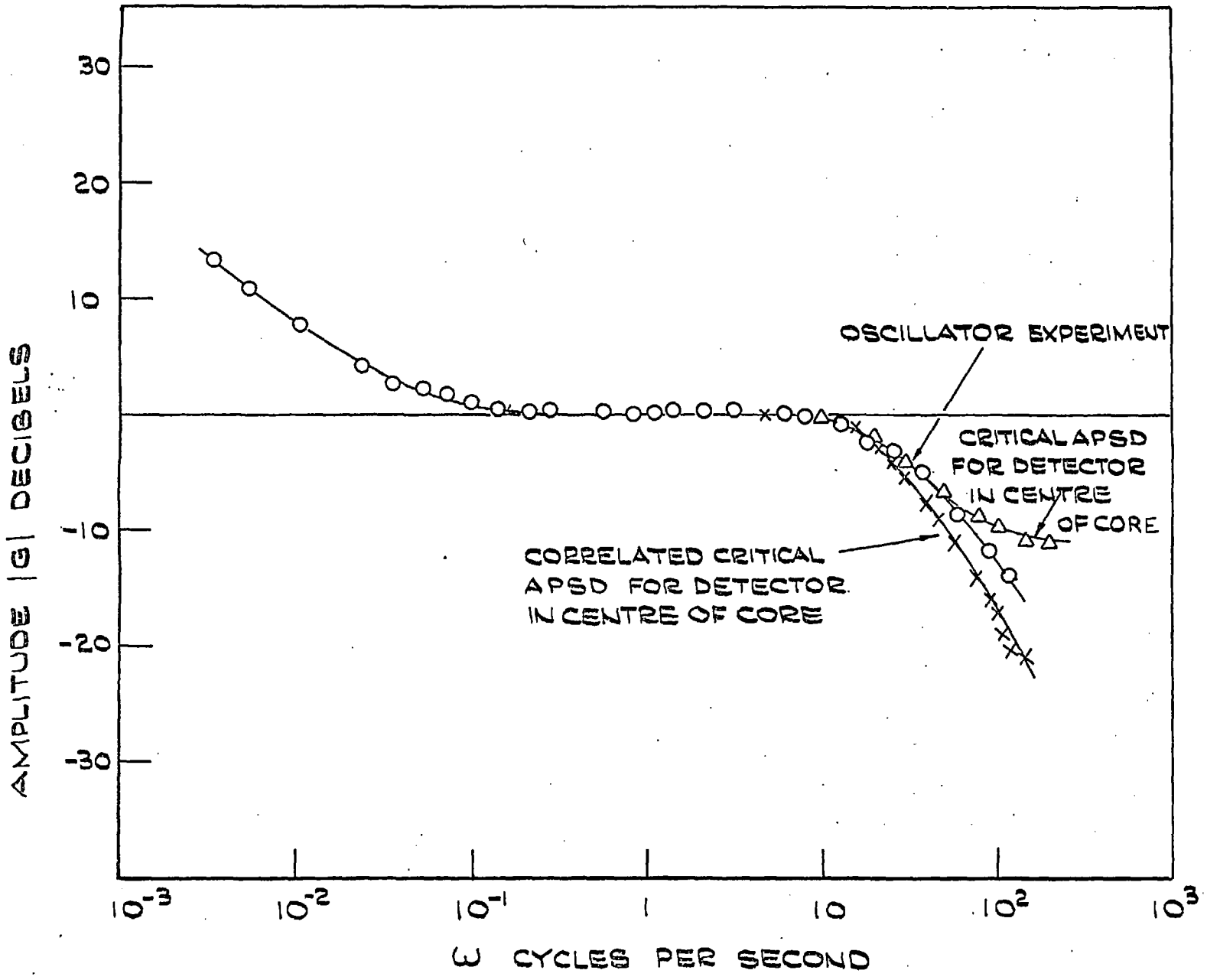

FIG. 43: COMPARISON OF OSCILLATOR, APSD & CORRELATED ASPD FUNCTION FOR CONSORT REACTOR

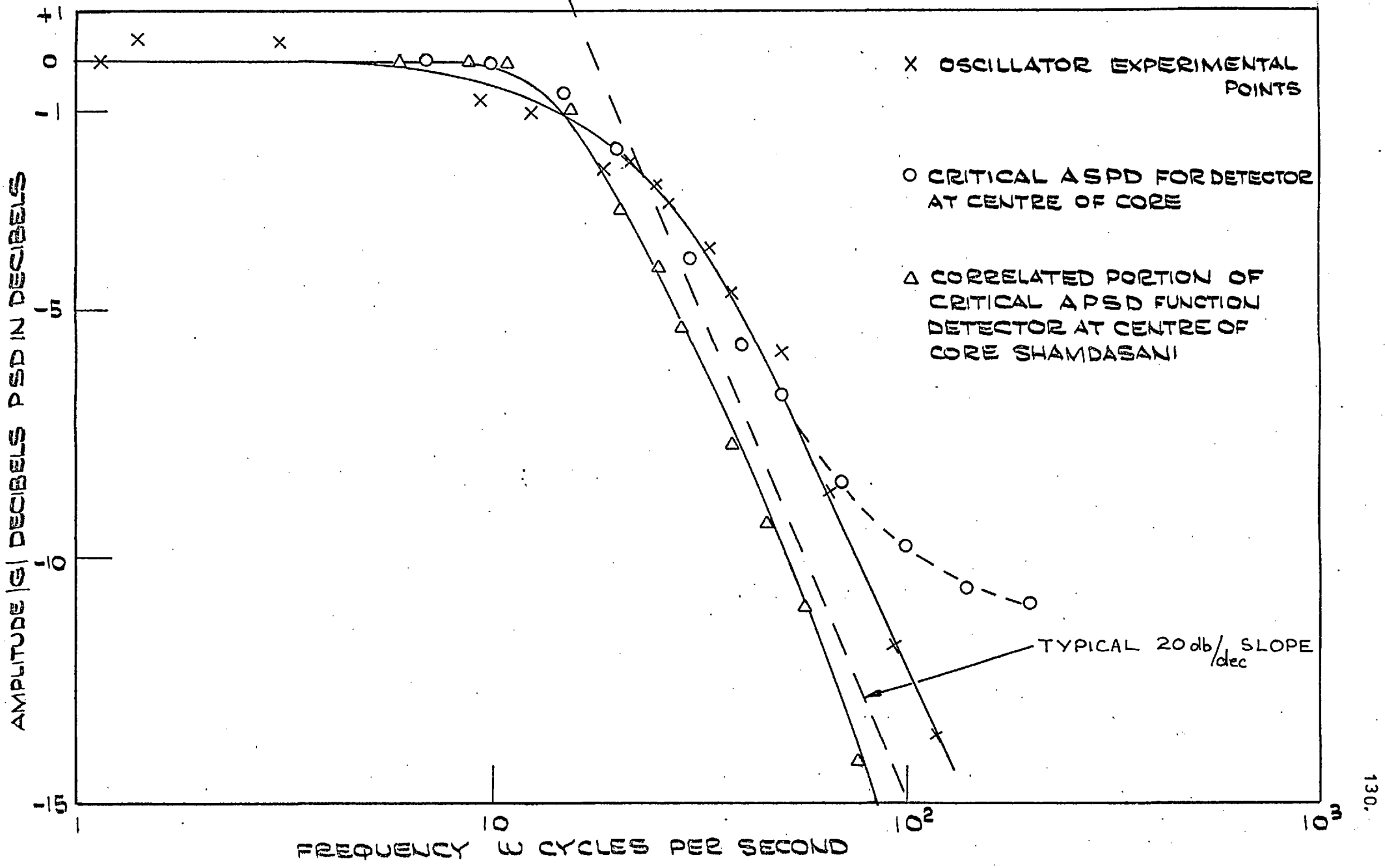

FIG. 44: COMPARISON OSCILLATOR, ASPD & CORRELATED ASPD FUNCTIONS FOR CONSORT

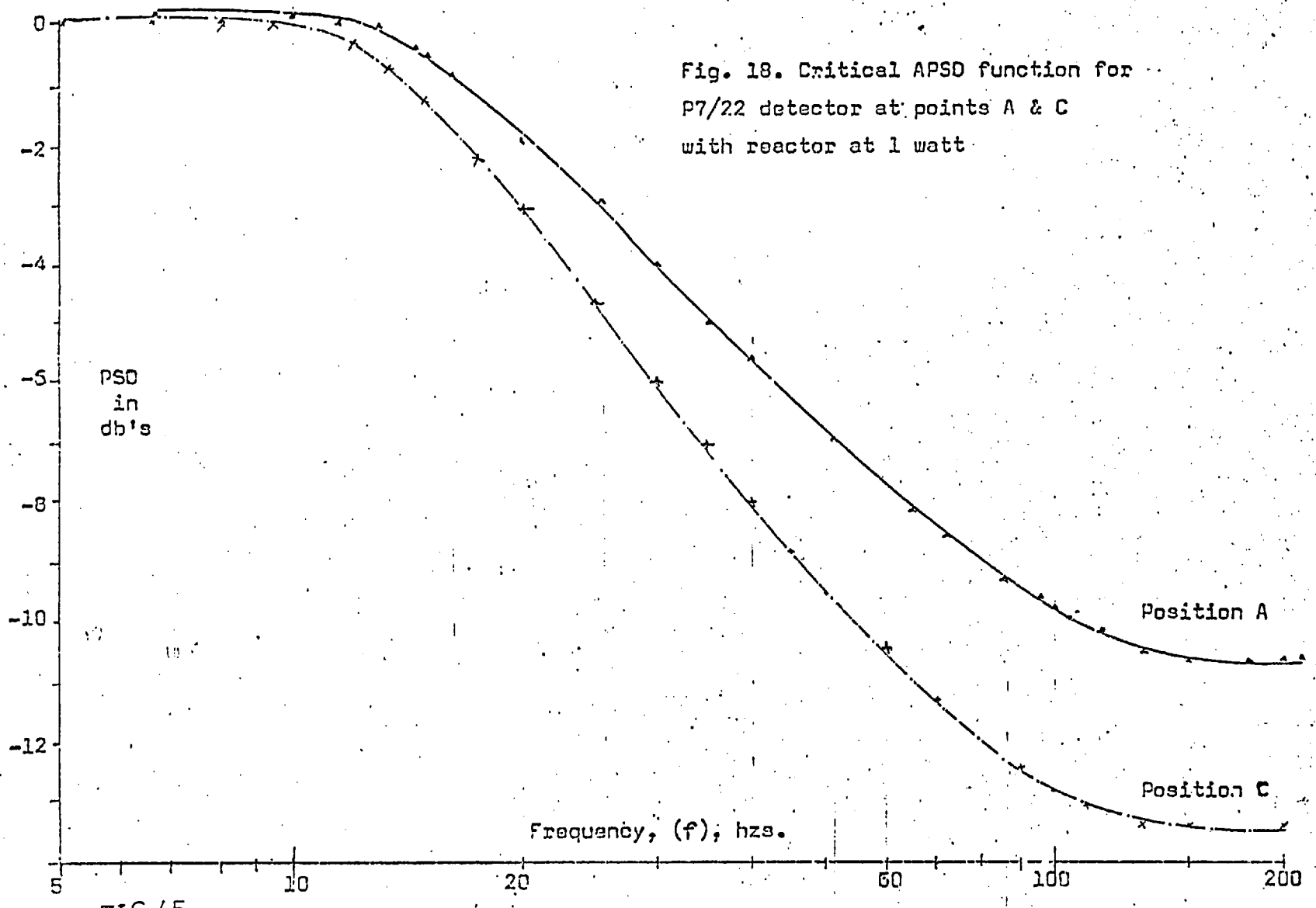

Fig. 18. Critical APSD function for P7/22 detector at points A & C with reactor at 1 watt

FIG 45.

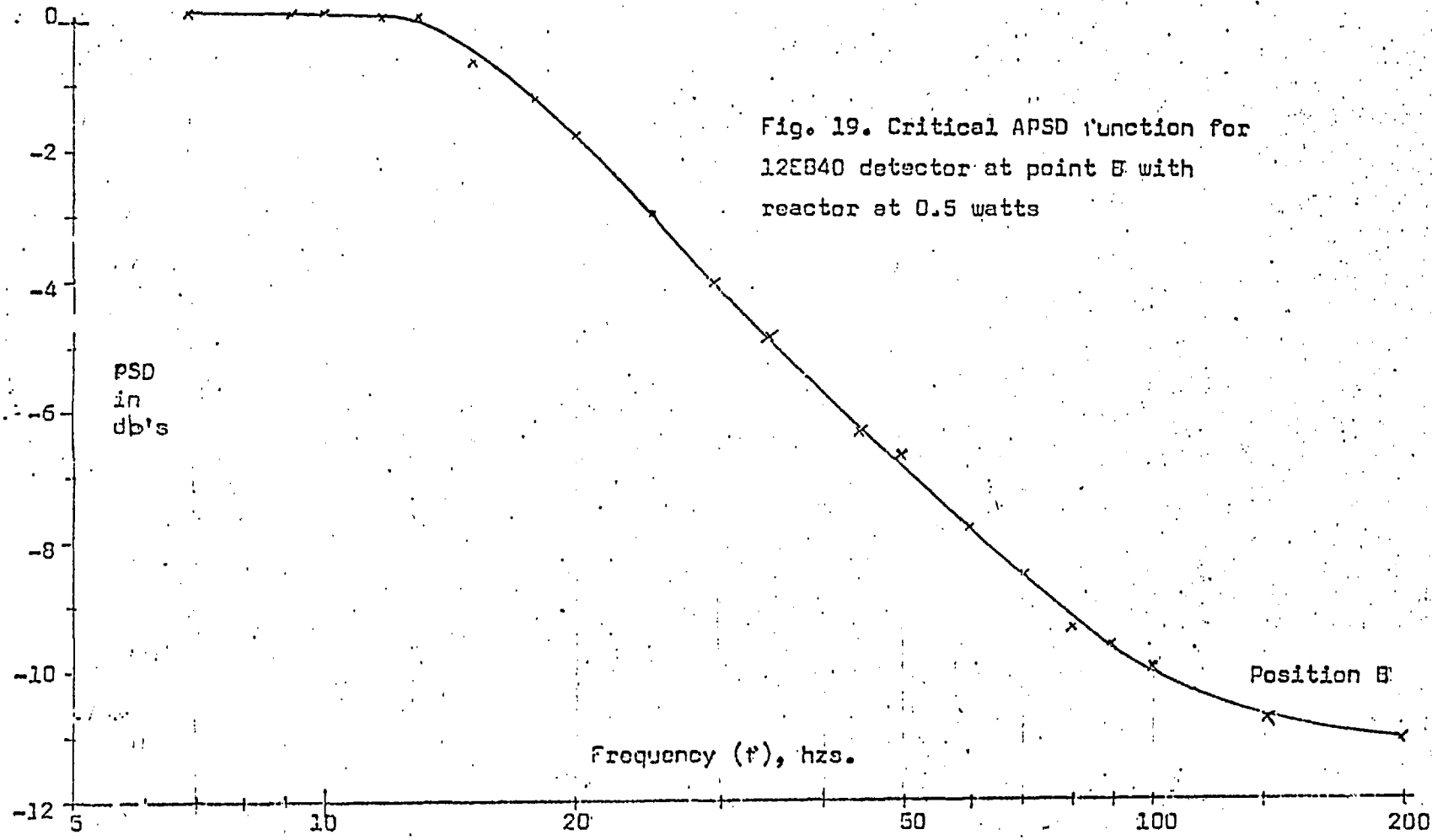

Fig. 19. Critical APSD function for 12E840 detector at point B with reactor at 0.5 watts

FIG46.

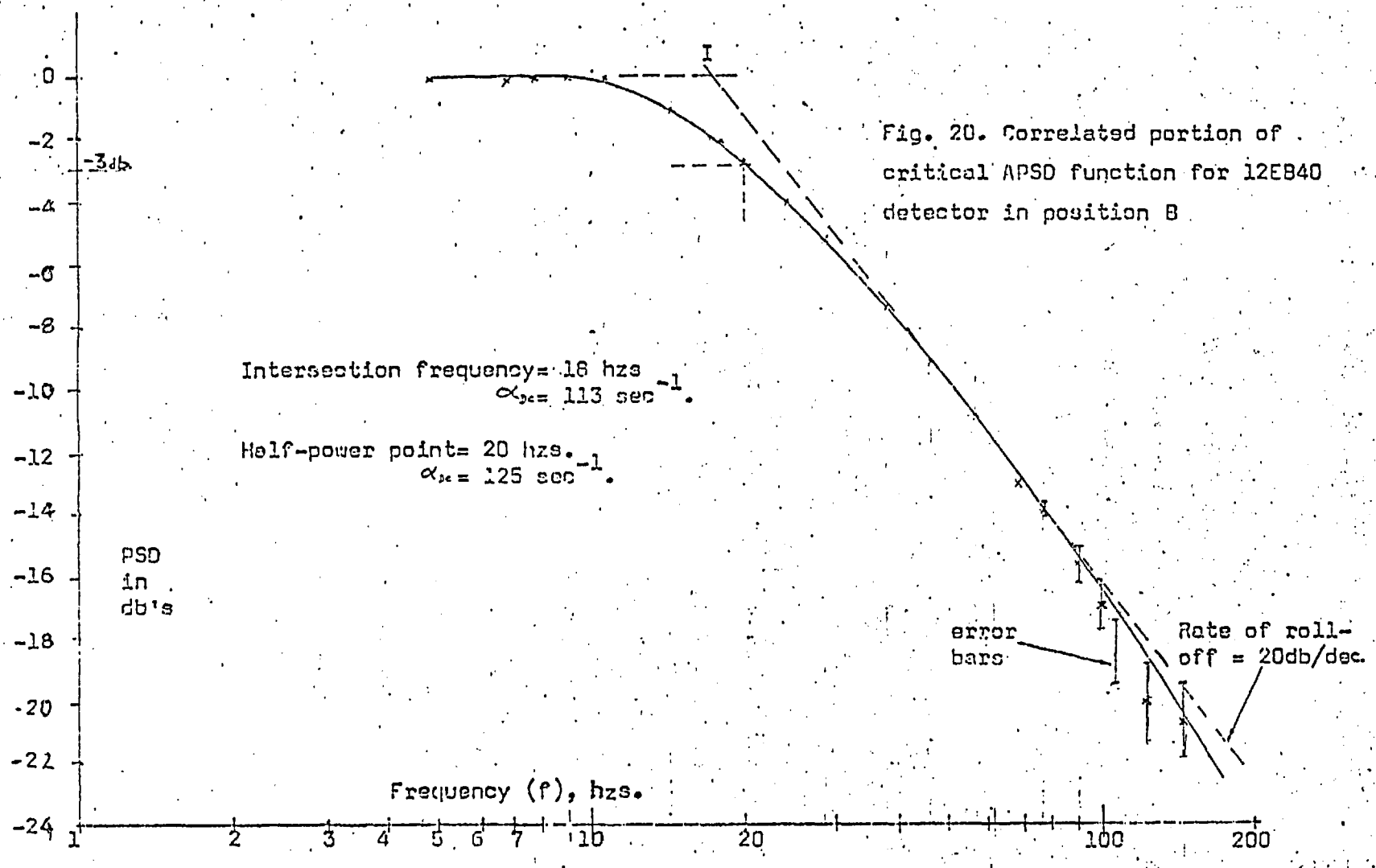

Fig. 20. Correlated portion of critical APSD function for 12EB40 detector in position B

FIG47

be inserted in the core or the reactor tank so measurements were made in the reactor thermal column. According to the results reported by Shamdasani[34] and agreed with by this work, the rates of roll-off in the critical experiments varied between 18.7 and 21.4 db/decade, whilst the value of α_{DC} as determined by the intersection of the half power frequencies varied between 113 and 130 $secs^{-1}$ with an average of 120 $sec^{-1} \pm 5\ sec^{-1}$. As stated in the earlier part of this chapter the intention was to only demonstrate, if possible, any spatial dependency using noise as an alternative to the oscillator for its determination. The results from the two detector measurements are not included since they were mainly carried out for sub-critical measurements which are not the subject of this particular study. It should be pointed out that if one of the main reasons for going to two detector experiments for sub-critical noise measurements was the fact that the signal to noise ratio was much lower, hence errors present in the ASPD particularly at higher frequencies can cause inaccuracies in the estimates of roll off frequencies and intersection frequencies.

Conclusions drawn from these results are given in Chapter 6 of this thesis.

CHAPTER 6

Conclusions, Comments and Suggestions for Further Work

6.1. Conclusions

6.1(1) Zero Power Transfer Function

The zero power reactor transfer function plotted on Figs. 28 and 29 is of the expected shape and amplitude. The phase shift Fig. 29 changing from approximately -90 degrees in the low frequency range through approximately zero degrees in the middle frequency range to -90 degrees again in the high frequency range. This behaviour pattern is expected from the study of the transfer function derived from the point reactor kinetic equations (1) and (2) section 2.1(1) Chapter 2.

The error bands for the experiments are shown on Fig. 33 and 34 respectively, these will become more important when observations and conclusions are made on the space dependency of the transfer function.

It is of interest to investigate the zero power transfer function amplitude response graph in more detail. H.C. Corben[47] analysed the zero power reactor transfer function for a series of isotopes, ranging from U^{238} to U^{233}, utilising data from Keepin[12]. Extrapolating the lower end of the frequency range of the experimentally determined transfer function Fig.28a (for $W \ll \lambda$) yields a value of 8.75 for a frequency of $W = 10^{-2}$ radians per second which compares with a value of 7.8 predicted by Corben[47] for a pure U^{235} isotope. Drawing the asymtote to this curve gives an intercept on the unity axis of 8.0×10^{-2}, the slope of the asymptote being 1.094 which

compares with a value of -1.0 predicted by Corben[47]. The intercept on the unity axis 8.0×10^{-2} yields a value of decay constant $\lambda = 12.5$ seconds which compares with a figure of 12.753 ± 0.1834 table 10.1 Keepin[12]. The actual value obtained from the experimental curves must be treated with care since a small movement on the slope of the asymptote could cause estimated differences of up to $\pm$ 10% in the value of the slope. One has to bear in mind that the Keepin[12] data was determined for a sphere of pure U^{235}. The leakage from the sphere will be less than that for the U.L.R. CONSORT Reactor.

Constructing the asymptote to the high frequency range of the transfer function, Fig.28a, yields a cross over point of $W = 115.5$ radians/second at $G = 1$. This intercept according to Corben[47] and the theory given in Chapter 2 section 2.2(3) yields an expression $G = \frac{\beta^*}{\ell W}$ where β^* is the effective delayed neutron fraction. Assuming values for β of 0.0064 ± 0.0002 Keepin[12] and 0.00755 Caesar[20] (Consort specification), Hughes et al[52] and allowing for an effectiveness factor of $\bar{\gamma} = 1.03$, this latter factor being that obtained from experiments carried out on Godiva[48] (bare metal assembly 93.8% U^{235}) two values of ℓ the neutron generation times are 57.07 μsec and 67.36 μsec respectively. If one does not assume an effectiveness factor of $\bar{\gamma} = 1.03$ the two values are 55.41 μsec and 65.37 μsec respectively. The design figure for the U.L.R. Consort Reactor is 62.5 μsec Caesar[29]. From Fig. 29 the maximum phase shift occurs at a frequency of 6.0 radians per second. The analysis of Corben [47] indicated that the value of the maximum phase shift should obey the expression

$$\tan\theta = \frac{-2\ell W_o}{\beta^*}$$

Where W_o is the frequency at which the maximum phase shift occurs.

From the experimental curve Fig. 29 W_o = 6.0 radians per second and the angle from zero degrees is 5.5°.

$$\therefore \quad \tan = \tan 5.5 = 0.0963 = \frac{2\ell\ 6.0}{0.00659}$$

$$\therefore \quad \ell = \frac{0.00659 \times 0.0963}{2 \times 6.0}$$

$$= 52.88\ \mu \text{ seconds.}$$

If a value of β^* of 0.00778 is used the resulting value of is 62.43 μ seconds.

Summary

β^*	$\bar{\gamma}$=1.00 0.0064	$\bar{\gamma}$ =1.03 0.00659	$\bar{\gamma}$=1.00 0.00755	$\bar{\gamma}$=1.03 0.00778	0.0075
values from high frequency asymptote intercept	55.41	57.07	65.37	67.36	62.5
values from maximum phase shift point	51.35	52.88	60.6	62.43	

The values tend to suggest that the design value of 62.5 μsec is reasonably accurate. It is interesting to note that using the old delayed neutron data produces a value of ℓ close to the design value, within 5% when a value of β^* of 0.00755 is assumed. The value of $\beta^* = 0.0064 \pm 0.0002$. Keepin[12] was experimentally determined using a sphere of U^{235} whereas the reactor involves a cube shaped geometry of metal sheathed fuel elements arranged in a lattice structure immersed in light water.

The β^* for the U.L.R. CONSORT should be near to the

Keepin[12] value since the amount of U^{238} in the core is low with respect to the U^{235} (U^{235} content of CONSORT is 92%).

Assuming that the design figure of 62.5 μ seconds for ℓ is substantially correct and that the higher frequency asymptotic intercept method is the more accurate determination of ℓ than the maximum phase shift position since the latter method is more imprecise due to the rather flat top to the phase shift response curve Fig. 29.

It is felt that the results are reasonable when the errors are considered.

For $\beta^* = 0.0064$ and $\beta^* = 0.00659$ corresponding to $\bar{\gamma} = 1.0$ and $\bar{\gamma} = 1.03$ the errors are -11.35% and -8.79% respectively. For $\beta^* = 0.00755$ and $\beta^* = 0.00778$ corresponding to $\bar{\gamma} = 1.0$ and $\bar{\gamma} = 1.03$ the errors are +4.59% and +7.78% respectively. A figure of $\pm$ 10% error band is reasonable dependent upon the choice of delayed neutron fraction and effectiveness factor.

Fig. 28 gives the transfer function amplitude response for forward and reverse rotation of the oscillator, it was not possible to identify any significant differences between the results for forward and reverse rotation, the results lying within the experimental error bands shown on Fig. 33. The phase shift response plotted on Fig. 29 is the mean of the values obtained for forward and reverse rotation of the oscillator, there was no significant difference between the two that lay outside the error bands shown on Fig. 34. The fact that signal recovery was used tended to reduce errors since an average of many repetitive cycles was taken at each frequency reading.

The comparison of the amplitude and phase shift responses with a range predicted for U^{235} by Keepin[12] data, Figs. 30 and 31, shows good agreement, no value of Keepin data was available for the exact value of the prompt neutron lifetime but interpolation between the values of $\ell = 10^{-4}$ and $\ell = 10^{-5}$ shows that the amplitude and phase responses are of the expected correct shape and magnitude. These values tend to justify the experimental and analysis techniques employed.

6.1(2) Space Dependency

Shamdasani[34] reported in previous noise experiments using one and two detector techniques, that CONSORT exhibited no spatial dependency. For the series of oscillator/detector configurations used in the series of experiments, see Fig. 25, Chapter 4 section 4.2., one is inclined to agree with this statement since no amplitude or phase response experimental results lay outside the error bands quoted for the experiment nor was there any systematic trend to the results that lay within the error band. The reactor core appeared as a point with respect to the configurations shown as Fig. 25. In fact the reversal of the oscillator/detector position produced no significant change in the spread of the results.

What is of significance is the reason why no spatial dependency was apparent Beckurts and Wirtz[49] give expressions for the diffusion of mono-energetic neutrons from a harmonically modulated source and arrive at the conclusion that the modulated part of the neutron flux is a modulated wave with a depth of penetration:

$$\frac{1}{K} = \frac{\sqrt{\frac{2Dv}{w}}}{1 + \frac{v\Sigma a}{2w}} \approx \sqrt{\frac{2Dv}{w}}$$

with a wavelength $\backsimeq 2\pi \sqrt{\frac{2Dv}{w}}$

and a phase velocity

$$\frac{w}{k} \backsimeq \sqrt{2Dvw}$$

response is given by

$$\frac{/\delta\Phi_o(r)/}{\Phi(r)} = \frac{\delta Q}{Q_o} \cdot \frac{e^{-Kr}}{e^{-r/L}}$$

CONSORT is a light water moderated and reflected reactor, using a value of D = 0.114 cm. provided by previous experiments carried out on the reactor Besant [50]. Which compares with a value of 0.14 Jakeman [51], appendix table A1, and assuming velocities of 2200 metres/sec and 200 metres/sec the latter figure allowing for a Maxwellian distribution of neutron velocities. For w = 500 radians/sec per second the values of penetration depth are approximately 10.5 cm. and 3.0 cm. For w = 1 radian per second the values of penetration depth are approximately 224 cm. and 67.5 cm. respectively. Thus as one can see as the frequency goes up the depth of penetration decreases causing the response to fall off rapidly with the core radius. This, of course, explains the attenuation as frequency increases. It has to be remembered that there are neutrons of all velocities within the spectrum. Bearing in mind that the CONSORT core is approximately a 60 cm. cube it can be seen, from the previous penetration values, that a spatial dependency would be difficult to measure, at the high frequency, no spatial depending was indicated by the experiment. In the previous calculations one must bear in mind that an oscillating absorber not a source was used, nevertheless the implied wave behaviour is the same. Also it must be remembered that the core

is a dispersive medium and the neutron waves would propagate in all directions thus causing a diffusive effect on the results. One final contributory factor is that the detector active length was 12 cm. thus the relative positions vertically in the core, Fig. 7 Chapter 3 section 3.1(2), and the neutron collection area would tend to increase the diffusion of the results. Experiments were carried out by Hansson[26] using an oscillator to determine the spatial dependency of the NORA D_2O moderator and reflector reactor. For an w of 1 radian per second and neutron velocities of 2200 metres per second and 200 metres per second using a D for D_2O of 0.82 Jakeman[51] appendix table A1, gives penetration depth of approximately 600 and 180 cm. Bearing in mind that these results must be treated with care the part of these experiments that caused very significant spatial dependency was when the detector was within 7 cm. of the oscillator at a frequency of approximately 1 cycle per second. This is well within the penetration depth using the former approximate calculation methods.

Not too much significance should be placed upon the comparison of the NORA and CONSORT reactors since not enough information was available on the NORA structure, also detailed lattice calculations might be necessary before a true comparison was possible. There is the problem, when the detector and oscillator are very close to the core, of local heterogeneity problems, this was posed as a possible cause of the error between the NORA predicted and experimentally determined results.

The CONSORT reactor exhibited no spatial dependency for the oscillator/detector configurations used in the experiments.

6.1(3) Noise Results

Due to the afore-mentioned reasons it was not expected that the noise experiments would exhibit any spatial dependency. The slope of the high frequency asymptote, Fig. 44, is as expected within experimental errors. The joint work undertaken with Shamdasani[34] substantiates this conclusion. Shamdasani[34] supports his conclusions with the use of one and two detector experiments using the three detectors discussed in Chapter 3 section 3.2 of this thesis.

The critical ASPD function Fig. 44 demonstrates the difficulties of unwanted noise when at high frequencies where the amplitude is attenuated. The corresponding correlated ASPD is shown on Fig. 44 for comparison, this curve being derived by Shamdasani[34] does not completely agree with the oscillator plot though the uncorrelated ASPD does appear to have a better agreement in the frequency range 15 to 55 cycles per second. It is possible that some of the basic neutron fluctuations could have been correlated and in addition to the unwanted instrumentation and analysis noise, no evaluation of this can be made.

The value of $\alpha_{DC} = 120 \text{ sec}^{-1} \pm 5 \text{ sec}^{-1}$ obtained from the ASPD function compares favourably with the value of 128 sec^{-1} obtained from the oscillator amplitude response curve, Fig. 32.

Some comment must be made upon the total curve plotted on Fig. 43. As can be seen the only range produced from the noise measurements is in the upper frequency range. To cover the low frequency range the recording time would have to be extremely long before any averaging or correlation was undertaken. The auto correlation function only provides the amplitude response of

the reactor, it is necessary to utilise cross-correlation methods so that the phase shift can be determined, this requires the excitation of the reactor with a known random reactivity input before a cross-correlation can be utilised. This was unfortunately outside the scope of these experiments.

As stated before, the noise experiments were only undertaken as a check for the oscillator results since the two experiments were running concurrently, but some comment upon noise measurements in general is necessary at this time. Many workers have investigated noise experimentally and theoretically with particular reference to zero power reactors and assemblies. One stated major advantage of noise techniques is that the reactor need not be disturbed, this is, of course, true for many of the studies undertaken but if phase information is necessary then the most convenient method in noise analysis is to inject a known random fluctuation into the core, that will affect reactivity, and for this to be used in cross-correlation analysis.

For higher frequency work noise is of advantage since not too long a recording time is necessary but this figure increases as the frequency reduces. The question of noise analysis of power reactors poses an additional problem. Whereas on the one hand it is not necessary to perturb the reactor there are many other sources of noise in the reactor that affect the reactivity, thus the pure neutron noise becomes more difficult to decipher. Especially when one considers the size of the reactor and the attenuation of any local neutron flux perturbation that are only due to the inherent fluctuations in the reactor chain reaction.

The analysis of the noise from sources other than the statistical nature of the neutron chain reactor become of much

greater interest, i.e. the rattling of control rods in the coolant flow. It is the auto correlation and cross-correlation techniques that become of great interest.

To summarise noise can be a powerful tool, not necessarily adding to the knowledge of the basic fission process, but confirming measurements or predictions made by other methods. The techniques used in noise analysis will be of greater use in power reactors for effects that are not directly due to inherent fluctuation. Care should be taken that noise investigations are not pursued only for the sake of the noise itself.

It is interesting to note the plot of fluctuating power obtained during the very slow speed runs, Fig. 42. The reactor operator did not trim the reactor during each run only at the beginning and end of each run to establish steady state.

The slow oscillatory runs were allowed to run for 45 minutes, during which time the reactor was observed not to drift from a mean power. This was most probably due to the fact that the reactor was effectively at zero power and most probably few fission products were present.

6.2. Suggestions for Further Work

The results obtained indicate that for the positions and frequency range concerned no spatial dependency was observable. It would appear necessary to insert the detector at points within the actual radius of the core, i.e. within the fuel element lattice. This was not possible with the CONSORT core with the detectors that were available. The use of pencil slim BF_3 counters would, of course, enable such in core detector positions to be investigated

the spatial dependency could then be investigated as a function of radius. By rearranging the lattice of CONSORT it would of course be possible to obtain a suitable size hole within the core boundaries, this was not possible within the experiments described but it could be of interest in the future providing the position for the entry hole could be chosen to exhibit a large spatial dependency.

The techniques used in the general measurement were proved satisfactorily though the coupling of the on-line Hewlett Packard to its own on-line computer would provide a very compact on site measurement and analysis system. The correlator itself is useful in displaying the correlation functions to verify the results. It is thus recommended that the unit be used as at least an indication in all future experiments.

The use of square wave and triangular wave modulators instead of the sine wave used in the oscillator in the former experiments would yield further information on the question of whether or not it was necessary for the input modulation to be a pure sine wave. Its effect on the propagation through the core would be of interest especially since a Fourier analysis could be quite readily undertaken.

None of the detector chambers were capable of operating at power, it is thus suggested that two chambers capable of operating in the core, should be used to determine the Power Transfer Function, this would lead to a knowledge of the intrinsic reactivity sources due to heat removal.

Both at zero power and full power it would be interesting to inject a known random input and to use cross-correlation functions to determine both the reactor amplitude and phase shift transfer

function responses. This latter condition could be achieved by either driving one of the control rods in a random manner or by injecting bubbles into a coolant channel, the injection being controlled by a known randomly driven value. This latter experiment has been suggested to and accepted by the U.L.R. Safety Committee.

APPENDIX 1

Fig. 6. University of London Reactor.

Power		
Maximum for continuous operation		100 KW (thermal)
Fuel Element	U.K.A.E.A. standard M.T.R. type	
Material of plates	Uranium-aluminium alloy	
Enrichment		c 80%
Cladding		aluminium
No. of plates per element (normal)		12
Wt of U-235 per plate		11.5 g
Core		
Maximum no. of elements		24
Wt of U-235 in critical assembly		c 2810 g
Moderator, Reflector, Coolant		H_2O
Maximum excess reactivity		c 0.1%
Control absorbers		
	1 fine control rod	
	2 coarse control rods (shut down)	
	1 safety rod	
Shielding	Water, Cadmium, Concrete	
Neutron Flux		
Centre of core, fast		4×10^{12} n/cm^{2}sec
thermal		2×10^{12} n/cm^{2}sec

Bare face and thermal column, at tank/graphite interface,	fast	2×10^{11} n/cm^{2}sec
	thermal	3×10^{11} n/cm^{2}sec
Main beam tube entry,	fast	1×10^{11} n/cm^{2}sec
	thermal	3×10^{11} n/cm^{2}sec

Coolant circuit

Flow rate	9100 l/h

Principal dimensions

Tank diameter	1142 mm.
Water depth, total	7772 mm.
above fuel plates	5245 mm.
Biological shield	
across flats of octagon	6400 mm.
height above ground level	6858 mm.
depth below ground level	1524 mm.

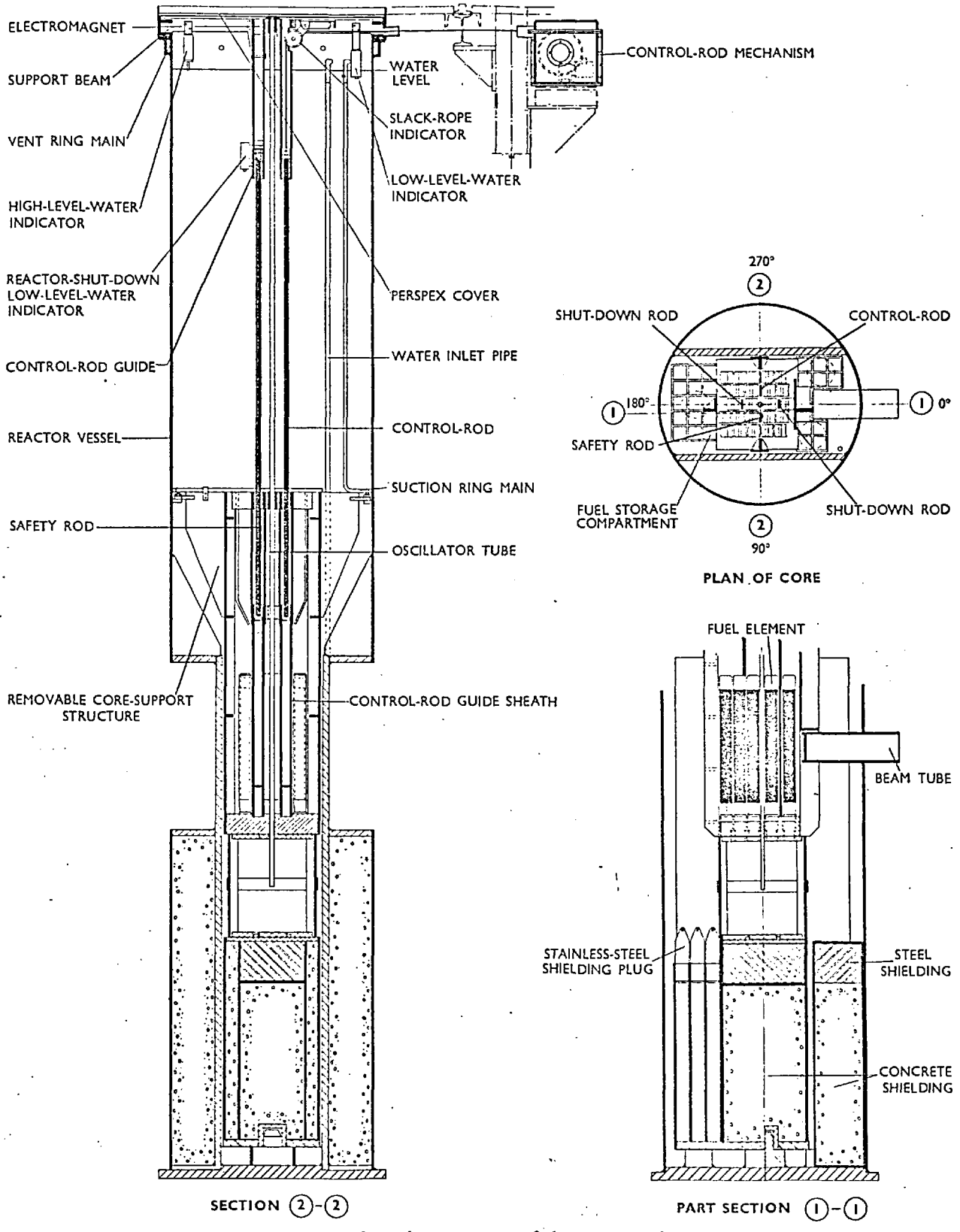

Fig. 3. General arrangement of the reactor tank.

L.U.R. 251.

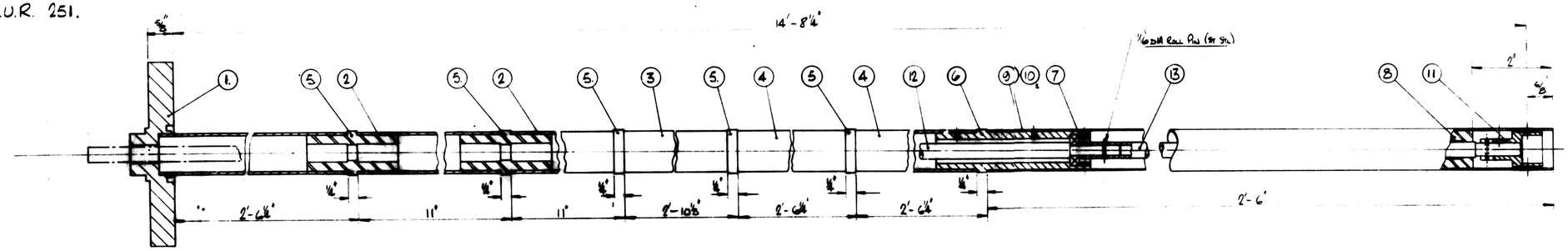

(1) USE ST. STL SCREWS THROUGHOUT

(2) PURCHASE HOFFMAN "S10 RACE ~ 1off
2 HOFFMAN "S1 RACE ~ 1off

UNIVERSITY OF LONDON REACTOR
SILWOOD PARK,
SUNNINGHILL ASCOT.
BERKS

DRG N° LUR 251.

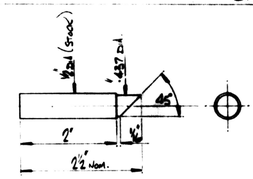

1off

CADMIUM PLATED — MATERIAL MILD STEEL

REACTIVITY OSCILLATOR

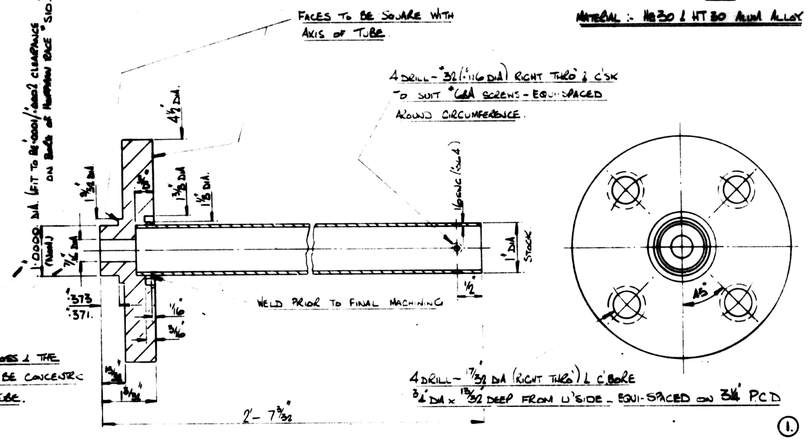

ITEM N°	DIM. 'X'	N° OFF
2	10⅜"	2
3	33⅜"	1
4	30"	2

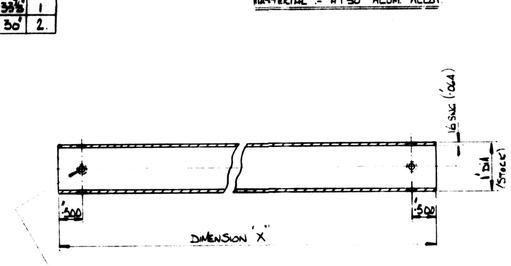

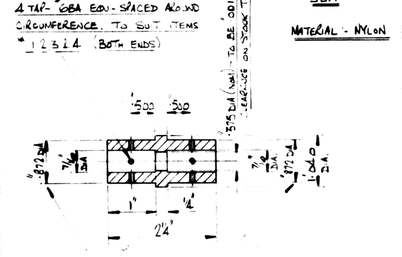

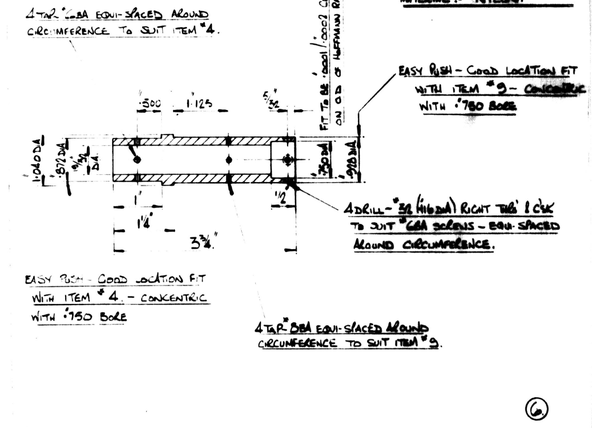

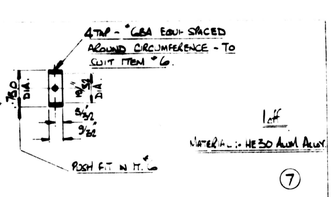

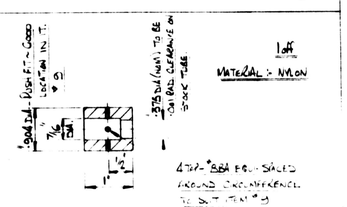

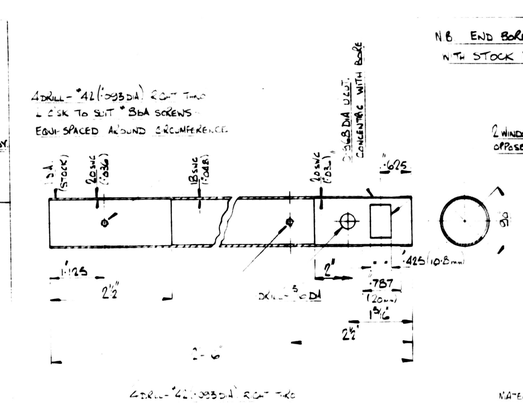

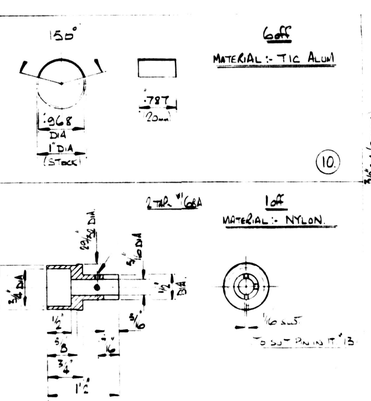

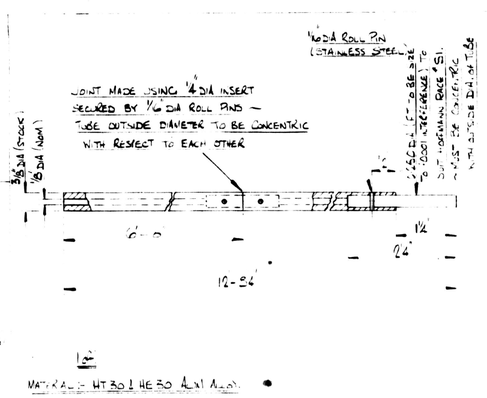

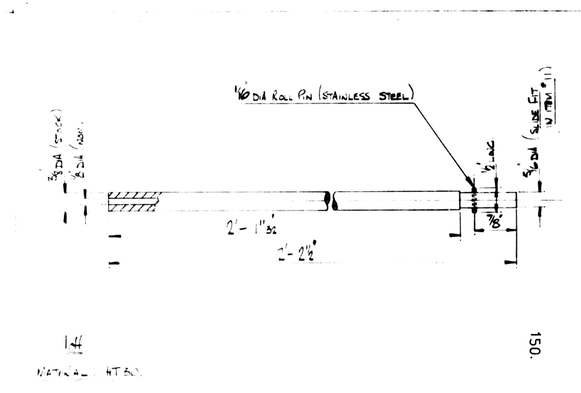

APPENDIX 3

Zero Power Reactor Transfer Function For U^{235}

is the prompt neutron lifetime. All values calculated using the delayed neutron data of table 4-7, Keepin[12].

W RADS/SEC	= 10^{-4} /G/ DOLLARS	= 10^{-4} ∅ DEGREES	= 10^{-3} /G/ DOLLARS	= 10^{-3} ∅ DEGREES
1 -02	8.6468 00	-72.041	8.5494 00	-72.250
2 -02	5.0585 00	-61.295	4.9970 00	-61.676
3 -02	3.9089 00	-54.474	3.8578 00	-55.007
4 -02	3.3435 00	-49.969	3.2965 00	-50.642
5 -02	2.9976 00	-46.901	2.9525 00	-47.702
1 -01	2.2002 00	-39.501	2.1578 00	-40.822
4 -01	1.3286 00	-24.134	1.2871 00	-27.864
6 -01	1.2200 00	-19.424	1.1752 00	-24.707
1 00	1.1340 00	-14.864	1.0787 00	-23.164
2 00	1.0593 00	-10.850	9.6846 -01	-26.122
3 00	1.0316 00	- 9.449	8.9641 -01	-30.998
4 00	1.0175 00	- 8.962	8.3266 -01	-36.061
5 00	1.0088 00	- 8.922	7.7272 -01	-40.825
6 00	1.0028 00	- 9.135	7.1654 -01	-45.131
7 00	9.9811 -01	- 9.507	6.6460 -01	-48.950
8 00	9.9419 -01	- 9.985	6.1720 -01	-52.309
9 00	9.9067 -01	-10.537	5.7431 -01	-55.254
1 01	9.8734 -01	-11.141	5.3568 -01	-57.838
2 01	9.5128 -01	-18.251	3.0719 -01	-72.141
3 01	9.0349 -01	-25.470	2.1113 -01	-77.821
4 01	8.4779 -01	-32.067	1.6012 -01	-80.790
5 01	7.8943 -01	-37.888	1.2877 -01	-82.603
6 01	7.3223 -01	-42.938	1.0762 -01	-83.823
7 01	6.7839 -01	-47.289	9.2407 -02	-84.699
8 01	6.2894 -01	-51.033	8.0948 -02	-85.358
9 01	5.8417 -01	-54.259	7.2010 -02	-85.871
1 02	5.4392 -01	-57.052	6.4845 -02	-86.282
2 02	3.0889 -01	-72.008	3.2481 -02	-88.139
3 02	2.1169 -01	-77.779	2.1661 -02	-88.759
4 02	1.6037 -01	-80.772	1.6248 -02	-89.069
5 02	1.2890 -01	-82.594	1.2999 -02	-89.255
6 02	1.0770 -01	-83.818	1.0833 -02	-89.379
7 02	9.2454 -02	-84.695	9.2853 -03	-89.468
8 02	8.0980 -02	-85.355	8.1247 -03	-89.586
9 02	7.2032 -02	-85.869	7.2220 -03	-89.586
1 03	6.4861 -02	-86.251	6.4998 -03	-89.628

APPENDIX 4

Preliminary Measurements Utilising an Existing Standard Multi-Channel Analyser

As a result of the intention that undergraduate and postgraduate experiments should be available using the oscillator it was decided that attempts at measurement and analysis of the transfer function should be made utilising an existing standard 400 channel multi-channel analyser.

The pulse from the oscillator drive shaft was used to trigger the multi-channel analyser to read the output of the neutron detector. Succeeding trigger pulses (every revolution) would effectively top up the analyser reading so that a steady state reading should be achieved.

Several difficulties were encountered immediately, the analyser was remote from the reactor and a pulse amplifying and shaping unit was required to trigger the unit.

The remoteness had to be accepted and the fact that ideally suited cables were not available. A standard Harwell 2000 pulse amplifier and shaper was used to drive the analyser. To achieve the 'top up' principle a repeat trigger pulse would be required. This was available from the oscillator shaft once every revolution or every two cycles. This gives a measurement of 1 cycle in 180 channels, i.e. a phase reading every 2 degrees.

This latter point plus the uncertainty in the trigger timing due to the cable delay and the pulse shaper meant that the method was not suitable for the present study though the results on Fig. 48 show that an experiment using the analyser is possible particularly if both equipment and analysis methods were modified.

The spread of points at the peaks and troughs of the sine wave shape shown on Fig.48 is mainly due to the channel measurements only being read to the first decimal place.

The method will be investigated at a later stage.

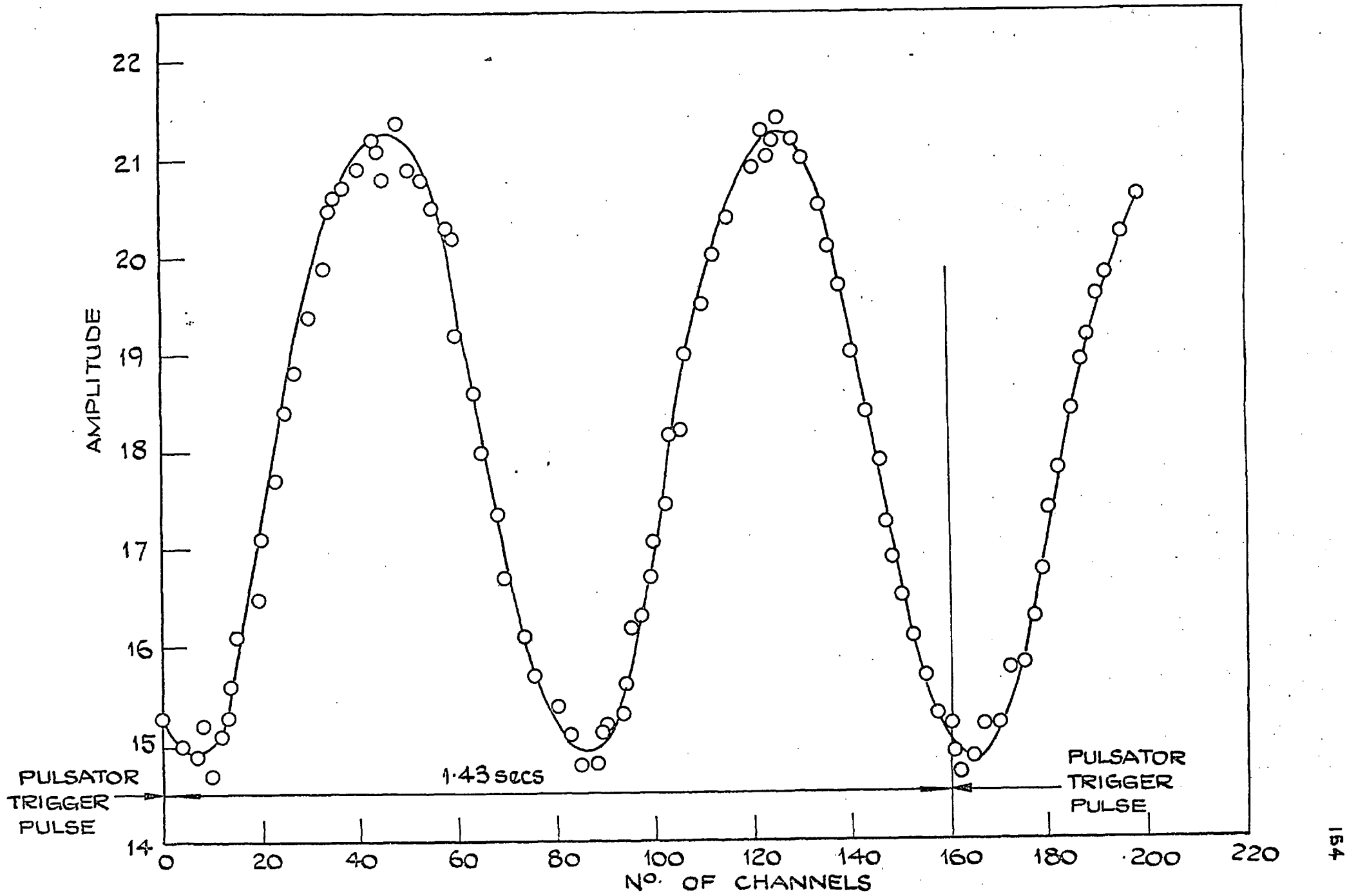

FIG.48 OSCILLATOR OUTPUT ON MULTI-CHANNEL ANAYSER.

APPENDIX 5

Experimental Points Experiment No. 1

Frequency C/S	Frequency RADS/SEC	Amplitude Dollars	Gain db's	Phase Degrees
3.49 - 03	2.19 - 02	4.66 00	13.368	60.4
5.39 - 03	3.37 - 02	3.43 00	10.706	52.1
1.11 - 02	6.96 - 02	2.395 00	7.596	44.8
2.3 - 02	1.44 - 01	1.633 00	4.26	34.9
3.4 - 02	2.185- 01	1.374 00	2.766	29.1
5.32 - 02	3.34 - 01	1.284 00	2.172	25.0
7 - 02	4.398- 01	1.21 00	1.0656	22.2
9.8 - 02	6.15 - 01	1.15 00	1.214	19.0
1.4 - 01	8.8 - 01	1.13 00	1.062	14.6
2.1 - 01	1.3 00	1.08 00	6.68 - 01	12.2
2.4 - 01	1.51 00	1.06 00	5.06 - 01	10.1
2.8 - 01	1.76 00	1.05 00	4.24 - 01	10.0
3.5 - 01	2.184 00	1.02 00	1.28 - 01	8.7
4.2 - 01	2.86 00	1.005 00	8.6 - 02	7.4
5.6 - 01	3.515 00	1.000 00	0.0000 00	7.05
7.0 - 01	4.395 00	1.000 00	0.0000 00	5.59
8.4 - 01	5.15 00	1.000 00	0.0000 00	5.49
9.8 - 01	6.157 00	1.03 00	2.56 - 01	5.35
1.12 00	7.04 00	1.000 00	0.0000 00	5.8
1.22 00	7.66 00	1.05 00	4.24 - 01	6.15
1.24 00	7.79 00	9.99 - 01	0.08 - 01	6.1
1.4 00	8.79 00	1.05 00	4.24 - 01	6.2
2.17 00	1.3625 01	9.95 - 01	-1.088 - 01	6.95
3.1 00	1.947 01	1.05 00	4.24 - 01	10.6
6.1 00	3.83 01	9.7 - 01	-2.640 - 01	18.4
9.3 00	5.845 01	9.25 - 01	-7.780 - 01	29
1.24 01	7.79 01	8.9 - 01	-1.012 00	36
1.55 01	9.74 01	8.9 - 01	-1.012 00	39.4
1.86 01	1.186 02	7.78 - 01	-2.18 00	41
2.17 01	1.362 02	7.9 - 01	-2.028 00	48.5
2.48 01	1.56 02	7.5 - 01	-2.498 00	50.8
2.635 01	1.654 02	7.2 - 01	-2.854 00	51.5
3.368 01	2.16 02	6.5 - 01	-3.742 00	59.3
3.74 01	2.37 02	5.8 - 01	-4.732 00	61.8
5.0 01	3.142 02	5.1 - 01	-5.934 00	71.4
6.52 01	4.095 02	3.65 - 01	-8.754 00	75.3
9.45 01	5.934 02	2.6 - 01	-1.17 01	77.9
1.19 02	7.46 02	2.08 - 01	-1.364 01	80.0

REFERENCES

1. HARRER, J.M.
D. Van Nostrand, Princeton N.J. (1963).

2. SCHULTZ, M.A.
1st Edition, McGraw-Hill, New York.

3. JEBB, A.
Imperial College, ME2. (1962).

4. SINGER, S.
LA-2654. (1962).

5. SCHULTZ, M.A.
2nd Edition, McGraw-Hill, New York. (1961).

6. GLASSTONE, S. and EDLUND, M.C.
C.V. Nostrand, Princeton N.J. (1952).

7. HARRER, J.M. et al.
Nucleonics, Vol. 10, No. 8, pp.32. (1952).

8. HASSITT, A.
PRG Report 229R, U.K.A.E.A. Risley.

9. LAMARSH, J.R.
Addison-Wesley, Reading, Mass. (1966).

10. WEINBERG, A.M. and WIGNER, E.P.
University of Chicago Press, Chicago, U.S.A. (1958).

11. HOFFMAN, F.de.
AECD-3051. (1944).

12. KEEPIN, G.R.
Addison-Wesley, Reading, Mass. (1965).

13. THIE, J.A.
Rowman and Littlefield, New York. (1963).

14. NORDHEIM, L.W.
MDDC-35. (1946).

15. WEINBERG, A.M. et al.
Phys. Rev. 74:851. (1948).

16. FRANZ, J.P.
AECD-3260. (1949).

17. HARRER, J.M. et al.
Nucleonics 10(8):32 (see also ANL-4373). (1952).

18. KERLIN, T.W.
Nucl. Safety 8:339. (1967).

19. CARTER, J.C. et al.
Ed. L.E. Weaver, Oak Ridge, Tenn. U.S.A.E.C. Division of Technical Information Extension. (1964).

20. GARABEDIAN, H.L. et al.
Nuc. Sci. and Eng., 6, 26. (1959).

21. HENRY, A.F.
Nuc. Sci. and Eng., 8, 532. (1958).

22. STACEY, W.M. (Jnr.)
Academic Press, New York.

23. LOEWE, W.E.
Nuc. Sci. and Eng., 21, 536. (1965).

24. SAJI, G.
Nuc. Sci. and Eng., 32, 93-100. (1968).

25. HAUGSET, K.
Institute for Atomenegi Kjeller, Norway. (1963).

26. HANSSON, P.T. et al.
Nuc. Sci. and Eng., 17, 528. (1963).

27. COHN, C.F. et al.
Nuc. Sci. and Eng., 26, 198. (1966).

28. KLYSTRA, C.D.
Ph.D. Thesis, University of Florida. (1963).

29. CAESAR, E.A.Y.
Imperial College, London. (1964).

30. ROUX, D.P.
Nuclear Applications, Vol. 3. (1963).

31. KIEHN, R.M.L.
ANL 6205.

32. WILSON, W.E. et al.
ANL 6410. (1961).

33. FOWLER, P.
Private Communication, U.K.A.E.A., Winfrith, England.

34. SHAMDASANI, R.
Ph.D. Thesis, University of London.

35. MOORE, M.N.
Nuc. Sci. and Eng., 3, 388. (1958).
Nuc. Sci. and Eng., 4, 134. (1958).
TID-7679, p.13, U.S.A.E.C. (1964).

36. ARGONNE, et al.
Nuc. Sci. and Eng., 5, 331. (1959).

37. COHN, C.E.
Nuc. Sci. and Eng., 4, 472. (1960).

38. WAX, N.
Dover Publications. (1954).

39. COHN, C.E.
A.E.C. Symposium, 4. (1964).

40. FEYMAN, R. et al.
J. Nuc. Energy, 3, 64. (1956).

41. HURWITZ, et al.
Nuc. Sci. and Eng., 15, 166. (1963).

42. HANSEN, G.E.
Nuc. Sci. and Eng., 8, 709. (1960).

43. SHEFF, R.
Nuc. Sci. and Eng., 24, 246. (1966).
and 26, 207. (1966).

44. NATELSON, N. et al.
J. of Nuc. Energy, P + A and B, 20, 557-585. (1967).

45. BENDAT, S.S. and PIERSOL
John Wiley & Sons. (1958).

46. NIETO, J.M. et al.
J. Nuc. Energy, 22, 175. (1968).

47. CORBEN, H.C.
Nuc. Sci. and Eng., 6, 461-465. (1959).

48. PETERSON, R.E. et al.
Nuc. Sci. and Eng., 1, 112. (1956).

49. BECKURTS, K.H. and WIRTZ, K.
Springer Verlag. (1964).

50. BESANT, C.B.
Ph.D. Thesis. (1965).

51. JAKEMAN, D.
English Universities Press. (1966).

52. HUGHES, D.J. et al.
Phys Rev. 107. 1044 (1957).